

Final Report

ULTRASONIC TEMPERATURE MEASURING DEVICE

by

L. C. Lynnworth and E. H. Carnevale

prepared for

NATIONAL AERONAUTICS AND SPACE ADMINISTRATION

August 1967

CONTRACT NAS3-7981

Technical Management  
NASA Lewis Research Center  
Cleveland, Ohio  
Nuclear Systems Division  
Miles O. Dustin

Advanced Systems Division  
Dr. John C. Liwosz

PANAMETRICS, INC.  
221 Crescent Street  
Waltham, Massachusetts 02154

6506

(ACCESSION NUMBER)	(THRU)	(CODE)	(CATEGORY)
143	1	14	

41-79-339

(PAGES)

(NASA CR OR TMX OR AD NUMBER)

FACILITY FORM 602

## NOTICE

This report was prepared as an account of Government sponsored work. Neither the United States, nor the National Aeronautics and Space Administration (NASA), nor any person acting on behalf of NASA:

- A) Makes any warranty or representation, expressed or implied, with respect to the accuracy, completeness, or usefulness of the information contained in this report, or that the use of any information, apparatus, method, or process disclosed in this report may not infringe privately owned rights; or
- B) Assumes any liabilities with respect to the use of, or for damages resulting from the use of any information, apparatus, method or process disclosed in this report.

As used above, "person acting on behalf of NASA" includes any employee or contractor of NASA, or employee of such contractor, to the extent that such employee or contractor of NASA, or employee of such contractor prepares, disseminates, or provides access to, any information pursuant to his employment or contract with NASA, or his employment with such contractor.

Requests for copies of this report should be referred to

National Aeronautics and Space Administration  
Office of Scientific and Technical Information  
Attention: AFSS-A  
Washington, D. C. 20546

## Ultrasonic Temperature Measuring Device

by

L. C. Lynnworth and E. H. Carnevale

### ABSTRACT

A pulse-echo ultrasonic system was designed, constructed and tested for automatically determining temperature by measuring the round trip transit time in a wire sensor. Laboratory tests were conducted to the melting point of Re in carbon-free vacuum, and up to the Re/C eutectic in a graphite environment. Rhenium wires irradiated to  $8.7 \times 10^{19}$  integrated thermal flux and  $2.6 \times 10^{19}$  integrated fast flux showed no significant differences in the velocity/temperature characteristic. In field tests in a graphite/hydrogen environment, bare Re sensors survived to temperatures ranging up to  $4765^{\circ}\text{R}$ .

## TABLE OF CONTENTS

	<u>Page</u>
SUMMARY . . . . .	1
INTRODUCTION . . . . .	4
Statement of the Problem . . . . .	4
Historical Review and Background - Ultrasonic Thermometry . .	4
Present Ultrasonic Approach . . . . .	6
Wire Sensors . . . . .	6
BASIC PRINCIPLES . . . . .	8
Propagation of Elastic Waves in Solids . . . . .	8
Wave Reflection and Transmission . . . . .	8
Methods of Generating Ultrasonic Elastic Waves in Wires . . .	10
Application to Acoustic Thermometry . . . . .	14
Bends, Kinks . . . . .	16
The Sensor . . . . .	16
Graphites . . . . .	19
Carbides . . . . .	20
Polycrystalline Metals . . . . .	21
Single Crystal Metals . . . . .	23
Comparison of Materials Based on Velocity . . . . .	23
EXPERIMENTAL APPARATUS AND TECHNIQUES . . . . .	24
Electronics . . . . .	24
Pana-Therm Model 5000 . . . . .	24
High Temperature Sources . . . . .	27
SRI Oven . . . . .	28
WANL Oven . . . . .	28
Abar Oven . . . . .	28
Self-Heating Oven . . . . .	28
RADIATION TESTS - BABCOCK AND WILCOX TEST REACTOR . .	29
Radiation Experiment and Analysis . . . . .	29
Radiation Effects in Rhenium . . . . .	31
HIGH TEMPERATURE TESTS AT PANAMETRICS . . . . .	33
Velocity Measurements in Molybdenum . . . . .	33
Velocity Measurements in Rhenium . . . . .	33

Tests in Tungsten/Vacuum Environment Beyond 5000°R . . .	33
Self-Heating Tests in Carbon-Free Vacuum Beyond 6000°R	35
Tests in Graphite/Helium Environment to ~ 5000°R . . .	35
Self-Heating Tests in Graphite/Vacuum Environment to ~ 5000°R . . . . .	37
FIELD TESTS AT WANL - GRAPHITE/HYDROGEN ENVIRONMENT TO 5000°R . . . . .	38
Tests on June 28, 1967 . . . . .	39
Results in All-Rhenium Line . . . . .	39
Results in Tungsten Lead-in/Rhenium Sensor . . . . .	40
Summary . . . . .	42
Tests on June 30, 1967 . . . . .	43
Bare Sensors . . . . .	43
Sheathed Sensor . . . . .	45
Summary . . . . .	45
CONCLUSIONS . . . . .	46
Disadvantages of Ultrasonic Thermometers . . . . .	47
Advantages of Ultrasonic Thermometers . . . . .	47
RECOMMENDATIONS FOR FUTURE WORK . . . . .	50
APPENDIX I - EFFECT OF TEMPERATURE DISTRIBUTION ON THE ACCURACY OF THE ULTRASONIC TEMPERA- TURE MEASUREMENT . . . . .	51
Case I. Triangular Temperature Distribution . . . . .	52
Case II. Parabolic Temperature Distribution . . . . .	53
Temperature Profiling . . . . .	55
APPENDIX II - METHODS FOR MEASURING ULTRASONIC VELOCITY . . . . .	58
APPENDIX III - ULTRASONIC THERMOMETRY BASED ON AMPLITUDE MEASUREMENTS . . . . .	60
APPENDIX IV - METHODS OF TEMPERATURE MEASUREMENT	62
APPENDIX V - RADIATION TEST CAPSULE DESIGNS . . . . .	64
Unheated, Acoustically Monitored Capsule . . . . .	64
Heated, Monitored Capsule . . . . .	64
Gamma Plus Electrical Heating . . . . .	64
APPENDIX VI - ATTENUATION MEASUREMENTS . . . . .	68
ACKNOWLEDGMENTS . . . . .	71
REFERENCES . . . . .	72

# LIST OF TABLES

<u>Table</u>		<u>Page</u>
I	Torsional Wave Impedance ( $Z_{tors} = \rho V_T J$ , $J$ = polar moment of inertia) of Shapes Having Constant Total Area ( $\pi D^2/4$ ) . . . . .	11
II	Maximum Frequencies for Propagating Torsional Mode in Thin Wires . . . . .	14
III	Comparison of Some Carbides . . . . .	21
IV	Effect of Composition on Extensional Wave Sound Velocity in Carbides of Tungsten and Molybdenum at Room Temperature . . . . .	22
V	Comparison of Irradiated and Non-irradiated Rhenium Sensors vs Temperature . . . . .	32
VI	Comparison of Annealed and Non-annealed Re Sensors . . . . .	34
VII	Behavior of Rhenium During Cycling . . . . .	36
VIII	Results in All-Rhenium Line (June 28, 1967) . . . . .	40
IX	Comparison of Results in Tungsten Lead-in/Rhenium Sensors with Each Other and with Optical Pyrometer Readings . . . . .	41
X	Materials and Dimensions for Lines Tested June 30, 1967 . . . . .	43
XI	Comparison of Ultrasonic Temperatures with Thermocouple and Pyrometric Determinations for Tests in WANL Graphite/Hydrogen Oven, June 30, 1967 . . . . .	44

## LIST OF FIGURES

### Figure

- 1 Nuclear rocket engine
- 2 Ultrasonic thermometry system developed by Bell (8-11), Thorne (18) et al in Dragon Project
- 3 Pana-Therm Model 5000 system block diagram
- 4 Pana-Therm Model 5000 automatically measures transit time in sensor, from which temperature is determined
- 5a Typical ultrasonic line
- 5b Polarity of echoes for different ratios among  $Z_2$ ,  $Z_3$  and  $Z_4$
- 6 Shear wave characteristic impedance nomogram
- 7 Extensional wave characteristic impedance nomogram
- 8 Schematic of automatic measurement of pulse transit time in sensor, using Pana-Therm Model 5000
- 9 Young's modulus of elasticity vs temperature in Mo and Re
- 10 Velocity vs temperature in various metals and ceramics
- 11 Sound velocity measurements in Mo wire show annealing effects on initial heating run
- 12 Normalized extensional wave sound velocity in polycrystalline tungsten vs temperature
- 13 Normalized velocity vs temperature in two nonirradiated rhenium specimens
- 14 Room temperature echoes obtained with Pana-Therm Model 5000 from front and rear of 0.5 mm dia molybdenum sensor, flash butt welded to 1 mm dia molybdenum lead-in wire
- 15a Calculated echo amplitude ratio vs diameter ratio for lead-in and sensor of same material, for extensional and torsional waves
- 15b Calculated extensional wave echo ratio, for Ni-W, W-Re, and Re-W
- 15c Calculated torsional wave echo ratio, for Ni-W, W-Re, and Re-W
- 15d Flash butt welder for joining refractory metal wires, strip, etc.
- 16 Oscillograms show echo patterns from two adjacent 0.5 mm dia molybdenum sensors

## LIST OF FIGURES (Cont'd)

### Figure

- 35 Schematic of capsule for studying radiation effects at elevated temperatures
- 36 Representative oscillograms show echoes from front and rear of control and irradiated rhenium sensors
- 37 Confirming tests in second pair of control and irradiated rhenium sensors show reproducibility obtained in ultrasonic experiment
- 38 Normalized velocity vs temperature in control and irradiated rhenium specimens
- 39 Normalized velocity vs temperature in control and irradiated rhenium specimens
- 40 Temperature dependence of sound velocity in molybdenum, normalized to the room temperature annealed value
- 41 Tests on kinked rhenium wire in zirconium diboride coated tantalum sheath, heated in SRI oven
- 42 Self-heating apparatus to test survival of rhenium sensor in graphite felt
- 43 Oscillograms showing attenuation in bare rhenium sensor self-heated in graphite felt
- 44 Preliminary measurements of attenuation vs temperature, in several refractory wires, at  $f \sim 250$  kHz
- 45a Schematic of a resonance method for the measurement of the modulus of elasticity and damping
- 45b Schematic of attenuation measurement using multiple echoes in bar
- 45c Measurement of the Attenuation coefficient using differential path length
- 46 Oscillograms showing attenuation in self-heated tungsten wire
- 47 Identification of key items in WANL tests of June 28, 1967
- 48 Oscillograms of bare all-rhenium wire line tested June 28, 1967 at WANL
- 49 Oscillograms of echoes in 0.020" dia x 5" long rhenium sensor, welded to 0.030" dia centerless ground tungsten lead-in

## LIST OF FIGURES (Cont'd)

### Figure

- 17 Pulse echo experiment in Mo wire at 1 MHz
- 18 Modulus vs temperature in AUF and SA-25 graphites, after Faris, Green and Smith (1952)
- 19 Young's modulus versus temperature of a highly anisotropic graphite, after Johnson and Dull (1963)
- 20 Young's modulus vs temperature for representative commercial graphites, after Armstrong and Brown (1964)
- 21 Extensional wave velocity in CS
- 22 Extensional wave velocity in EY9
- 23 Reciprocal velocity vs temperature in several non-metallic materials
- 24 Reciprocal of extensional wave velocity vs temperature, in several refractory materials
- 25 Schematic of waveforms on ultrasonic line
- 26 Oscillograms for rhenium sensor of dimensions 0.5 mm diameter x 50 mm long
- 27a Schematic of movable reflector using dial indicator
- 27b Schematic of movable reflector using micrometer spindle
- 28 Two-point reflector for monitoring uniformity and quality of wire
- 29 Impedance vs temperature
- 30 Schematic of the 7000<sup>o</sup>R radiant heating source for testing thin wire ultrasonic thermometer in graphite environment (SRI oven)
- 31a Hot zone details of Abar oven
- 31b Ultrasonic, thermocouple and pyrometric temperature measurements in Abar oven
- 32 Photograph of lab set-up for ultrasonically testing self-heated wires
- 33 Trimetric view of BAWTR
- 34 Schematic of capsule with coiled foil for studying radiation effects at elevated temperatures

## LIST OF FIGURES (Cont'd)

### Figure

- 50 Oscillograms of 5" bare rhenium sensor, 0.020" dia flash butt welded to 0.030" dia tungsten lead-in wire
- 51 Oscillograms of 2" bare rhenium sensor 0.030" dia flash butt welded to 0.040" dia tungsten lead-in wire
- 52 Echoes from lead-in wires, after loss of sensors in WANL test, June 30, 1967
- 53 Comparison of temperatures in WANL graphite/hydrogen oven using ultrasonic, pyrometric and thermocouple means

## SUMMARY

The object of this program was to design, construct and test an ultrasonic system for determining localized temperatures to an accuracy of  $\pm 50^{\circ}\text{R}$  up to  $5000^{\circ}\text{R}$  for one hour in the core of a nuclear rocket engine. The present approach is based on the temperature dependence of sound velocity in solid materials. Temperature is determined by using a pulse-echo technique to measure the ultrasonic round trip transit time in a small sensor, e. g., a wire 0.5 mm (0.020 inches) dia x 50 mm (2 inches) long. More generally, the sensor diameter should be small compared to the wavelength of extensional waves, and of a length which is at least long enough for echoes from the front and rear of the sensor to be distinguishable at the ultrasonic test frequency. This minimum length turns out to be about one wavelength, for the typical video triplet pulse used herein.

The sensor is made of a material which is potentially compatible with the environment, and which exhibits a sound velocity sufficiently sensitive to temperature. This velocity may be the extensional wave velocity  $V_o = \sqrt{E/\rho}$  or the shear (torsional) wave velocity  $V_T = \sqrt{G/\rho}$  where  $E$  = Young's modulus,  $G$  = shear modulus and  $\rho$  = density.

After studying and/or testing various candidates including columbium, molybdenum, tantalum, tungsten and tungsten/rhenium alloys, some of the platinum metals, as well as graphite, carbides and several other non-metals, rhenium was selected for the sensor and then tested in wire form up to its melting point,  $6216^{\circ}\text{R}$ , in vacuum, and up to  $\sim 4966^{\circ}\text{R}$  (the rhenium/carbon eutectic) in a graphite environment. These tests established the velocity and preliminary attenuation characteristics of extensional waves in rhenium. These tests also established tungsten, rhenium and possibly tungsten/rhenium alloys as lead-in members. Tests were also conducted to determine the reflectivity and attenuation characteristics of various vacuum and pressure seals (feedthroughs), the effects of curvature, bends and long lead-in lengths up to  $\sim 30$  m ( $\sim 100$  ft), effects of immersion in water or various granulated, powdered or fibrous materials, etc. Soldering, brazing, welding and mechanical joining techniques were also compared experimentally, to determine the optimum methods for connecting segments of the ultrasonic wire line: transducer/lead-in/sensor.

Rhenium wires, irradiated to  $8.7 \times 10^{19}$  integrated thermal flux and  $2.6 \times 10^{19}$  integrated fast flux, were annealed and ultrasonically tested in vacuum (Abar oven with tungsten strip heater) up to  $\sim 4000^{\circ}\text{R}$ , together with non-irradiated rhenium control wires. Sound velocities were measured during heating and cooling. These control wire and irradiated wire velocity data exhibited no significant differences. From this it was concluded that structural or compositional radiation effects due to the above radiation levels were negligibly small with respect to the present ultrasonic thermometry application. The scatter in these velocity data corresponds to uncertainties in ultrasonically determined temperatures as follows: near  $2000^{\circ}\text{R}$ ,  $\pm 2\%$ ; near  $3000^{\circ}\text{R}$ ,  $\pm 1\%$ ; near  $4000^{\circ}\text{R}$ , less than  $\pm 1\%$ . In addition to comparing these control and irradiated wires up to  $\sim 4000^{\circ}\text{R}$ , two non-irradiated rhenium wires, one annealed and one not annealed, were tested in this same oven to  $\sim 5500^{\circ}\text{R}$ . Up to  $4000^{\circ}\text{R}$ , i. e., before the second wire became annealed, the two ultrasonically indicated temperatures differed as follows: near  $2000^{\circ}\text{R}$ ,  $10\%$ ; near  $3000^{\circ}\text{R}$ ,  $8.5\%$ ; near  $4000^{\circ}\text{R}$ ,  $2.5\%$ . Above  $4000^{\circ}\text{R}$ , annealing brought the two ultrasonically indicated temperatures into closer agreement: near  $5000^{\circ}\text{R}$ ,  $1/2\%$ ; near  $5350^{\circ}\text{R}$ , better than  $1/2\%$ .

Self-heated rhenium was cycled in carbon-free vacuum five times to  $5000^{\circ}\text{R}$ , including a total dwell of one hour at  $5000^{\circ}\text{R}$ , and exhibited excellent reproducibility. After cycling, specimens were tested up to the melting point,  $6216^{\circ}\text{R}$ .

A new instrument, the Pana-Therm Model 5000, was developed to automatically measure the transit time in the sensor to  $0.1$  microsecond. In field tests in a graphite/hydrogen environment at Westinghouse Astronuclear Laboratory (WANL), Re sensors survived to temperatures beyond  $4700^{\circ}\text{R}$ .

Disadvantages of ultrasonic thermometers, compared to thermocouples, include: more complicated electronics; certain limitations with regard to negotiating very sharp contours or passing through some types of feedthroughs; operators require some degree of specialized training; temperature is not measured at a point, but instead is averaged over the length of the sensor (in some situations, however, this can be an advantage); attenuation may limit allowable frequencies and lengths for lead-in and sensor; elastic hysteresis effects should be annealed out of sensors; applications experience is limited; and effects of long-term heating in a graphite/hydrogen environment have not yet been determined, with respect to ultrasonic propagation.

The present ultrasonic thermometer offers several advantages over thermocouples in the range  $\sim 3000$  to  $6000^{\circ}\text{R}$ . These advantages accrue partly because of the greater choice of ultrasonic sensor materials. The ultrasonic thermometer does not require electrical insulation at high temperature (no shunting error), and avoids calibration shifts which in thermocouples are due to diffusion of one leg into another, and preferential vaporization of certain alloy constituents. When one can replace two thermocouple wires, insulator and sheath with a single ultrasonic wire line, this one line can perhaps be substantially simpler, and/or larger in diameter than the thermocouple wires. In this case, a monolithic, more rugged ultrasonic sensor can sometimes be fabricated, with prospects of longer life, even in unfavorable environments. On the other hand, a single thin wire,  $\sim 1/2$  mm diameter, occupies less space than any practical thermocouple pair for use to comparable temperatures in extreme environments. The measurement of two or more temperatures with only one ultrasonic wire line is a unique advantage with respect to temperature profiling. Because of the marked changes in velocity and amplitude at phase changes, there may exist possibilities to use certain ultrasonic sensors in simple and automatic go/no go devices. Accuracy increases at elevated temperature.

## INTRODUCTION

### Statement of the Problem

One of the more important measurements required in nuclear rocket engine technology is the measurement of temperature. This measurement has proven to be extremely difficult because of the high temperatures involved ( $\sim 5000^{\circ}\text{R}$ ), because of compatibility problems with some of the materials involved (graphite and hydrogen) and because of the intense and sustained neutron and gamma fluxes. Additional difficulties stem from the high ambient noise, shock and vibration levels expected in some locations, the accuracy and response time required, possibility of temperature overshoot, high pressure, flow, accessibility and geometrical restrictions, etc.

Up to now, thermometry based on thermocouple developments has received the greatest attention, with respect to operating in the above nuclear rocket engine core environment. At this time, however, a number of thermocouple problems still remain unsolved.

### Historical Review and Background - Ultrasonic Thermometry

The concept of acoustically measuring temperature, based on the temperature dependence of sound speed, dates back to the last century(1). One might therefore expect acoustic thermometry to be a rather well developed and widely used technology at this time. Until recently, however, most of the acoustic techniques have been restricted to relatively low temperatures, i. e., below about  $1500^{\circ}\text{R}$ .<sup>\*</sup> There are at least two reasons for this restriction. First, available acoustic transducers could not operate above  $1500^{\circ}\text{R}$ . Second, the need for high temperature properties, especially temperature and other properties which could be measured acoustically, was not sufficiently established.

The need for high temperature data became more obvious during the last ten years as man began his entry into space. Also important, transducer materials with Curie points in excess of  $2500^{\circ}\text{R}$  are now becoming available. During this decade, new acoustic techniques have been developed to measure properties at elevated temperatures, for

---

<sup>\*</sup> A graph for converting from  $^{\circ}\text{R}$  to other scales appears on the inside rear cover.

example, elastic moduli, Poisson's ratio and phase transformations in solids, and transport properties (viscosity, thermal conductivity and diffusion) in gases. Determining these properties requires accurate temperature measurements since the properties must be specified as a function of temperature. Temperature measurements are also important for control purposes. At temperatures substantially in excess of  $3000^{\circ}\text{R}$ , the more common thermometry methods are not free of serious difficulties. At higher and higher temperatures, there is increased motivation to consider ultrasonic thermometry methods, especially those techniques that are being developed to determine temperature in solids up to at least  $5000^{\circ}\text{R}$ , and in gases up to  $\sim 30,000^{\circ}\text{R}$ .

Historically, the use of sound velocity in temperature determinations was demonstrated over ninety years ago(1). The earliest acoustic measurements of temperature were obtained in gases. In 1926, Anderson and Smith(2) reflected sound waves from exploding wires back into the discharge for measuring the temperature of the metal vapor. Sherratt and Griffiths(3) obtained specific heat measurements in CO up to  $3600^{\circ}\text{R}$  using an acoustic interferometer. This method could just as well be used in determining temperature. Apfel(4) used a resonant cavity method for temperature measurements to  $2300^{\circ}\text{R}$ . Suits(5) generated a sound wave ( $\sim 75\text{ kHz}$ ) by a spark discharge in air and passed it through a  $10,000^{\circ}\text{R}$  stabilized arc column. Livengood et al.(6) used an ultrasonic pulse technique to determine the temperature within an internal combustion engine. Carnevale et al.(7) used a technique similar to Livengood's in determining temperatures of plasma jets. Since about 1962 ultrasonic pulse techniques have been used in determining the temperature of gases heated by shock waves, combustion, induction (rf plasmas), conduction and convection (dc transfer arcs and ovens).

In solids, the active exploitation of sound velocity as an indicator of temperature appears to be due to Jaques of the A. E. E., Winfrith, England(8). Almost ten years ago, Jaques recognized the potential value to thermometry of ultrasonic thin wire techniques that had been developed by Bell(9). While Bell did not perform the earliest high temperature ultrasonic measurements in solids, his continuing work (10, 11) has significantly influenced ultrasonic thermometry using thin wire sensors. Bell's ultrasonic techniques are in some ways analogous to those of Frederick(12), who tested notched solid bars ("bulk" specimens) up to  $\sim 2300^{\circ}\text{R}$  some twenty years ago. During the past few years, Lynnworth and Carnevale(13, 14) have considered some

of the problems in ultrasonically measuring temperature averages and temperature distributions in large solid bodies ("bulk" specimens) wherein the specimen itself is the sensor material.

### Present Ultrasonic Approach

Ultrasonic measurements of temperature in a nuclear rocket engine may be applied in the core and also in the thrust chamber (Fig. 1). Our work on through-transmission gas thermometry is reported elsewhere (15-17), the most recent instrumentation development being the Pana-Therm Model 10K, which is designed to automatically measure transit time across the hot gas. Core thermometry, on the other hand, exploits the pulse-echo technique applied to a thin wire sensor.\* The rest of this report is devoted to the thin wire approach to ultrasonic thermometry in the core of a nuclear rocket engine.

Wire Sensors. There are several ultrasonic systems available for measuring high temperatures in solid wire sensors, based on the temperature dependence of sound velocity. One of these systems uses double pulses, and was developed ten years ago by Bell(9). Bell and his co-workers ultrasonically measured temperatures(18), phase changes (10), nitriding(10) and other effects(11) up to  $\sim 5000^{\circ}\text{R}$ . This system is manually operated, and typically uses sensors  $\sim 1$  to 3 mm diameter x  $\sim 150$  mm long.\*\* Measurement of temperature in the Dragon Project reactor (A. E. E., Winfrith, England) up to  $\sim 3200^{\circ}\text{R}$  has been a principal thermometry goal in this work.

In Bell's unique double-pulse system (Fig. 2) the high accuracy of transit time measurement depends upon the fact that the pulses are transmitted in alternate pairs (spacing:  $T + \delta$ ,  $T - \delta$ ). The average time interval  $T$  between pulses is adjusted until the end echo from the first pulse approximately coincides with the shoulder echo from the second pulse. The principal disadvantage of this otherwise excellent arrangement is the difficulty of automatically adjusting  $T$ . Despite the efforts of Bell and his colleagues in England, and our efforts at Panametrics, a practical method of automating Bell's double-pulse technique has not yet evolved.

---

\* While the experiments in this program were confined to sensors in wire form, there may be important advantages associated with other shapes, particularly tubular lines, as explained subsequently.

\*\* Techniques for using shorter sensors,  $\sim 20$  to 50 mm long, are currently under investigation in the Dragon Project.

For this reason we decided to depart from our original intention of automating the double-pulse unit (Fig. 2) and instead embarked on a single-pulse approach more amenable to completely automatic temperature measurement and control. As a result, a new instrument, the Pana-Therm\* Model 5000, was developed (Figs. 3, 4). The physical, acoustic and electronic principles associated with this instrument are discussed below.

---

\* "Pana-Therm" trademark applied for.

## BASIC PRINCIPLES

### Propagation of Elastic Waves in Solids

The properties of elastic waves in solids have been generally established and extensively studied. For homogeneous, isotropic Hookean rods of uniform cross-sectional area, it may be shown that the propagational velocities of shear and extensional waves are

$$v_T = \sqrt{\frac{G}{\rho}} \quad (1)$$

and

$$v_o = \sqrt{\frac{E}{\rho}} \quad (2)$$

where  $G$  and  $E$  are the moduli of shear and elasticity, respectively, and  $\rho$  is the density. Equation (2) holds only for "acoustically slender" rods. By this we mean that

$$\frac{d}{\lambda} \ll 1$$

where  $d$  is the rod diameter and  $\lambda$  is the wavelength at the excitation frequency.

### Wave Reflection and Transmission

A wave will generally be partially reflected and partially transmitted upon reaching a geometric discontinuity or a boundary between two different media. The amplitudes of the reflected and transmitted waves relative to the incident wave may be determined by solving the wave equation and imposing the conditions of continuity of force and velocity at the boundary. For a wave propagating from medium 1 to 2, the force amplitudes are given by

$$\frac{F_{\text{reflected}}}{F_{\text{incident}}} = \frac{r-1}{r+1} \quad (3)$$

$$\frac{F_{\text{transmitted}}}{F_{\text{incident}}} = \frac{2r}{r+1} \quad (4)$$

where  $r \equiv \frac{Z_2}{Z_1}$  (5)

is the ratio of mechanical impedances at the boundary. Expressions (3) and (4) hold for torsional as well as extensional waves. The mechanical torsional wave impedance is

$$Z_T \equiv \rho V_T J \quad (6)$$

whereas the mechanical extensional wave impedance is

$$Z_O \equiv \rho V_O A \quad (7)$$

where  $J$  is the polar moment of inertia and  $A$  is the cross-sectional area.

Equations (3) and (4) can be applied to wire lines containing more than one boundary. Consider, for example, the case of a two-junction line (Fig. 5a). Let the boundary 1-2 be such that  $Z_1 = Z_2$ , i. e.:  $r = 1$  ("matched" impedance). Applying Equations (3) and (4) one can determine the "echo ratio" defined as the ratio of the amplitude of the pulse reflected from the mismatched boundary 2-3 ( $Z_2 \neq Z_3$ ) to that of the pulse reflected off the end of the line and transmitted through the same boundary. The result is:

$$ER = \frac{4r}{1-r^2} \quad (8)$$

The relative polarity of the echoes generated at typical impedance discontinuities is illustrated in Fig. 5b.

The further concept of "characteristic" impedance is useful in matching lines of the same diameter but of different materials. The characteristic impedance of a material for shear (transverse or torsional) waves is

$$Z = \rho V_T$$

and for extensional waves is

$$Z = \rho V_o .$$

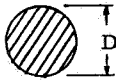
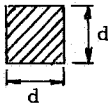
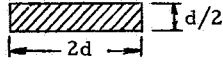
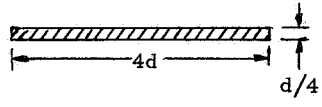
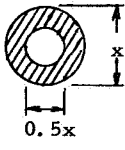
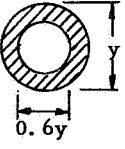
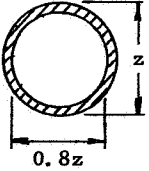
Values for both shear and extensional wave characteristic impedances for a number of materials are plotted in Figs. 6 and 7, on a log-log scale, where the loci of constant characteristic impedance are straight lines inclined at  $-45^\circ$  as shown.

The effect of shape on the torsional wave mechanical impedance is indicated in Table 1.

#### Methods of Generating Ultrasonic Elastic Waves in Wires

The most common methods of generating ultrasonic elastic waves in solids exploit the coupling between the electromagnetic and elastic fields inherent in certain materials at the molecular level; for example, the piezoelectric and magnetostrictive effects. With the piezoelectric effect, the coupling is between the electric and elastic fields, while magnetostriction involves the coupling between the magnetic and elastic fields. Choosing between piezoelectric and magnetostrictive transducers is principally determined by the test frequency and pulse shape required. For example, regarding frequency, below about 1 MHz, magnetostrictive

Table I. Torsional Wave Impedance ( $Z_{tors} = \rho V_T J$ ,  $J$  = polar moment of inertia) of Shapes Having Constant Total Area ( $\pi D^2/4$ )

Section	Area = $\frac{\pi D^2}{4}$	Polar Moment of Inertia $J$	Normalized Torsional Wave Impedance
	$\frac{\pi D^2}{4}$	$\frac{\pi D^4}{32} = 0.098 D^4$	1.00
	$d^2$ ( $d \approx 0.9 D$ )	$\frac{d^4}{6} = 0.103 D^4$	1.05
	$d^2$	$\frac{17d^4}{48} = .218 D^4$	2.23
	$d^2$	$\frac{257d^4}{192} = .825 D^4$	8.42
	$\frac{3\pi x^2}{16}$ ( $x = 2D/\sqrt{3}$ $\approx 1.15 D$ )	$\frac{15\pi x^4}{512} \approx 0.164 D^4$	1.67
	$0.16\pi y^2$ ( $y = 1.25 D$ )	$0.0855 y^4 \approx 0.208 D^4$	2.12
	$0.09\pi z^2$ ( $z = 1.67 D$ )	$0.0578 z^4 \approx 0.447 D^4$	4.55

transducers are usually preferred, where above 1 MHz, piezoelectric transducers are preferred. Reasons for this approximate limit on the maximum permissible excitation frequency in any given magnetostrictively-driven line include the capacitive coupling between turns in the transducer coil, coil size vs pulse width, number of turns that can be fitted close enough to the wire to couple efficiently, the skin effect in wires at the higher frequencies, and the increase in attenuation with frequency. Therefore, as a practical matter, excitation frequencies rarely exceed 1 to 2 MHz in magnetostrictively driven ultrasonic wire lines. Conversely, as the operating frequency of a piezoelectric crystal is raised above  $\sim 1$  MHz, the crystal can be vibrated to maximum permissible amplitudes using reasonable voltage levels - fraction of a kv to the low kv range. Below about 1 MHz, to drive the crystal to maximum amplitudes requires voltages substantially in excess of 1 kv.

Regarding pulse shape, video pulses are most easily launched using magnetostrictive transducers, while rf pulses are usually generated more efficiently by taking advantage of the resonant behavior of piezoelectric crystals. Now the condition  $\frac{d}{\lambda} \ll 1$  imposes an upper bound on the maximum permissible excitation frequency for extensional waves in a particular wire. In practice, it is found that the curve of velocity versus  $d/\lambda$  is sufficiently flat in the interval  $0 < \frac{d}{\lambda} < 0.1$  so that the dispersion in  $V_0$  may be neglected. If we then set  $d/\lambda = df/V_0 < 0.1$  we get  $f < 0.1 V_0/d$ .

For a typical value of  $V_0 = 5 \times 10^5$  cm/sec and a wire of 0.5 mm diameter,  $f$  should be  $< 10^6$  Hz to avoid dispersion of extensional waves. Hence, magnetostrictive transducers are emphasized in this work. (In determining the maximum usable frequency imposed by this equation, one must consider the minimum  $V_0$  to be encountered over the temperature range of interest. As the melting point is approached, velocity may decrease to only 75%, and possibly to only 50% of the room temperature value.) The simplicity achievable with video pulses, compared to rf pulses, also indicates that magnetostrictive transducers are preferred for the present work.

Regarding torsional waves (19), which are most commonly used in ultrasonic wire delay lines, one upper limit on frequency is imposed by the wire's diameter, shear modulus and density, according to the equation

$$f_c = \frac{5.136\sqrt{G/\rho}}{\pi d} = \frac{5.136}{\pi d} V_T \approx \frac{V_T}{r}$$

where  $f_c$  = maximum frequency\*  
 $G$  = shear modulus  
 $\rho$  = density  
 $V_T = \sqrt{G/\rho}$  = shear wave velocity  
 $d$  = wire diameter =  $2r$ .

Table II lists  $f_c$  in five metal wires, of 0.020 and 0.040 inch diameters. Since  $V_T$  decreases at the elevated temperatures of interest,  $f_c$  is actually determined by the sound velocity at the maximum temperature experienced by the wire. Near the melting point,  $V_T$  may be about half to three-quarters of the room temperature value.

Taken alone, Table II would suggest the use of wire diameters less than 0.020 in. to increase  $f_c$  as high as desired. However a second limit on maximum frequency is imposed by the scattering and absorption characteristics of the wire at high temperature. (Additionally, surface characteristics of some wires, such as Re, are better in larger diameter wires). Commercially available wire delay lines operate up to 2 MHz. It is unlikely that long refractory wires could operate at high temperature much above this practical frequency limit, and in fact lower frequencies,  $\sim 100$  kHz, appear necessary to overcome attenuation.

To construct a magnetostrictive transducer, a coil may be wound around a suitable wire, usually a nickel alloy (see Fig. 8). The coil is pulsed, thus producing an elastic strain in the wire. This effect is known as the "Joule" effect. In axially-magnetized wires, (19) an extensional wave then propagates along the wire, and is reflected and/or transmitted according to the geometry and materials used in the line. The reflected waves will generate a signal upon reaching the coil according to the inverse magnetostrictive effect, known as the "Villari" effect, namely: that a change in dimension will produce a change in magnetic field within the wire.

---

\*W. P. Mason, in Physical Acoustics and the Properties of Solids, p. 49, Van Nostrand, New York (1958), points out that by operating at a frequency  $f < 3f_c/4$ , one is assured that all the higher torsional modes will be highly attenuated and only the zero-order, dispersion-free mode will propagate over any appreciable distance.

Table II

Maximum Frequencies for Propagating Torsional Mode in Thin Wires

Wire Material	Melting Point*		$V_T$ at Rm Temp. in. / $\mu$ sec	$V_T/2$ in. / $\mu$ sec	$f_c$ at Rm Temp. MHz		$f_c/2$ MHz	
	$^{\circ}$ C	$^{\circ}$ R			d = 0.02"	0.04"	d = 0.02"	0.04"
W	3410	6630	0.113	0.057	9.4	4.7	4.7	2.4
Re	3180	6216	0.113	0.057	9.4	4.7	4.7	2.4
Ta	2996	5884	0.080	0.040	6.7	3.4	3.4	1.7
Mo	2610	5190	0.132	0.066	11.0	5.5	5.5	2.8
Cb	2415	4839	0.080	0.040	6.7	3.4	3.4	1.7

Application to Acoustic Thermometry

Eqs. (1) and (2) have been used to determine the moduli of shear and elasticity as functions of temperature in wires, rods, tubes and ribbon or strip materials at known temperatures (see Fig. 9). In this way, it is possible to calculate all of the elastic constants of a crystal by measuring the longitudinal and shear wave velocities along variously oriented crystal cuts(20). Determinations of phase transitions and eutectic points have also been accomplished in this manner. The object of the present program, however, was to determine temperatures from measurements of the normalized transit time in the sensor (reciprocal of normalized velocities  $V_T$  or  $V_O$ ) after first establishing the velocity-temperature characteristics (see Figs. 10-13).

While feasibility of using both shear waves and extensional waves has been demonstrated, most of the work during this program has

\* M. R. Nadler and C. P. Kempter, J. Chem. Phys. 64, 1468-1471 (1960).

been devoted to extensional waves which we shall almost exclusively refer to henceforth.

Consider the transmission line shown in Fig. 5a, and let the boundary 1-2 be perfectly matched, i. e.:  $Z_1 = Z_2$ . Assuming an ideal (reflectionless) damping termination, the oscilloscope display will consist of the driving "main bang" or "interrogation" pulse and two large echoes, one due to reflection from the boundary 2-3 and the other due to reflection from the end of the line. The time interval between these echoes is an indication of the wave velocity  $V_0$  in section 3 for known sensor length  $L$ . The remaining multiple echoes are due to the "ringing" of the last section in the line, and occur at regular intervals but with decreasing amplitude (Fig. 14). The echo ratio of the two main echoes is given by Eq. (8) and is plotted in Fig. 15a, b, c as a function of diameter ratio for both torsional and extensional waves.

Section 3 is known as the sensor, insofar as it is the temperature sensing element; section 1 is the transducer wire which is made of suitable magnetostrictive material; finally, the "lead-in" section 2 provides for accessibility in a given installation, and is chosen on the basis of ultrasonic propagation characteristics and materials compatibility.

A typical line would consist of a Remendur transducer,  $\sim 0.050$  in. diameter x 1 to 10 in. long, a tungsten lead-in,  $\sim 0.040$  in. diameter x 1 to 10 ft long, and a rhenium sensor,  $\sim 0.030$  in. diameter x 1 to 10 in. long.

Sections may be connected to each other by mechanical means (screwed or crimped together), by chemical means (adhesives, cements) or most commonly, by metallurgical means (soldering, brazing, welding). We have found flash butt welding to be the fastest technique, but this principal advantage is partly offset by joint embrittlement due to recrystallization at welds involving refractory metals (especially W). Brazing (silver soldering) is appropriate at the transducer/lead-in joint, and avoids recrystallization. To avoid recrystallization at the lead-in/sensor joint and attendant handling and installation problems, these two sections can be made of the same material, the required discontinuity being provided by a bend, kink or diameter change. In service above  $\sim 4000^\circ\text{R}$ , of course, the sensor and part of the lead-in would recrystallize anyway, and so avoiding recrystallization during assembly is not of major importance. Accordingly, we use flash butt welding almost exclusively for all metallic wire joints. The welder used in this work is shown in Fig. 15d. The theoretical echo ratios (Fig 15a, b, c) were essentially confirmed experimentally, for joints that were flash butt welded.

Bends, Kinks. Just as a wave is generally partially reflected and partially transmitted at an abrupt change in cross-sectional area, the same situation will hold at a sharp bend (radius of curvature  $\ll$  wavelength) or kink in a wire of uniform cross-section. The reason is that the kinked portion of the wire will be subjected to both extensional and lateral (flexural) vibrations, thus exhibiting an abrupt change in impedance to the incident wave. A kink angle of  $\sim 45^\circ$  gives extensional wave echoes of approximately equal amplitudes while an angle of  $90^\circ$  will produce virtually complete reflection owing to the impedance discontinuity (see Fig. 16). One can also see that the projected area of the bent portion, as seen looking down the straight portion, represents a reduced cross section, and so the pulse is inverted at the bend, as well as delayed an additional increment, depending on the discontinuity.

### The Sensor

The material, shape and size of the sensor will depend upon one or more of the following: the environment in which the sensor is required to operate, survival time required, the desired accuracy of the temperature measurement, and the time resolution of the supporting equipment.

An approximate error estimate in the temperature measurement may be arrived at as follows:

Let  $t$  be the time interval between sensor echoes at temperature  $T$ . Then  $t = 2L/V_o(T)$ . For a change in temperature from  $T_1$  to  $T_2$ , the change in transit time is

$$t_1 - t_2 = 2L \left[ \frac{1}{V_o(T_1)} - \frac{1}{V_o(T_2)} \right], \text{ and } \therefore \Delta t \equiv t_1 - t_2 = - \frac{2L\Delta V}{V_o(T_1) V_o(T_2)}$$

( $\Delta t$  is negative for  $T_2 > T_1$ )

$$\text{If } \frac{\Delta V}{V_o(T_1)} \ll 1, \text{ then } \Delta t = - \frac{2L\Delta V}{V_o^2(T_1)}$$

or

$$L = - \frac{1}{2} \frac{\Delta t V_o^2(T_1)}{\Delta V} \quad (9)$$

For rhenium at  $\sim 2500^{\circ}\text{K}$  ( $4500^{\circ}\text{R}$ ) the data presently available is:

$$V_o \approx 3.6 \times 10^5 \text{ cm/sec} ; dV_o/dt \approx -70 \text{ cm/sec } ^{\circ}\text{K}$$

$\therefore$  for an accuracy of  $\pm 1\%$ , i. e.: a temperature uncertainty of about  $25^{\circ}\text{K}$  (or  $\pm 50^{\circ}\text{R}$ ),

$$\Delta V \approx -70 \times 25 = -1750 \text{ cm/sec}$$

So, from (9), taking  $\Delta t = 0.1$  microsecond (resolution of present instrument),

$$L = \left(\frac{1}{2}\right) \frac{(0.1 \times 10^{-6}) (3.6 \times 10^5)^2}{1750}$$

$$= 3.6 \text{ cm}$$

$$= 1.4 \text{ in.}$$

The desirability of having the shortest possible sensor wire is, of course, quite evident in view of the temperature gradients that may exist in a long wire; in other words, the shorter the sensor wire, the more localized the temperature determination can be. However, as was shown above, the minimum sensor length is limited by the pulse or time resolution of the supporting equipment. This restriction may be overcome to a certain extent by observing the multiple echoes

(Fig. 14) or by coiling the sensor\* to give a greater acoustic length (see Fig. 17) or using a slower wave, such as the torsional wave. The torsional wave would yield  $\pm 50^\circ\text{R}$  accuracy or 1% at  $5000^\circ\text{R}$ , in a 1 in. Re sensor. (Localized temperature may also be determined despite relatively long sensors by measuring the difference in temperature between neighboring sensors - see Appendix I.)

In addition, it may be observed that while acoustic attenuation at high temperatures may appear at first sight to favor short sensor lengths, in some cases a predetermination of the attenuation characteristics of the sensor material might serve as an approximate cross-check on the temperatures derived from the velocity measurements.\*\* Two other methods of determining temperature based on amplitude measurements, as opposed to transit time measurements, are indicated in Appendix III.

The selection of the proper sensor material is not only based upon the temperatures to be measured and the steepness of the  $V_o(T)$  function to yield sensitive measurement, but is also critically dependent upon the environment in which the sensor is required to operate. Thus the operating environment introduces metallurgical problems relating to the compatibility of the sensor, either bare or

---

\* In a coiled sensor, there are several restrictions on how tightly the coil may be wound. One limit is mechanical, and is simply determined by the wire's brittleness or ductility at the winding temperature. Another limit is due to velocity dispersion (Brockelsby et al. Ref. 19, pp. 126-129). The outer part of the coiled wire is in tension, and so exhibits a different velocity than the inner part, which is in compression. (It might be possible, however, to reduce stress induced dispersion for transverse shear waves by twisting the wire before coiling, if the shear wave polarization follows the twist - see L. C. L., Materials Evaluation, 25, (12) (Dec. 1967). Finally, if the coil's radius of curvature is smaller than at least one wavelength, the pulse is scattered and highly attenuated. In this contract, the available room dictated a small coil radius, requiring a frequency much above 1 megahertz, but this high a frequency would obviously be attenuated due to absorption, even if the curvature per se were no longer a problem.

\*\* Use of longer sensors permits operation at proportionately lower frequencies. If  $\alpha = \text{const.} \times f^n$ , where  $n > 1$ , the term  $e^{-\alpha x}$  can be reduced by increasing  $x$  while decreasing  $f$  in the same proportion.

protected by packing material, coating, metallizing (21), a sheath or combinations of these.

It is now appropriate to briefly review potential sensor materials such as graphites, carbides, polycrystalline metals and single crystal metals.

Graphites. To minimize or avoid reactions with the graphite core, graphite is a natural first choice as a candidate sensor material. In this program, however, we did not test graphite ultrasonically, for the following reasons. Faris, Green and Smith's early work in AUF and SA-25 graphites (22) (Fig. 18), Johnson and Dull's more recent work (23) in an unspecified "highly anisotropic graphite" (Fig. 19), and Armstrong and Brown's recent work (24, 25) in AUC, G and H4LM graphites (Fig. 20), indicate that sound velocity varies considerably from sample to sample, and that the velocity is often insensitive to temperatures over wide ranges, and also two different temperatures yield the same velocity (Figs. 19, 20). Bell, Hub and Smith (8) tested CS and EY9 graphites up to about 1100°R and observed hysteresis effects which they attributed to water absorption (Figs. 21, 22). Additional hysteresis effects are to be expected near 5000°R due to creep and annealing processes. Available Young's modulus data\* for pyrolytic graphite (PG) indicates that sound velocity is not very sensitive to temperature in the range 3000 to ~4500°R. Between ~4500 and 6000°R, however, it appears that PG would be a sensitive ultrasonic thermometer sensor.

Other available graphite forms, particularly cloth-like or rope-like filaments, can be produced in ~1/8 inch diameters up to several feet long. Such filament structures typically exhibit strength and modulus which increase up to ~5000 to 6000°R, and then decrease at higher temperatures. Thus, the same velocity is found at two temperatures, making such forms somewhat undesirable as sensors for use over broad temperature extremes, because of the ambiguity.

---

\* Lockheed Missile & Space Co., Pyrolytic Graphite Data Book, LMSC 288186 (June 26, 1961). Data also in Fig. 16, p. 21 in High Temperature Materials, Inc. (Union Carbide Corp., Carbon Products Div.) PG data sheet (Oct. 6, 1961).

However, by using the filament-type graphite\* as a lead-in, PG as the sensor, and carbonaceous cement as the bonding agent between the two, a composite line might be formed having potential thermometry capability up to  $\sim 6000^{\circ}\text{R}$  in a graphite environment.

Carbides. After graphite, the second choice material likely to withstand the graphite environment would appear to be one in which the carbide reaction has gone to completion, i. e., a carbide.

Unfortunately, the task of fabricating a carbide which will remain stable at  $5000^{\circ}\text{R}$  is difficult. Moreover, reliable modulus data is meager and scatter in the data even at room temperature is substantial (Young's modulus in WC has been reported ranging from 75 to 103 million psi) (26). Although the carbides generally have rather high melting points, Table III shows that the maximum useful temperature in the present carbon/hydrogen environment is generally below  $5000^{\circ}\text{R}$ .

Carbides tend to be unstable near  $5000^{\circ}\text{R}$ . Depending on temperature, pressure and hydrogen flow conditions, the net reaction may be either decarburization or formation of a higher carbide. The effect of composition on sound velocity is illustrated in Table IV for W,  $\text{W}_2\text{C}$ , WC and C (diamond), calculated at room temperature from Köster and Rauscher's data (27). Velocities in  $\text{MoC}$  and  $\text{Mo}_2\text{C}$  were also calculated from Shaffer's data (26). Uncertainties in composition as severe as these could lead to temperature errors of thousands of  $^{\circ}\text{R}$ . Even in a given carbide there are uncertainties. For example, in  $\text{W}_2\text{C}$ , Schwarzkopf and Kieffer (28) point out that the transformation from  $\beta - \text{W}_2\text{C}$  into  $\alpha - \text{W}_2\text{C}$  occurs near  $4800^{\circ}\text{R}$ . The lattice structure of the modification stable at high temperatures had not been fully established at the time of that writing (1953).

Another problem relevant to a carbide sensor is the difficulty of handling pure carbides in lengths greater than about five diameters. Pure carbides are also characterized by poor thermal shock resistance.

In the case of near stoichiometric UC, sound velocity is not sensitive to temperature over the range 500 to  $2000^{\circ}\text{R}$ , and attenuation

---

\* "Thornel 40," for example, is a graphite yarn with a room temperature modulus of elasticity of 40 million psi (Carbon Products Div., Union Carbide Corp., New York).

Table III

Comparison of Some Carbides\*

<u>Carbide</u>	<u>M. Pt., °R</u>	<u>Reactivity/Mechanical Properties</u>	<u>Max. Use Temp. in Graphite/Hydrogen Environment, °R</u>
MoC	5100-5250	Decomposes to Mo <sub>2</sub> at 2100°R	2100
Mo <sub>2</sub> C	4800-5400	Decarburizes rapidly in H <sub>2</sub> above 3200°R	3200
TaC	7200-7300	Attacked by H <sub>2</sub> above 3200°R	3200
WC	5200-5700	Decarburizes above 3200°R in H <sub>2</sub>	3200
W <sub>2</sub> C	5400-5700	Decarburizes in H <sub>2</sub> , hydrocarbons above 5000°R	5000 (?)

\* Data and remarks extracted from Shaffer (Ref. 26). See also Ref. 43, 29.

increases above 2000°R, in a nonreproducible manner.\*\*

In summary, the presently available carbides, despite attractively high melting points, at this time appear generally unsuited for reliable use from 1000 to 5000°R, as a thin wire temperature sensor.

Polycrystalline Metals. Polycrystalline refractory metals are readily available in wire form in relatively unlimited lengths, except for Re, which until welded, is typically available in lengths of ~ 5 ft in diameters of ~ 0.040 inches. The Dragon Project concluded that Re was the preferred sensor material, and our results to date confirm this.

\*\* G. Ervin, Jr., Atomics International, private communication (August 17, 1966). See Atomics International Quarterly Prog. Rpt. 7551-4539, p. 2 (April 6, 1964).

Table IV

Effect of Composition on Extensional Wave Sound Velocity  
in Carbides of Tungsten and Molybdenum at Room Temperature\*

<u>Material</u>	<u>Young's Modulus, psi</u>	<u>Density, g/cc</u>	<u>Extensional Wave Sound Velocity in. /<math>\mu</math> sec</u>
W	$59 \times 10^6$	19.3	0.181
W <sub>2</sub> C	$62 \times 10^6$	17.3	0.195
WC	$104 \times 10^6$	15.8	0.265
C (diamond)	$115 \times 10^6$	3.5	0.592
Mo	$46 \times 10^6$	10.2	0.214
Mo <sub>2</sub> C	$32.5 \times 10^6$	8.9	0.193
MoC	$29 \times 10^6$	7.6**	0.197

\* Velocity calculations based on data in Shaffer (Ref. 26) and Köster and Rauscher (Ref. 27).

\*\* (Pycnometer density = 8.5-8.8 g/cc).

In preliminary tests conducted with 0.030" dia Re wire in intimate contact with graphite at elevated temperature, it was found that on returning to room temperature, velocity was virtually unaffected by carbon diffusion. Tests have not yet been run for periods of one hour at temperatures just below the eutectic. The Re-C phase diagram (30) shows 4.5 at. % carbon in the range 3500-4000°R, increasing to 11.7 at. % carbon at the reported 4966°R eutectic. To retard carbon diffusion into rhenium, at temperatures over 4966°R, coating, sheathing or sheathing plus flushing may be required.

Single Crystal Metals. Single crystal metals offer several potential advantages over polycrystalline metals: (1) No grain reorientations during thermal cycling; (2) More linear velocity/temperature curve; (3) No grain boundaries for carbon attack, slip, etc. Disadvantages are: (1) Length limited; (2) Diameter limited; (3) Machining O.D. is difficult; (4) Cost is high, ~\$100 to \$200 per inch (however, use of short single crystal sensor welded to a polycrystalline lead-in would be reasonable in cost).

Comparison of Materials Based on Velocity. Figs. 23 and 24 compare the reciprocal velocity in a number of materials to the extent that data are available. The slope of these curves gives the sensitivity to temperature. Since the Pana-Therm Model 5000 measures transit time to  $\pm 0.1 \mu\text{sec}$ , the curves can be used to determine the sensor length required for  $\pm 50^\circ\text{R}$  resolution (note that 1 inch sensor yields 2 inch path).

The transit times shown are for extensional waves. These times would approximately double for shear waves, i. e., sensor length could be halved, for a given sensitivity.\*

---

\* A better approximation for the ratio of transit times can be obtained if Poisson's ratio  $\sigma$  is known:

$$\frac{t_{\text{shear}}}{t_{\text{ext}}} = \frac{V_o}{V_T} = \sqrt{2(\sigma+1)}.$$

This function is plotted in McMaster, R. C. (ed.), Nondestructive Testing Handbook, Vol. II, Sect. 43, page 11, Ronald Press, N. Y. (1959).

## EXPERIMENTAL APPARATUS AND TECHNIQUES

### Electronics

Pana-Therm Model 5000. To clarify the details of transit time measurement in the Pana-Therm Model 5000 (Figs. 3, 4, 8), consider a typical basic wire line and the associated waveshapes (Figs. 25, 26).

The "main bang" pulse is applied to the transmitter coil T 120 times per second. Elastic pulses, generated magnetostrictively, propagate away from T. For simplicity, assume that the pulse going to the left is fully absorbed in the pad (silicone rubber, for example). The pulse going to the right induces a voltage (1) in receiver coil R as it passes through R. This pulse continues to the right, and is partly reflected at the junction with the lead-in (2) but mostly transmitted toward the sensor. If there is a pressure seal, another small echo (3) arises. The pulse continues to the sensor, generating the important echoes (4) and (5). Between these echoes, time is to be measured automatically.

To avoid false measurements due to echoes such as (1), (2) or (3), a suppressor gate is adjusted by means of a 3-step capacitance range switch and a parallel potentiometer such that the RC time constant of a "delay flop" prevents any pulses within a predetermined interval from being "counted."

To avoid false measurements due to noise present after the suppressed interval, an amplitude threshold adjustment is set so that pulses below, say, 2 volts, are neglected. That is, low level noise pulses cannot trigger the counting circuits.

Having adjusted the RC time constant as indicated schematically by the dashed line between echoes (3) and (4), and having adjusted the electro-acoustic system such that echoes (4) and (5) are above the noise level ( $S/N$  usually  $> 2$ ),  $t$  is measured as follows. Consider the expanded wave diagram and a cycle of 12 pulses. Of these 12, the first two are steered such that the amplitudes  $A_4$  and  $A_5$  of echoes (4) and (5) are sampled and held. The third pulse in the cycle of 12 now travels down the line, yielding echoes (4) and (5) again. During the time  $t_4$  when the amplitude of echo (4) exceeds a preset percentage of  $A_4$ , say 70.7% of  $A_4$  (3 db points), every other output cycle of a 10 MHz

oscillator is counted, resulting in a stored count of  $t_4/2$ . Likewise, during the time  $t_5$  that echo (5) exceeds 70.7% of  $A_5$ , every other output cycle is counted, adding an amount  $t_5/2$  to the accumulated count. During the interval  $t_{45}$  between (4) and (5), the oscillator output is directly counted, adding  $t_{45}$  to the count. This pattern is then repeated. Thus, after the sample and hold pulses, the next 10 driving pulses, 3, 4, 5.....12, each raise the count by an amount  $t$  given by

$$t = \frac{t_4}{2} + t_{45} + \frac{t_5}{2} .$$

By accumulating 10  $t$  and "dropping the last digit," i. e., dividing 10  $t$  by 10, the resultant count is  $t$ . The reason for first accumulating  $t_4/2 + t_{45} + t_5/2$  ten times and then dividing by ten is to improve the accuracy over a single measurement of  $t$  by roughly  $\sqrt{10}$ . This "averaging" process reduces errors due to random noise.

Note that  $t$  is effectively measured between the "centerline" of the upper portion of echoes (4) and (5). This measurement is superior to measurements between fuzzy "leading edges" or between the rather flat "peaks."

As an example of the time intervals involved in a 2 inch rhenium sensor,  $t$  is about 20  $\mu\text{sec}$  at room temperature, and about 30  $\mu\text{sec}$  at 5500°R. For echoes typically 3  $\mu\text{sec}$  wide at their baseline, and about 2  $\mu\text{sec}$  wide at their half power (3 db) points,

$$t_4 \approx t_5 \approx 2 \mu\text{sec}$$

$$t_{45} \approx 18 \text{ to } 28 \mu\text{sec} .$$

Use of a 10 MHz oscillator permits each of the intervals  $t_4/2$ ,  $t_{45}$  and  $t_5/2$  to be measured to the nearest cycle, or 0.1  $\mu\text{sec}$ . The maximum accumulated error for any one pulse is 0.3  $\mu\text{sec}$ . By dividing the total count by ten, the error is cut down to about 0.3/ $\sqrt{10}$   $\mu\text{sec}$ , or < 0.1  $\mu\text{sec}$ . The actual errors in any particular case depend on the signal to noise ratio. Due to nonlinearity in the velocity/temperature

curve, sensitivity varies, with accuracy improving as temperature increases.

The choice of 3  $\mu$ sec driving pulses is a compromise. For example, higher frequencies yield better resolution (shorter sensor) but higher attenuation. Lower frequencies yield poorer resolution, but stronger echoes and less attenuation. The 3  $\mu$ sec width has been generally used to date, for sensor lengths of  $\sim 1$  to 2 inches heated to  $\sim 6000^\circ\text{R}$  in vacuum. When long portions of the lead-in are also at high temperatures, pulse widths on the order of 10  $\mu$ sec or longer may be required.

#### SPECIFICATIONS

Automatic Readouts: Digital: Transit Time, 0.1 to 999.9  $\mu$ sec digital display presents average of 10 measurements.

Analog: Meter display, dc output to recorder, 0 to 100 mv across  $200\Omega$  proportional to transit time.

Accuracy:  $\pm 0.1 \mu\text{sec}$

Response Time: 0.1 sec

Pulse Repetition Frequency: Manual, 60, 120 pps

Ultrasonic Pulse Width: 1, 2 or 3  $\mu$ sec, or externally adjustable beyond or between these limits.

Transducer: Magnetostrictive

Instrument Size: 3-1/2" x 17" x 19"

Weight: 20 lbs.

Power Requirements: 105-130 volts; 3 amperes

Mounting: Rack Mountable, or Bench Model with Carrying Handle

Number of Sensors: Function of commutation and response time requirements.

In this contract, the Pana-Therm Model 5000 has been used to measure transit times which are normalized to the room temperature value. This normalization avoids the need for accurate measurement of sensor length. Measurement of absolute velocity, as distinct from relative (normalized) velocity, is discussed in Appendix II in connection with Figs. 27 and 28.

Because of potential academic interest, we mention the possibility of using the Pana-Therm Model 5000, or other pulse generator and receiving equipment, to determine temperature based on amplitude measurements. This technique, while not demonstrated in this program, is explained in Appendix III (see Fig. 29).

## High Temperature Sources

Appropriate high temperature sources are required to conduct experiments and simulation studies. Consideration of the total anticipated environment shows that this unique combination of parameters - temperature, pressure, materials, geometry, fluxes, noise, etc. - appears to be obtainable only in a nuclear rocket engine. Ultimately, then, tests may be conducted in this particular high temperature source.

Until nuclear rocket engine tests are justified, however, it is necessary to study the ultrasonic thermometer system in a variety of sources providing one or more of the principal environmental ingredients.

In this program, the following high temperature sources were considered:

1. Graphite heater plus vacuum or helium or argon atmosphere (SRI).
2. Graphite heater plus hydrogen atmosphere (WANL).
3. Muffle tube ovens plus vacuum or inert atmosphere (Hevi-Duty, Panametrics).
4. Tungsten filament plus vacuum (Abar).
5. Electron beam heating of sensor.
6. Induction heating of sensor.
7. Induction heating of susceptor.
8. Torch heating of sensor.
9. Plasma heating of sensor.
10. Gamma heating (Babcock & Wilcox, NASA-Plumbrook)
11. Gamma plus electrical heating.
12. Self-heating of sensor.

Generic comparisons of the advantages and disadvantages of most of these source types appear in tables compiled by Rose and Metcalfe (31). Additional comparisons are tabulated in NASA CR-789 (32).

In this program, experiments were conducted using the sources listed as Items 1, 2, 3, 4, 7, 8 and 12. We confine the present discussion to those sources wherein significant tests were run, namely, Items 1, 2, 4 and 12. These four are henceforth denoted the SRI, WANL, Abar and self-heating ovens, respectively. Discussion of laboratory tests in these sources appears in later sections of this report.

SRI Oven. This oven has been fully described by Pears (33) of the Southern Research Institute, Birmingham, Ala. Panametrics built a slightly modified version of the original model. This oven has a hot zone  $\sim 1$  inch dia  $\times$  2 inches long, large enough to test wire sensors while simultaneously measuring temperature by thermocouple and pyrometric means (Fig. 30).

WANL Oven. This oven has been fully described by Ferris, Malarkey and Zellner (34) of the Westinghouse Astronuclear Laboratory, Large, Pa. The WANL oven permits several ultrasonic sensors to be tested side by side in a graphite/hydrogen atmosphere, with simultaneous thermocouple and pyrometric measurements (see section on Field Tests at WANL).

Abar Oven. This vacuum oven, Abar Corporation Model C3T2-Lab, utilizes a folded tungsten strip, 1 inch wide  $\times$  0.010 inches thick, as the heater element (Fig. 31). Due to electrode connections and shield placement, the hot zone is nonuniform. Temperature distribution, however, appeared to be reasonably reproducible, and so this oven was used to determine the effects of radiation on sound propagation in rhenium (see section on Radiation Tests).

Self-Heating Oven. This oven usually consists of a chamber surrounding the sensor. The sensor is heated by passing ac or dc current through it. Temperature distribution may be calculated by the methods of Jain and Krishnan (35). Temperature may be measured by pyrometer, thermocouple and resistivity techniques. In some cases, tables or nomograms are available for estimating the temperatures produced by various currents in different diameter wires (tungsten, rhenium, nichrome, etc.) (36, 37). This type oven was used to test wires from  $\sim 1$  in. long to 2 ft long, to establish preliminary attenuation data to  $\sim 5000^{\circ}\text{R}$ , and to determine effects of graphite on sound velocity. One arrangement is shown in Fig. 32.

Temperature was measured in the above ovens using routine thermocouple and pyrometric means. Additionally, four other methods were considered for possible future calibrations in the laboratory. Discussion of these methods is briefly summarized in Appendix IV (see also Ref. 37-40).

## RADIATION TESTS - BABCOCK AND WILCOX TEST REACTOR

Calculations of expected radiation effects in Re, W, Ta, Mo, Cb and their alloys showed that the intensities and dosages of interest to the present contract would probably produce no significant changes in the velocity/temperature curves. Details of these calculations are appended to our Second Monthly Progress Report (July 26 - August 25, 1965, Conf.).

To determine experimentally the magnitude of radiation effects, a number of possible radiation experiments were considered. Experimental considerations principally involved capsule designs appropriate for testing in the Babcock and Wilcox (Lynchburg, Va.) test reactor (Fig. 33). The capsule design used in the B & W test was a simple capsule containing many wire samples. These wires were irradiated at room temperature. Sound velocity was measured in the irradiated wire, and results were compared with velocity in a control wire. The capsule was fabricated of commercially pure aluminum, 6 inches long x  $\sim 1\frac{3}{4}$  inches diameter, welded closed at both ends. The flux was monitored by conventional Al-Co and Fe wires placed within the capsule. Other capsule designs, however, are discussed in Appendix V because of possible interest in future tests (Figs. 34, 35).

### Radiation Experiment and Analysis

On February 16, 1966, Babcock and Wilcox personnel visited Panametrics, Inc., to review radiation effects, handling hazards, and the conduct of the radiation test. Independent calculations performed by Babcock and Wilcox and by Panametrics, Inc., indicated that radiation effects and handling hazards would be minimum in pure grades of Re, Mo and Cb (these three materials, incidentally, are all ductile at room temperature, making it convenient to coil relatively long lengths into the test capsule). Isotopes with long half-lives and high activity render Ta and W more difficult to handle. It was agreed that several W-Re alloys would be tested. Use of alloys would appear to depend on the behavior of their separate constituents, i. e., if W and Re are acceptable individually, their alloys should likewise be acceptable, from the radiation standpoint.

The calculations indicated that after irradiation, pure Cb, Mo and Re could be safely handled, without shielding, in 0, 30 and 60 days,

respectively. W, Ta and the W/Re alloys could be ultrasonically tested in a hot cell, if required in subsequent studies.

Some consideration was also devoted to the platinum metals (42), notably osmium, ruthenium and iridium. There is some experimental evidence\* of solid state reactions with carbon, leading to a lowering of these melting points substantially below 5000°R, except in the case of osmium (43). Osmium is otherwise unfavorable because it is generally considered mechanically unworkable.

From the above considerations, it was decided to irradiate, at room temperature, thirty encapsulated samples of seven different refractory elements and alloys.\*\*Babcock and Wilcox personnel analyzed the iron and cobalt-aluminum flux wires which were placed in the capsule. The results of the analyses are as follows: integrated thermal flux was  $8.7 \times 10^{19}$  and integrated fast flux was  $2.6 \times 10^{19}$ . The fast flux is defined as being above 1 Mev in energy and is based on a  $\text{Fe}^{54} (n, p) \text{Mn}^{54}$  cross section of 95 mb. The thermal flux is defined at the 2200 m/s level. A cadmium correction has been applied for the thermal flux.

The capsule was opened in a hot cell approximately one month after pulling. Ta, W, and W-Re alloys are being stored at Babcock and Wilcox. Initial qualitative radiation measurements at Babcock and Wilcox showed traces of Co and Ta in Cb and Mo, and other impurities in Re (~330 millicuries). These results, not wholly unanticipated, delayed the return of irradiated Cb, Mo and Re until November, 1966. Subsequently, however, we conducted high temperature ultrasonic tests in the Abar oven on short specimens of irradiated Re wires (~2 inches long) instead of testing complete lengths at once. These test results were compared with our own preirradiation tests.

\* According to Nadler and Kempter (43) (See also footnote on p. 43.):

Metal	Melting Point		Eutectic with Carbon	
	$^{\circ}\text{C}$	$^{\circ}\text{R}$	$^{\circ}\text{C}$	$^{\circ}\text{R}$
Os	3000	5892	2732	5409
Ir	2442	4887	2296	4624
Ru	2250	4542	1942	3987

\*\* Wires of the following materials were irradiated: W, Re, Ta, Mo, Cb, W-5% Re and W-26% Re. Lengths ranged from several inches to 10 ft.

## Radiation Effects in Rhenium

Rhenium wires, previously irradiated to  $8.7 \times 10^{19}$  integrated thermal flux and  $2.6 \times 10^{19}$  integrated fast flux, were annealed and ultrasonically tested in vacuum (Abar oven, Fig. 31) up to  $\sim 4000^{\circ}\text{R}$ , together with non-irradiated rhenium control wires. Sound velocities were measured during heating and cooling. These control wire and irradiated wire velocity data exhibited no significant systematic differences. From this it was concluded that structural or compositional radiation effects due to the above radiation levels were negligibly small with respect to the present ultrasonic thermometry application. The scatter in these velocity data corresponds to uncertainties in ultrasonically determined temperatures as follows: near  $2000^{\circ}\text{R}$ ,  $\pm 2\%$ ; near  $3000^{\circ}\text{R}$ ,  $\pm 1\%$ ; near  $4000^{\circ}\text{R}$ , less than  $\pm 1\%$ .

Typical oscillograms are shown in Figs. 36 and 37. Fig. 36 oscillograms correspond to a first pair of control and irradiated Re specimens. Fig. 37 oscillograms correspond to a second pair of specimens. It is seen that as temperature increases, the transit time increases in the sensor. Also important, the echoes obtained from the front and rear of the sensor remained at substantially constant amplitude. Transit times can be estimated from the oscillograms, but are more easily obtained automatically with the Pana-Therm Model 5000 (Fig. 4). Data are shown in Table V, comparing control and irradiated wires. The tabulated transit times are rounded off to the nearest  $0.1 \mu\text{sec}$ . Normalized sound velocity vs temperature is plotted in Figs. 38 and 39. These graphs show that there are no significant systematic differences between the control and irradiated wires, all of which are from the same parent wire. Superposition of these graphs shows the excellent reproducibility of the Re data.

Table V

Comparison of Irradiated and Non-irradiated Rhenium Sensors vs Temperature

Time hrs (12/12/66)	Temperature		Measured Extensional Wave Transit Time, $\mu$ sec		Normalized Velocity	
	$^{\circ}$ C	$^{\circ}$ R	Control	Irradiated	Control	Irradiated
1030	25	536	22.0	22.1	1.0000	1.0000
1055	810	1949	23.6	23.6	.9321	.9363
1110	1050	2381	24.4	24.5	.9014	.9018
1125	1225	2696	24.9	25.0	.8833	.8838
1135	1375	2966	25.4	25.5	.8659	.8664
1153	1530	3245	25.8	26.0	.8524	.8497
1213	1625	3416	26.4	26.5	.8330	.8336
1230	1730	3605	26.8	26.9	.8206	.8212
1243	1850	3821	27.5	27.6	.7996	.8004
1250	1850	3821	27.5	27.6	.7996	.8004
1320	1750	3641	26.9	27.1	.8175	.8152
1330	1630	3425	26.4	26.6	.8330	.8305
1350	1520	3227	25.9	26.1	.8491	.8464
1405	1405	3020	25.5	25.7	.8625	.8596
1420	1205	2660	24.9	25.2	.8833	.8767
1435	1060	2399	24.4	24.6	.9014	.8982
1450	770	1880	23.5	23.6	.9360	.9363
(12/13/66)						
0845	25	536	22.0	22.1	1.0000	1.0000
(12/15/66)						
0900	25	536	22.1	22.1	1.0000	1.0000
0930	825	1976	23.6	23.6	.9363	.9363
1125	1070	2417	24.4	24.4	.9055	.9037
1135	1380	2975	25.4	25.5	.8681	.8664
1145	1650	3461	26.3	26.3	.8384	.8400
1155	1910	3929	27.7	27.6	.7975	.8004
1205	2090	4253	29.0	28.8	.7617	.7670
1215	1920	3947	27.6	27.5	.8004	.8018
1222	1640	3443	26.3	26.3	.8384	.8400
1230	1430	3065	25.6	25.6	.8601	.8601
1240	1070	2417	24.5	24.4	.9018	.9055
1255	800	1931	23.6	23.5	.9363	.9403
1500	25	536	22.1	22.0	1.0000	.9955

## HIGH TEMPERATURE TESTS AT PANAMETRICS

### Velocity Measurements in Molybdenum

In the SRI oven (Fig. 30 - graphite heater, helium atmosphere) refractory metals have been tested bare as well as in protective sheaths.

Molybdenum wire, for example, 0.040 inch diameter x 3 inches kink-to-end sensor length, was tested bare up to about 3200°R. Results are plotted in Fig. 40 and are compared with Mo data obtained in the Abar oven (Fig. 31). Note the characteristic annealing occurring at high temperature (40-minute soak at 3200°R). This wire was subsequently reheated to 4500°R, but reliable acoustic data were obtained on heating only up to 3500°R (Fig. 40). Carbiding caused embrittlement, and apparently gave rise to spurious echoes within the sensor. The significance of these tests is that Mo appears unsuitable for use as a sensor or lead-in in a high temperature carbonaceous environment (unless suitable protection - coating or sheath - were available).

### Velocity Measurements in Rhenium

Tests in Tungsten/Vacuum Environment Beyond 5000°R. Non-irradiated Re wires were tested to the maximum temperature capability of the Abar oven as follows. Two Re sensors, 0.020 inches diameter x 2 inches long, were flash butt-welded to 0.030 inch diameter Re lead-in wires. One of the sensors (specimen A) had previously been a control wire and so was annealed, while the other sensor (specimen B) had not been previously tested at high temperature. Data are tabulated in Table VI, and plotted in Fig. 13. Data were obtained on heating only, as the tungsten element failed at ~ 5500°R on rising temperature. Up to 4000°R, i. e., before the second wire became annealed, the two ultrasonically indicated temperatures differed as follows: near 2000°R, 10%; near 3000°R, 8.5%; near 4000°R, 2.5%. Above 4000°R, annealing brought the two ultrasonically indicated temperatures into closer agreement: near 5000°R, 1/2%; near 5350°R, better than 1/2%. It was observed that both sensors followed the rapid cooling in the furnace following heater failure. The good agreement between both sensors, and between these data and the data obtained earlier (Figs. 38 and 39) again shows that Re exhibits a substantially reproducible velocity vs temperature characteristic. From these tests, it appears that reliable thermometry accuracy of  $\pm 50^{\circ}\text{R}$  at temperatures

Table VI

Comparison of Annealed and Non-Annealed Re Sensors

Time hrs	Temperature		Measured Extensional Wave Transit Time, $\mu$ sec		Normalized Velocity	
	$^{\circ}$ C	$^{\circ}$ R	Specimen A	Specimen B	Specimen A	Specimen B
(12/16/66)						
1120	25	536	22.1	22.3	1.0000	.9910
1140	900	2111	24.1	24.4	.9168	.9055
1155	1150	2561	24.8	25.2	.8909	.8767
1210	1415	3038	25.6	26.1	.8630	.8464
1225	1640	3443	26.4	26.9	.8368	.8212
1240	1920	3947	27.5	27.8	.8033	.7946
1255	2100	4271	28.9	28.8	.7643	.7670
1305	2270	4577	30.2	30.2	.7314	.7313
1317	2490	4973	31.2	31.2	.7079	.7079
1334	2505	5000	31.2	31.3	.7079	.7045
1340	2580	5135	31.7	31.7	.6967	.6967
1345	2625	5216	32.3	32.3	.6837	.6837
1356	2700	5351	32.8	32.8	.6733	.6733
1400	2800	5531	-	-	-	-

Specimen A previously annealed.

Specimen B not previously annealed (note agreement in transit times above 4000 $^{\circ}$ R).

Neither specimen irradiated.

Normalized velocity: values shown are normalized to the room temperature annealed value of Specimen A. Data were obtained on heating only.

up to 5000°R are attainable in a 2 inch Re sensor, at least in a carbon-free vacuum environment.

#### Self-Heating Tests in Carbon-Free Vacuum Beyond 6000°R.

Rhenium wire, 0.020 inch diameter x 2 inches long was cyclically self-heated in a carbon-free vacuum environment (Fig. 32) to 5000°R five times, with a total dwell of one hour at 5000°R. Results are tabulated in Table VII. Again, the annealed material exhibits good reproducibility in vacuum. After cycling, the sensor was heated to its melting point, 6216°R. The effects of gradients in such tests will be determined in the future by testing wires of various lengths (differential path).

The performance of Re in graphite is discussed in the following sections.

Tests in Graphite/Helium Environment to ~ 5000°R. Although Re does not carbide, it is well known that it becomes embrittled when heated in the presence of graphite (30). Therefore, initial tests on Re in the SRI oven included sheaths to minimize transport of carbon to the Re wire.

In one sheath test, for example, a 0.030 inch diameter Re wire, kinked to provide a 2 inch sensor, was placed in a 3/8 inch O. D. x 12 inch long Ta tube coated with zirconium diboride. Data were obtained up to ~ 3800°R (Fig. 41) but echoes and the sheath were lost after a 15 minute soak at this temperature.

In another sheath test, a 2 inch Re sensor was packed with boron nitride fiber in a W-clad W-26% Re thermowell, 0.075 inch I. D. (provided by WANL). Data were obtained to 4000 and 4200°R at which temperatures echoes were attenuated into the noise, terminating the run.

Since these and other sheath tests had not yet led to a successful run to 4500°R or beyond, it was decided to again test bare Re in the SRI oven without a sheath (this had been attempted twice before in the SRI oven, with unexplained attenuation causing the run to be terminated). A bare Re wire sensor, 0.030 inch diameter x 2-inch kink-to-end length, was heated in 20 minutes to a brightness temperature (measured with disappearing filament L&N pyrometer) of 4575°R and yielded readable echoes for 12 minutes at this apparent temperature. The run was terminated after the echoes were lost. Post mortem examination showed that the Re had

Table VII. Behavior of Rhenium During Cycling

Clock Time, hrs.	Temperature °R			Ultrasonic Transit Time, $\mu$ sec		Self-heating Current, amperes
	Observed	Corrected for Wall Loss	Corrected for Emissivity	Observed*	Normalized	
1343		Room temperature		21.09	1.0014	0
1344	2768	3200	3447	-	-	6.5
1345	2949	3380	3654	25.10	.8414	8.0
1347	3287	3731	4070	26.34	.8018	10.2
1349	3444	3893	4270	27.56	.7663	12.0
1352	3876	4334	4824	28.88	.7313	14.0
1356	4092	4559	5094	30.51	.6922	16.5
1404	-	-	-	30.47	.6931	16.5
1408	-	-	-	30.47	.6931	16.5
1445		Room temperature		21.15	.9986	0
1453	2652	3083	3312	24.60	.8585	6.5
1457	2922	3353	3618	25.06	.8428	8.0
1500	3219	3659	3978	26.12	.8086	10.2
1502	3435	3884	4266	27.43	.7700	12.0
1504	3912	4388	4892	29.01	.7280	14.0
1507	4092	4559	5094	30.61	.6900	16.5
1525	-	-	-	26.48	.7976	16.5
1545		Room temperature		21.12	1.0000	0
1548	2760	3191	3429	24.45	.8638	6.5
1549	2970	3407	3690	25.06	.8427	8.0
1550	3300	3749	4095	26.34	.8018	10.2
1552	3461	3911	4284	27.31	.7724	12.0
1555	4002	4469	4986	28.91	.7305	14.0
1558	4092	4559	5094	30.49	.6926	16.5
1610	-	-	-	30.40	.6947	16.5
1622	-	-	-	30.39	.6949	16.5
1630	-	-	-	30.40	.6947	16.5
1002		Room temperature		21.14	.9991	0
1005	2652	3083	3294	24.70	.8551	6.5
1007	2913	3344	3618	25.16	.8394	8.0
1012	3111	3551	3852	26.33	.8021	10.2
1014	3290	3731	4068	27.39	.7711	12.0
1016	3516	3965	4356	29.03	.7275	14.0
1018	3876	4343	4824	30.58	.6906	16.5
1037	3995	4253	4482	30.49	.6927	16.5
1100	-	-	-	30.51	.6922	16.5
1148		Room temperature		21.12	1.0000	0
1150	2628	3062	3285	24.60	.8585	6.5
1152	2805	3200	3456	25.06	.8428	8.0
-	3102	3548	3852	26.23	.8052	10.2
1153	3273	3713	4050	27.51	.7677	12.0
1154	3462	3911	4284	29.05	.7270	14.0
1155	3768	4226	4680	30.63	.6895	16.5
1220	-	-	-	30.60	.6902	16.5
1230	-	-	-	30.60	.6902	16.5
1235	-	-	-	30.54	.6915	16.5
1240	-	-	-	30.47	.6931	16.5
1242	-	-	-	30.89	.6837	16.5
1315	-	-	-	29.99	.7042	16.5

\*Transit time measured using double pulse technique (Fig. 2). Note reproducibility of current and transit time data. Self-heating of 0.020 in. diameter Re sensor requires less than 40 watts per inch at 5000°R. Corrected L&N optical pyrometer readings correlate in first three runs. Discrepancy in last two runs due to vapor deposition on inside surface of tube. Transit times normalized to 21.12  $\mu$ sec.

melted or broken off at the kink between Re lead-in and sensor. Therefore, it is considered not out of the question that the Re actually survived to the eutectic point,  $4966^{\circ}\text{R}$ . In any event, this test demonstrated the use of a Re sensor, bare, to at least  $4575^{\circ}\text{R}$  in a graphite/helium environment. In this test, since there was no apparent reason for the Re to have melted below  $\sim 4966^{\circ}\text{R}$ , it appears that the pyrometer reading was in error, probably due to misalignment of the sight port (Fig. 30).

Self-Heating Tests in Graphite/Vacuum Environment to  $\sim 5000^{\circ}\text{R}$ . Bare Re was self-heated in direct physical contact with graphite felt (Fig. 42). In this self-heating test, the graphite felt was pierced by a 2 inch Re sensor. The Re sensor survived one hour at an ultrasonically determined temperature of  $4400^{\circ}\text{R}$ , and, on cooling to room temperature, the velocity reproduced the value observed prior to heating. The same sensor was then self-heated to about  $5000^{\circ}\text{R}$ , at which temperature it survived (i. e., produced readable echoes) for 15 minutes, and then melted. Oscillograms obtained in these self-heating tests are shown in Fig. 43, and depict the changes in transit time and echo amplitudes in Re up to  $\sim 5000^{\circ}\text{R}$ . Analysis of these oscillograms is summarized below.

#### Preliminary Computation of $\alpha$ for Bare Rhenium Wire in Contact with Graphite Felt

Round Trip Time, ( $\mu$ sec)	Relative Velocity, $V/V_o$	Estimated Temperature ( $^{\circ}\text{R}$ )	Attenuation, $\alpha$ at $\sim 250$ kHz (db/ft)
21.4	1	530	0
28.1	0.762	4400	7
30.3	0.706	5000	10

The estimates for attenuation  $\alpha$  are only coarse approximations because of the signal to noise ratio being only  $\sim 2:1$ , and further, because the sensor is so short. For reliable measurement of  $\alpha$ , the echo amplitude itself should decrease by  $\sim 10$  db. Note that since the amplitude  $A = A_o e^{-\alpha x}$ , increasing length from 2 to 10 inches changes  $A$  by  $e^5$  or a factor of 150. To offset the increase in length from 2 to 10 inches,  $\alpha$  must be

reduced by the same factor, i. e., from  $\sim 10$  db/ft to  $\sim 2$  db/ft. Now if  $\alpha$  is proportional to frequency\* to the first power,  $f$  must be reduced from  $\sim 250$  kHz to  $\sim 50$  kHz. If  $\alpha$  obeys an  $f^2$  law, then  $f$  need be reduced only to  $\sim 250/\sqrt{5}$  kHz, or 110 kHz. Further testing is required to establish the frequency dependence of  $\alpha$  at high temperatures. Attenuation measurements are discussed in Appendix VI (see also Figs. 44-46 and Ref. 44).

#### FIELD TESTS AT WANL - GRAPHITE/HYDROGEN ENVIRONMENT, TO 5000°R

To evaluate the ultrasonic system in a graphite/hydrogen environment, while simulating certain geometrical and other parameters of interest, field tests were conducted at the Westinghouse Astronuclear Laboratory, Large, Pa., during the week of June 26, 1967. The particular oven used in these tests is described elsewhere (34). This oven was run to  $\sim 4000^\circ\text{R}$  on June 28, and to beyond  $5000^\circ\text{R}$  on June 30.

In planning for these field tests at WANL, the temperature objective was originally set at  $4500^\circ\text{R}$ . This temperature objective was chosen under the assumption that a W-clad W/Re sheath would be used, and allows approximately a  $200^\circ\text{R}$  safety factor with respect to the W/Re/C eutectic. Prior to testing at WANL, however, it became clear from the SRI tests that the available W-clad W/Re sheath presently used for protecting thermocouples was not necessarily the optimum choice for protecting the ultrasonic sensor. Besides the question of the sheath itself (materials and dimensions), the question of how to acoustically isolate the sensor and lead-in within the sheath had not been answered satisfactorily. That is to say, while boron nitride fiber, as well as various tubes and beads ( $\text{BeO}$ ,  $\text{HfO}_2$ ) and powdered materials ( $\text{ThO}_2$ ) had been tested with sheathed lines up to about one foot long, and found satisfactory, at least with regard to isolation, the full-length sheath required for the WANL tests posed new problems of packing and assembly. To deal adequately with all the full-scale sheath problems requires an effort beyond the scope of the present program. Thus, the WANL tests were finally approached

---

\* The "frequency" of the pulses used in this work is estimated from the pulse width. Most of the pulse's energy is distributed between dc and a frequency approximately equal to the reciprocal of the pulse width. This distribution is rather symmetrical, and is peaked in the middle of the band, as is shown, for example, by Bell, Ref. 9.

with the understanding that the sheath was not yet optimized for use with an ultrasonic line. It was further recognized that bare Re wires might even yield signals and/or survive to higher temperatures than Re in a sheath. At this stage, thermometry accuracy was not considered of paramount importance, in view of the other unresolved questions.

#### Tests on June 28, 1967

On June 28, three bare Re sensors were tested. Each sensor measured 0.020 inches diameter x ~ 5 inches long. The purpose of this test was to coordinate general assembly procedures, and to simultaneously conduct ultrasonic, thermocouple and pyrometric tests in this particular facility. Sensors were positioned so their centers would approximately correspond to oven sight ports. Positioning was verified by radiographing the assembly before inserting it in the oven (Fig. 47).

X-ray positives (Fig. 47) show the relative positions of two centerless ground 0.030 inch diameter W lead-ins, and the single 0.040 inch diameter Re lead-in, and the three 0.020 inch diameter Re sensors. Other items of interest are also identified.

The two Re sensors which are welded to the W lead-ins were inserted to the same depth in the assembly, and subsequently were heated up to  $\sim 3000^{\circ}\text{R}$ . The Re sensor which is welded to the Re lead-in was inserted deeper, and was heated to  $\sim 4000^{\circ}\text{R}$ .

Results in All-Rhenium Line. Oscillograms in Fig. 48, a through f, show the ultrasonic signals on rising and falling temperature. Attenuation of the 3  $\mu\text{sec}$  pulses in the 5-inch sensor is indicated in Figs. 48 c and d, while additional attenuation in the lead-in is indicated in Fig. 48e (diameter discontinuity still visible, but end echo lost in the noise). Shortly after this last oscillogram was obtained an apparent hydrogen leak necessitated oven shutdown. On cooling, the sensor echoes returned (Fig. 48f). This experiment showed that a bare all-Re line could survive physically to at least  $4000^{\circ}\text{R}$ , but attenuation at 3  $\mu\text{sec}$  pulse widths ( $\sim 330\text{ kHz}$ ) was excessive in a 5-inch sensor (see results on June 30, however, where data were obtained at  $\sim 6\text{ }\mu\text{sec}$  pulse widths ( $\sim 170\text{ kHz}$ ) in a 2-inch bare Re sensor to  $4765^{\circ}\text{R}$ ). Test results are tabulated in Table VIII. The discrepancy in indicated

temperatures may be due to the hydrogen leak, which could have caused a substantial gradient in the assembly. Again, the major purpose at this point was merely to check out general operating procedures. The question of accuracy demands subsequent study.

Table VIII

Results in All-Rhenium Line (June 28, 1967)

<u>Figure</u>	<u>Clock Time, Hrs.</u>	<u>Transit Time in Sensor, <math>\mu</math>sec</u>	$\tau_o / \tau$	<u>Temperature, <math>^{\circ}</math>R</u>		
				<u>Ultrasonic</u>	<u>Thermocouple</u>	<u>Pyrometer</u>
48a	1337	53.5	1.00	Room temperature		-
b	1409	61.5	.87	2600	2810	2800
c	1428	64.5	.83	3200	2740	3745
d	1434	65.0	.82	3400	3755	3760
e	1441	-	-	-	4060	-
f	1500	55.0	.97	1000	-	-

NOTE: Thermocouple and pyrometer data are taken as the values tabulated by WANL (Bldg. 15, Run 18, Test Piece 0667D1) at the times closest to the listed clock times at which the ultrasonic data were recorded. Transit times are estimated from oscillograms. The long non-isolated line attenuated the sensor echoes below the pre-set threshold of the Pana-Therm, and so prevented it from reading automatically.

Results in Tungsten Lead-in/Rhenium Sensor. The placement of these lines is shown in Fig. 47, while the corresponding oscillograms are shown in Fig. 49. Transit times were read to the nearest micro-second from the oscillograms, from which the ultrasonic temperatures shown in Table IX were obtained. Generally, sensor "A" ran about  $200^{\circ}$ R hotter than "B", while the pyrometer readings were  $\sim 200^{\circ}$ R hotter than "A". These discrepancies could be due in part to a radial temperature gradient, the plausibility of which is supported by the hydrogen leak and burnout which terminated the run. Also, the sensors were not centered exactly on the line of sight of the pyrometer. Finally,

TABLE IX

Comparison of results in tungsten lead-in/rhenium sensors with each other  
and with optical pyrometer readings\* (WANL Tests, June 28, 1967).

Clock Time, Hours	Rhenium Sensor "A"		Rhenium Sensor "B"		Corrected Optical Pyrometer Temperature, °R
	Sensor Transit Time, $\mu$ sec	$\frac{t_o}{t}$ Ultrasonic Temp., °R	Sensor Transit Time, $\mu$ sec	$\frac{t_o}{t}$ Ultrasonic Temp., °R	
1343			47	1.000	530
1344	48	1.000			
1410			52	.905	2000
1411					2365
1412	54	.889			
1427					2755
1430			53	.888	2250
1432	55	.873			
1433					2755
1437					3020
1443	56	.857	54	.870	2600
1445					3005
1507			47	1.000	530
1511	48	1.000			

\* Corrected pyrometer readings ( $T_4$ ) from WANL tabulation for Bldg. 15, Run 18, Test Piece 0667D1  
(June 28, 1967).

the resolution of transit time from these oscillograms (only to the nearest microsecond) is not conducive to high accuracy. With adequate set-up time in the future, uncertainties in sensor position and transit time could be reduced tenfold. It is noteworthy that both lead-ins and 5-inch sensors exhibited essentially no attenuation up to 3000°R, at an ultrasonic pulse width of about 4  $\mu$ sec (frequency bandwidth  $\sim$  250 kHz). As a practical matter, it is also noted that the straightness of the centerless-ground tungsten lead-ins enabled these lines to be inserted into the assembly with relative ease.

Summary. Perhaps the two most important results of these field tests (June 28, 1967) are (1) the general check-out and operating procedures were established for measuring temperature by simultaneous ultrasonic, thermocouple and pyrometer means, and (2) a new sequence for pre-assembling the test element was indicated, whereby potting and other time-consuming steps could be completed prior to and independent of the ultrasonic measurement.

Additionally, the following observations were made. Regarding transducer design, the unwanted rearward-traveling pulse could be dampened sufficiently in a three-foot length of steel wire, surrounded by shrink tubing, and coiled in a two-inch diameter loop. This design allows room for at least four transducers in the plenum. Manual switching or commutation of different transducers (sensors) introduced no electrical problems. However, it may sometimes be desirable to use lead-ins or sensors of different lengths, or employ other means (e. g., different frequencies for different sensors) to avoid any ambiguity in sensor/switch relationships. The integrity of the welded construction (lead-in/sensor joint) appears reasonably well-established so far. There was no difficulty in operating the magnetostrictive transducers despite the high dc currents flowing through the heater. Attenuation becomes excessive if too high a frequency is used.\*

---

\* Assuming attenuation in Re can be sufficiently overcome by reducing frequency (to  $\sim$  100 kHz, for example) the temperature limit is imposed by the Re/graphite eutectic. Nadler and Kempter at Los Alamos (43) empirically showed this limit to be  $2486 \pm 18^\circ\text{C}$ , or  $4966 \pm 32^\circ\text{R}$ . (In their experiments on thermocouples for use in carbon atmospheres, these authors (43) demonstrated the use of Re in direct contact with graphite to about  $4730^\circ\text{R}$ .) Thus, the maximum temperature range for pure Re in contact with graphite would appear to be  $4966^\circ\text{R}$ , less an appropriate safety margin. The practical upper limit might have to be further reduced, depending on the long term effects of carbon diffusion on sound velocity in Re. These limits apply to unprotected Re.

### Tests on June 30, 1967

Four rhenium sensors were tested on June 30 at elevated temperatures ranging up to 4765°R. Two of these sensors remained operable beyond 4600°R. Ultrasonic temperatures are compared below with both thermocouple and pyrometric determinations of temperature until 4600°R, where the thermocouple data became unreliable (junction opened), and with pyrometer readings only, for temperature above 4600°R. Tests were continued to 5000°R, i. e., above the rhenium/graphite/tungsten eutectic (reportedly  $4740 \pm 50^{\circ}\text{R}$ ),\* to observe propagation in all four lead-in wires. Materials and dimensions of lead-ins and sensors are given in Table X.

Table X

#### Materials and Dimensions for Lines Tested June 30, 1967

Switch Point	Lead-in Wire		Sensor Wire		
	Material	Diameter, in.	Material	Diameter, in.	Length, in.
1	W	0.030	Re	0.020	5
2	W	0.040	Re	0.030	2
3	Re	0.040	Re	0.030	5
4 (sheathed)	W	0.030	Re	0.020	2

Bare Sensors. Representative oscillograms for a bare 5-inch and a bare 2-inch Re sensor are shown in Figs. 50 and 51, respectively. Of the four ultrasonic sensors used in this test, these two ("switch points" 1 and 2) performed best, i. e., to pyrometrically observed temperatures of 4650 and 4765°R, respectively. Figure 52 shows end echoes from W and Re lead-in wires obtained after sensors were lost. Data from all four ultrasonic sensors are plotted in Figure 53. (See also Table XI.)

The 5-inch sensors exhibit the largest discrepancies, especially below 3000°R. Above 4000°R, however, the ultrasonic temperatures

\* In Ref. 45, the W/Re/C eutectic is shown to depend on the W/Re alloy composition as follows (see also footnote on p. 30):

Metal	W	W-5% Re	W-26% Re	Re
Eutectic, °R	5370	5244	4920	4966

Table XI. Comparison of ultrasonic temperatures with thermocouple and pyrometric determinations, \* for tests in WANL graphite/hydrogen oven, June 30, 1967.

Clock Time Hrs.	Minutes	Thermocouple Temp, °R	Corr. Optical Pyrometer Temp, °R	Rhenium Ultrasonic Sensor									
				Switch Point 1		Switch Point 2		Switch Point 3		Switch Point 4		T, μsec	τ o/τ Temp, °R
				τ, μsec	τ o/τ Temp, °R	τ, μsec	τ o/τ Temp, °R	τ, μsec	τ o/τ Temp, °R	τ, μsec	τ o/τ Temp, °R		
1322	0	Room Temperature		56	1.000 530	22.5	1.000 530	57	1.000 530	22.5	1.000 530		
1332	10	3050											
1335	13	3220	3105	64	.875 2500								
1336	14		3170			27.0	.833 3150	65	.877 2490				
1337	15		3160										
1340	18		3145										
1342	20	3680	3610										
1345	23		3620	66	.850 2900								
1347	25		3635			28.0	.803 3600	67	.851 2900				
1348	26		3645										
1349	27	3700	3650										
1352	30	4000	4010										
1355	33	4020	4080	71	.790 3770			72	.792 3750				
1356	34					28.5	.790 3770			28.6	.788 3770		
1358	36		4090										
1359	37		4120										
1401	39	4250	4300										
1403	41		4290	74	.758 4120								
1404	42		4300			30.0	.750 4220						
1407	45		4305			29.5	.763 4080	74	.771 4000				
1412	50	4400	4450										
1413	51		4455										
1415	53		4500			30.0	.750 4220						
1417	55	4450	4575	78	.718 4540	30.0	.750 4220						
1419	57		4630										
1420	58		4650	80	.700 4700								
1421	59	4600, (tc failure)	4680			30.5	.737 4350						
1426	64		4700										
1427	65		4720										
1428	66		4765			33.0	.682 4800						
1430	68		4990										
1434	72		5050										
1440	78		4075										

\* Thermocouple data obtained from WANL temperature-time plot for thermocouple Z-70. Pyrometer data primarily from WANL T<sub>2</sub> tabulation for Bldg. 15, Run 19. Ultrasonic transit times read from oscillograms.

are generally within a few percent of the thermocouple and pyrometer temperatures. Again, it was not intended to establish the accuracy of the ultrasonic system at this stage, and so the observed discrepancies, or agreements, are not yet considered significant.

Sheathed Sensor. Regarding the sheathed ultrasonic sensor, we note the following. Considerable difficulty was encountered in attempting to pack either boron nitride fiber or thoria powder between the lead-in and sensor and the long sheath. In view of time limitations, these packing approaches were abandoned, and the line was tested with negligible acoustic isolation material between itself and the sheath. Except for possibly one point, no useful temperature data were obtained. With proper acoustic isolation within the sheath, however, the sheathed acoustic line might offer important advantages over bare acoustic lines. \*, \*\*

Summary. While the accuracy of the above ultrasonic results leaves considerable ground for improvement, it is considered encouraging that, in these (June 30, 1967) field tests with four sensors tested at once, three operated up to at least 4000°R, two beyond 4600°R, and one beyond 4750°R. (The sheathed thermocouple opened up at 4600°R.)

---

\* Note added in proof: further testing of Re wire in contact with graphite near 4500°R for periods of one hour and longer show that carbon diffusion increases the sound velocity at high temperature (compared to carbon-free velocity at same temperature). Further, carbon diffusion severely reduces the temperature sensitivity of sound velocity in Re. (These experiments, conducted in Contract NAS3-10284, will be fully reported in Dec. 1967.) It therefore appears that if Re is to be a useful sensor, it must be kept free of carbon. If it can indeed be protected from carbon, then its maximum operating temperature is independent of the Re/C eutectic. Thus, operation to 5300°R may not be unrealistic. (Again, tests reported above, in the Abar oven and in the self-heating oven, were conducted beyond 5300°R.)

\*\* While tightly packed material extending over a substantial lead-in distance can attenuate the signal to a large degree, loosely packed materials over short lengths hardly attenuate the signal at all. This was determined in tests of 1 mm dia sensor wires which were inserted several inches deep into test tubes filled with 0.03 in. dia lead shot, sawdust, waxed sawdust, sugar, sand, Al<sub>2</sub>O<sub>3</sub> powder, borax, graphite cloth, felt and powder, Fiberfrax and boron nitride fiber. Low density materials (e.g., carbon motor brushes) in pressure contact over only local areas also have little effect on 100 to 300 kHz signal amplitudes in high density wires. Attenuation due to immersion in water is also negligible.

## CONCLUSIONS

The object of this program was to design, construct and test an ultrasonic system for determining localized temperatures to  $\pm 50^{\circ}\text{R}$  up to  $5000^{\circ}\text{R}$  in the core of a nuclear rocket engine. The principal elements of the ultrasonic system include a transducer, a lead-in line, a sensor, a sheath (in some cases), and an automatic electronic instrument capable of transmitting pulses, and measuring the time between their reflections from the front and rear of the sensor. For the anticipated nuclear rocket engine application, one should use an extensional wave magnetostrictive transducer operated below 250 kHz, a lead-in of W or possibly W/Re up to  $\sim 4700^{\circ}\text{R}$ , but pure Re lead-in above  $\sim 4700^{\circ}\text{R}$ ,\* and a sensor of Re of length up to 5 inches. If a sheath is used, the acoustic line must be properly isolated from it, to avoid attenuation and unwanted reflections. Potentially of some importance, Re can survive to about  $5000^{\circ}\text{R}$  in intimate contact with graphite, whereas W/Re thermocouples are limited in the present application by the W/Re/graphite eutectic,  $\sim 4740^{\circ}\text{R}$ . If the Re/C eutectic limit of  $4966^{\circ}\text{R}$  can be overcome by sheathing, flushing or some other approach, Re sensors (melting point  $6216^{\circ}\text{R}$ ) might then be used up to a temperature limited by attenuation. It appears, however, that attenuation may be overcome by operating at lower frequencies, perhaps as low as  $\sim 100$  kHz. Near  $5000^{\circ}\text{R}$ , temperature sensitivity of  $50^{\circ}\text{R}$  is achievable in a Re sensor 1.4 inches long if extensional waves are used, and in a 1 inch sensor, if shear (torsional) waves are used, assuming transit time is measured to  $0.1\ \mu\text{sec}$ . This result is based on tests on Re wires which established the velocity and preliminary attenuation characteristics of extensional waves to the melting point,  $6216^{\circ}\text{R}$ . Additional measurements of ultrasonic propagation up to and beyond  $4000^{\circ}\text{R}$  in non-irradiated rhenium wires and in rhenium wires irradiated to  $8.7 \times 10^{19}$  integrated thermal flux and  $2.6 \times 10^{19}$  integrated fast flux showed no significant differences.

To measure temperature automatically, it was decided to depart from the double-pulse approach used in the Dragon Project. Accordingly, a new instrument, the Pana-Therm Model 5000, was designed, built and tested. This device averages ten measurements of transit time in the sensor to  $\pm 0.1\ \mu\text{sec}$ , and provides this average reading in digital and analog form with an instrument response time of 0.1 sec.

The present ultrasonic system is being developed to complement other temperature measuring systems, particularly thermocouples.

\* These temperature limits (see Ref. 45) assume the line is in contact with graphite. If a protection system can isolate the line from graphite, lead-in lines can be chosen on the basis of mechanical integrity and ultrasonic attenuation characteristics. In this case, the carbon eutectic does not govern the choice of materials for use to  $5000^{\circ}\text{R}$  or beyond.

To appreciate the potential contribution of ultrasonic sensors, it is useful to compile the advantages and disadvantages of the ultrasonic system. Since thermometry applications of thin wire ultrasonics have been developed only during the present decade, and since the present program has spanned only two years, it is understandable that only certain advantages and disadvantages have been clearly demonstrated. Future applications will probably clarify limitations not yet anticipated. On the other hand, new methods often yield unexpected advantages as their applications are pursued.

#### Disadvantages of Ultrasonic Thermometers

Disadvantages of ultrasonic thermometers, compared to thermocouples, include: more complicated electronics; certain limitations with regard to negotiating very sharp contours or passing through sheaths and some types of feedthroughs; operators require some degree of specialized training; temperature is not measured at a point, but is averaged over the length of the sensor (in some situations, however, this type measurement might be desired)\*; high frequency components of the vibration and noise spectrum,\* if present, may be more troublesome to an acoustic system than to a thermoelectric system; attenuation may limit allowable frequencies and lengths for lead-in and sensor for some vibration modes; elastic hysteresis effects that cannot be annealed out may limit the choice of sensor materials; applications and lifetime experience is limited; changes in acoustic propagation characteristics due to long-term heating in a graphite/hydrogen environment are still to be determined.

#### Advantages of Ultrasonic Thermometers

The present ultrasonic thermometer offers several inherent and/or demonstrated advantages over thermocouples up to  $\sim 6000^{\circ}\text{R}$  or higher, depending on the environment and accuracy required. These advantages accrue partly because of the greater choice of ultrasonic sensor materials (Figs. 10 - 13). Also, only one material, not two or three, need be selected, at least in some situations. The ultrasonic thermometer does not require electrical insulation at high

---

\* H. P. Eckstein, Studies of Random Noise: An Annotated Bibliography, AD 651 308 (Dec. 1966).

temperature (no shunting error). Consequently the sensor can be installed bare (at least to the extent that there are no materials compatibility problems) in electrically conducting media, with attendant improvement in response time. Regarding pressure or vacuum seals on the line itself, the ultrasonic line requires only one small access hole. The line can be brazed or welded at this access hole, provided this hole is through a diaphragm which, in the vicinity of the wire, is thin compared to wavelength. Alternatively, one may use electrical feedthroughs, or compression seals on a sheath, while in non-nuclear cases, use of an elastomeric compression seal directly on the lead-in is suitable. The ultrasonic sensor, composed of only one material, avoids calibration shifts which in thermocouples are due to diffusion of one leg into another. There exists the practical possibility of calibrating an individual ultrasonic sensor such as Re (hexagonal structure) which is not embrittled as much as W (cubic structure) when heated above recrystallization temperatures. (W/Re thermocouples are usually calibrated on a sampling basis, to avoid embrittling the particular wires which are to be installed for a test.) When one can replace two thermocouple wires, insulator and sheath with a single ultrasonic wire line, this one line can be substantially simpler, and/or larger in diameter than the thermocouple wires. In this case, a monolithic, more rugged ultrasonic sensor can sometimes be fabricated, with prospects of longer life. If desired, brazed or welded joints between sensor and lead-in can be completely avoided by grinding the last inch or two of the lead-in down to the size required for the sensor. On the other hand, flash butt welded joints can be made in air or under a protective atmosphere in a few seconds, with standard welding equipment. A single thin wire,  $\sim 1/2$  mm diameter, occupies less space than any practical thermocouple pair for use to comparable temperatures in extreme environments. The measurement of two or more temperatures on each side of only one ultrasonic line is a unique advantage with respect to temperature profiling. (This may simplify certain data acquisition systems, i. e., one may interrogate sensors according to their distance from the transducer.) Also significant, accuracy increases at elevated temperature.

Thermocouple difficulties are elaborated on in the literature (45-49).<sup>\*</sup> In this report we do not compare the advantages and disadvantages of ultrasonic thermometers vs pyrometers, for even though important advances are being made in pyrometry (50) the geometry and environment of particular interest here precludes their consideration. Likewise, comparison with resistance thermometers, non-instrumented techniques (51) or other new, and in some cases proprietary techniques, is beyond the scope of this report.

---

\* Some of the precautions which may be necessary to fabricate thermocouples in a sufficiently controlled manner are spelled out in NASA Lewis RFP No. C-320898 Q, Exhibit "A," pp. 1-6 (Sept. 26, 1967). See also P. Bliss and S. Fanciullo, PWAC-462, High Temperature Thermometry at P&WA-Canel, TID-4500 (41st Ed.) (June 2, 1965).

## RECOMMENDATIONS FOR FUTURE WORK

As the present two-year program drew to a close, it became apparent that the potentialities of thin wire ultrasonic thermometry could be more fully developed in these areas:

1. Sensor lengths in the range 1 to 5 inches;
2. Sensor diameters in the range 0.01 to 0.1 inch (bare and sheathed);
3. Simultaneous or sequential measurements at two sensors in the same wire, especially using two modes of vibration (one for each sensor);
4. Evaluation of sheaths to protect ultrasonic sensor and lead-in;
5. Additional field tests in the graphite/hydrogen environment available at WANL.

Other areas of future nuclear-oriented interest include tests in gamma-heated systems, effects of long-term heating, special sensor configurations for thermal equilibrium between sensor and adjacent materials, with presence of intense gamma heating and flowing hydrogen, design and testing of nuclear-hardened transducers, use of transducers with Curie points above  $2000^{\circ}\text{R}$ , for possible use in locations of high gamma heating, and development of commutation schemes for use with one hundred or more sensors.

## APPENDIX I

### EFFECT OF TEMPERATURE DISTRIBUTION ON THE ACCURACY OF THE ULTRASONIC TEMPERATURE MEASUREMENT

In evaluating the accuracy of the temperature deduced from ultrasonic measurements, one must distinguish between the arithmetic mean temperature (sometimes referred to as the "true temperature"), the harmonic mean temperature, and the temperature determined from the measured sound velocity. The velocity determined by a measurement of the transit time in the sensor is the harmonic mean velocity. In general, the harmonic mean temperature is not necessarily equal to the temperature corresponding to the harmonic mean velocity.

Consider a temperature distribution  $T(x)$  along a wire of length  $L$ , whose velocity-temperature characteristic is  $V(T)$ .

$$\text{Then} \quad T_A \equiv \frac{1}{L} \int_0^L T(x) \, dx \quad (1)$$

$$T_H \equiv \frac{L}{\int_0^L \frac{dx}{T(x)}} \quad (2)$$

$$V_H \equiv \frac{L}{\int_0^L \frac{dx}{V(T)}} = \frac{L}{\int_0^L \frac{dx}{V\{T(x)\}}} \quad (3)$$

$$\text{and} \quad V(T_S) = V_H \quad (4)$$

where  $T_A$  = arithmetic mean temperature  
 $T_H$  = harmonic mean temperature  
 $V_H$  = harmonic mean velocity  
 and  $T_S$  = sonic or ultrasonic temperature

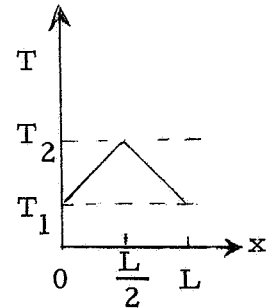
Clearly,  $T_S$  is not necessarily the same as  $T_H$  since it will depend upon the  $V(T)$  characteristic. Possible conditions for  $T_S = T_H$  are that  $V(T) = \text{constant} \times T$ , or  $T(x) = \text{constant}$ .

It is generally known that the arithmetic mean of any finite and discrete set of numbers is greater than the harmonic mean.\* The extension to well behaved functions is straightforward, where the same conclusion holds. However, no similarly general conclusion can be drawn for  $T_S$  versus  $T_H$  or  $T_A$ . Depending on  $T(x)$  and  $V(T)$ ,  $T_S$  may be greater or less than  $T_A$ .

#### Case I. Triangular Temperature Distribution

This distribution is given by:

$$\begin{cases} T(x) = T_1 + (T_2 - T_1) \frac{2x}{L} ; & 0 \leq x \leq \frac{L}{2} ; & T_2 > T_1 \\ T(x) = (2T_2 - T_1) - (T_2 - T_1) \frac{2x}{L} ; & \frac{L}{2} \leq x \leq L \end{cases}$$



Now if  $V(T) = \alpha - \beta T$  (approximating  $V(T)$  by a piecewise linear function) where  $\alpha, \beta$  are constants, then

$$T_A = \frac{1}{2} (T_1 + T_2)$$

---

\* This is readily illustrated as follows. The harmonic mean of two numbers  $a$  and  $b$  is  $H \equiv 2/(1/a + 1/b) = 2ab/(a+b)$ , and the arithmetic mean is  $A \equiv (a+b)/2$ . Their difference is  $A - H = \frac{(a-b)^2}{2(a+b)} > 0$  unless  $a = b$ . If  $a = b$ ,  $A = H$ .

$$T_H = \frac{T_2 - T_1}{\ln \frac{T_2}{T_1}}$$

$$T_S = \frac{a}{\beta} - \frac{(T_2 - T_1)}{\ln \left( \frac{a - \beta T_1}{a - \beta T_2} \right)}$$

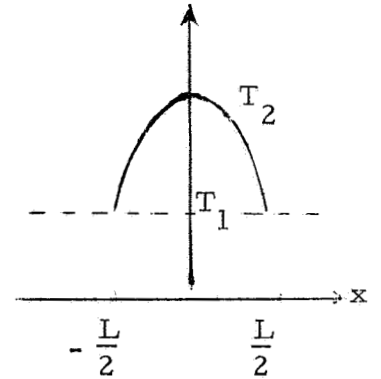
Case II. Parabolic Temperature Distribution (see Ref. 35)

This distribution may be given by:

$$T(x) = T_1 + (T_2 - T_1) \left[ 1 - \left( \frac{2x}{L} \right)^2 \right] ; -\frac{L}{2} \leq x \leq \frac{L}{2}$$

Then  $T_A = \frac{1}{3} T_1 + \frac{2}{3} T_2$

and



$$T_H = \frac{2T_2 \sqrt{\left(1 - \frac{1}{T_2}\right)}}{\ln \left\{ \frac{1 + \sqrt{\left(1 - \frac{1}{T_2}\right)}}{1 - \sqrt{\left(1 - \frac{1}{T_2}\right)}} \right\}} \approx \frac{T_2}{1 + \frac{1}{3} \left( \frac{T_2 - T_1}{T_2} \right) + \frac{1}{5} \left( \frac{T_2 - T_1}{T_2} \right)^2 + \dots}$$

Again assuming  $V(T) = a - \beta T$ ,

$$T_S = \frac{1}{\beta} \left\{ a - \frac{\sqrt{\beta (T_2 - T_1) (a - \beta T_2)}}{\tan^{-1} \sqrt{\left( \frac{\beta (T_2 - T_1)}{a - \beta T_2} \right)}} \right\}$$

For rhenium at  $2500^{\circ}\text{C}$  ( $\sim 5000^{\circ}\text{R}$ )

$$\alpha \approx 6.32 \times 10^5 \text{ cm/sec}$$

$$\beta \approx 105.38 \text{ cm/sec}^{\circ}\text{K}.$$

Now suppose there is a temperature difference of  $1000^{\circ}\text{C}$  ( $1800^{\circ}\text{R}$ ) over the length of the sensor.

$$\text{Let } T_1 = 2000^{\circ}\text{C} = 2273^{\circ}\text{K}$$

$$\text{and } T_2 = 3000^{\circ}\text{C} = 3273^{\circ}\text{K}$$

Triangular Case

$$T_A = 2500^{\circ}\text{C}$$

$$T_H = 2472^{\circ}\text{C}$$

$$T_S = 2526^{\circ}\text{C}$$

Parabolic Case

$$T_A = 2667^{\circ}\text{C}$$

$$T_H = 2634^{\circ}\text{C}$$

$$T_S = 2696^{\circ}\text{C}$$

$$\frac{T_S - T_A}{T_A} = \frac{26}{2773} = 0.94\%$$

$$\frac{T_S - T_A}{T_A} = \frac{29}{2940} = 0.99\%$$

The significance of these calculations is as follows. First and most important, even for temperature differences as extreme as  $1000^{\circ}\text{C}$  ( $1800^{\circ}\text{R}$ ) over the sensor,  $T_A$  and  $T_S$  differ by less than 1%. (Similar conclusions were reached in Ref. 14 and 17, for sinusoidal and other distributions.) Second, the difference between  $T_A$  and  $T_S$  is independent of sensor length for a given temperature difference. Third, the ultrasonic temperature is higher than the average temperature, when  $\beta$  is a positive constant (as is usual for solids, with but few exceptions), because the sound wave spends more time in the hotter portions of the sensor, thereby weighting the velocity in favor of higher temperatures. (An opposite weighting occurs in gaseous media, or where  $\beta$  is negative, because here the wave spends a "disproportionate" amount of time in the colder parts of the path.)

Temperature Profiling. From the above, it follows that a point-by-point profile may be obtained with reasonable accuracy (error =  $dT$ ) even if each of the sensors used is so long that the temperature difference  $\Delta T$  over their length is much greater than  $dT$ :  $\Delta T \gg dT$ . (This means that sensor length per se does not impose the limit on the shortest path over which temperature can be averaged ultrasonically.)

Theoretically, this is most easily illustrated with a hypothetical linear temperature distribution. Let the distribution be  $T = 100x$ , for  $0 \leq x \leq 50$  inches, and with  $T$  measured in  $^{\circ}R$ . The assumed distribution is sketched below, together with individual corrected ultrasonic temperatures that would be obtained in relatively long Re sensors positioned as shown.

In the following, we show that despite the use of a relatively long sensor (which might be necessitated by low frequency pulses, i. e., attenuation-free pulses), temperature may still be determined in small regions, only  $\sim 1$  to 2 inches long. For simplicity, we treat only the linear temperature distribution.

Referring to the sketch, the first pair of lines may be denoted "overlapping lead-in wires." Their possible application has been suggested in the Dragon Project. This pair may be useful to the extent that transit times are identical in both lines, up to the end of the shorter line. Their use is not restricted to situations wherein the approximate shape of the temperature distribution  $T(x)$  is known. In principle these two lines effectively define a 2 inch sensor between  $x = 48$  and  $x = 50$  inches, for the example illustrated on p. 57.

Consider next the overlapping 8 inch and 10 inch sensors. Again, the objective is to determine the average temperature between  $x = 48$  and  $x = 50$  inches. We assume a linear temperature distribution  $T(x) = ax + b$ , and make two observations:

$$4500^{\circ}R = \frac{1}{10} \int_{x=40}^{50} (ax + b) dx = \frac{1}{10} \left[ \frac{ax^2}{2} + bx \right]_{40}^{50} = 45a + b$$

$$4400^{\circ}R = \frac{1}{8} \int_{x=40}^{48} (ax + b) dx = \frac{1}{8} \left[ \frac{ax^2}{2} + bx \right]_{40}^{48} = 44a + b$$

from which  $a = 100^{\circ}\text{R/inch}$  and  $b = 0$ . From this one readily calculates the average temperature between  $x = 48$  and  $x = 50$  inches:

$$T_{48-50} = \frac{1}{2} \left[ 50 x^2 \right]_{48}^{50} = 4900^{\circ}\text{R}.$$

Consider next the two overlapping 10 inch sensors. Again assuming  $T(x) = ax + b$ , we observe:

$$4500 = 45 a + b$$

$$4300 = 43 a + b$$

from which  $a = 100^{\circ}\text{R/inch}$  and  $b = 0$  as before. Likewise,  
 $T_{48-50} = 4900^{\circ}\text{R}.$

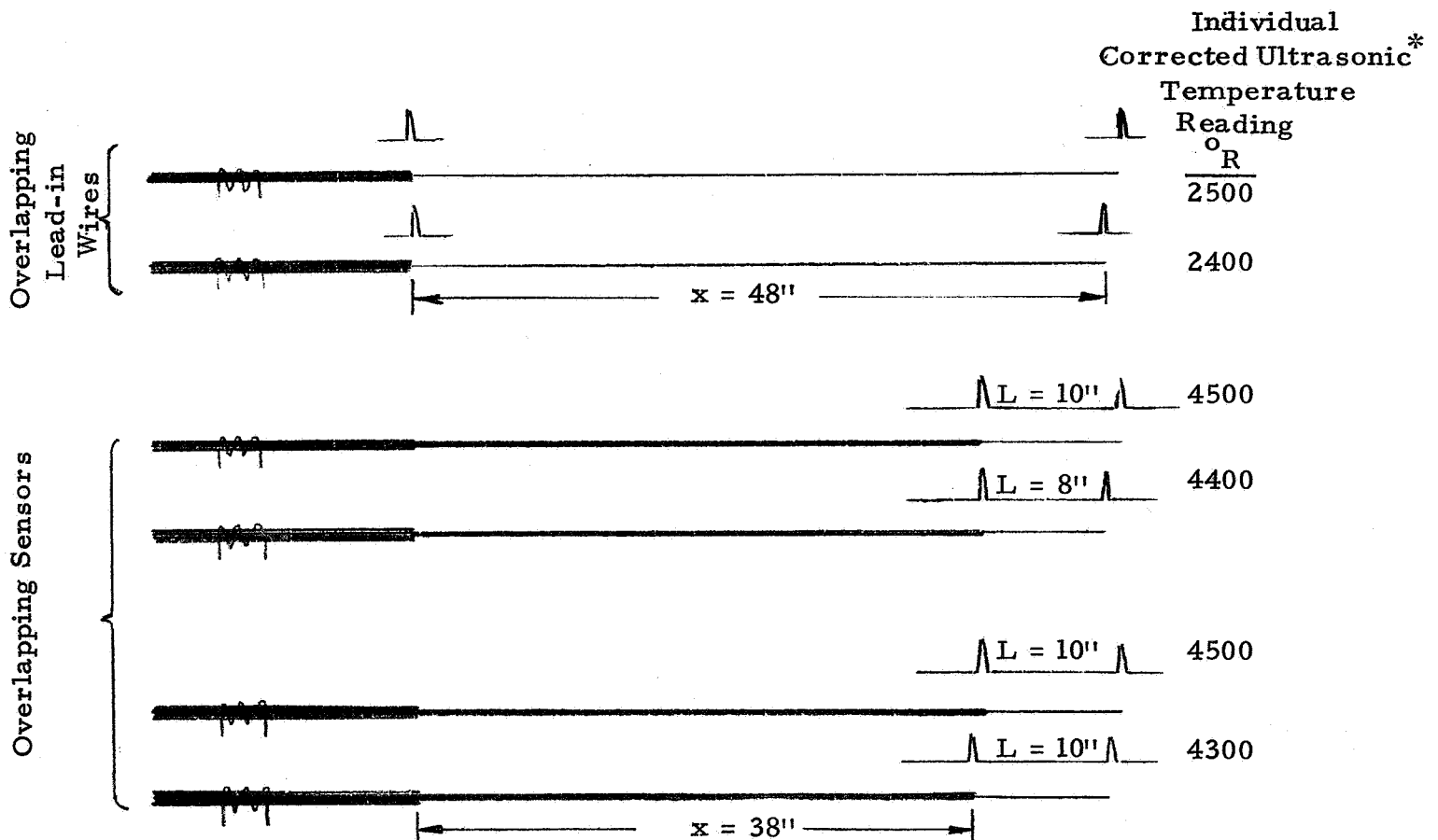
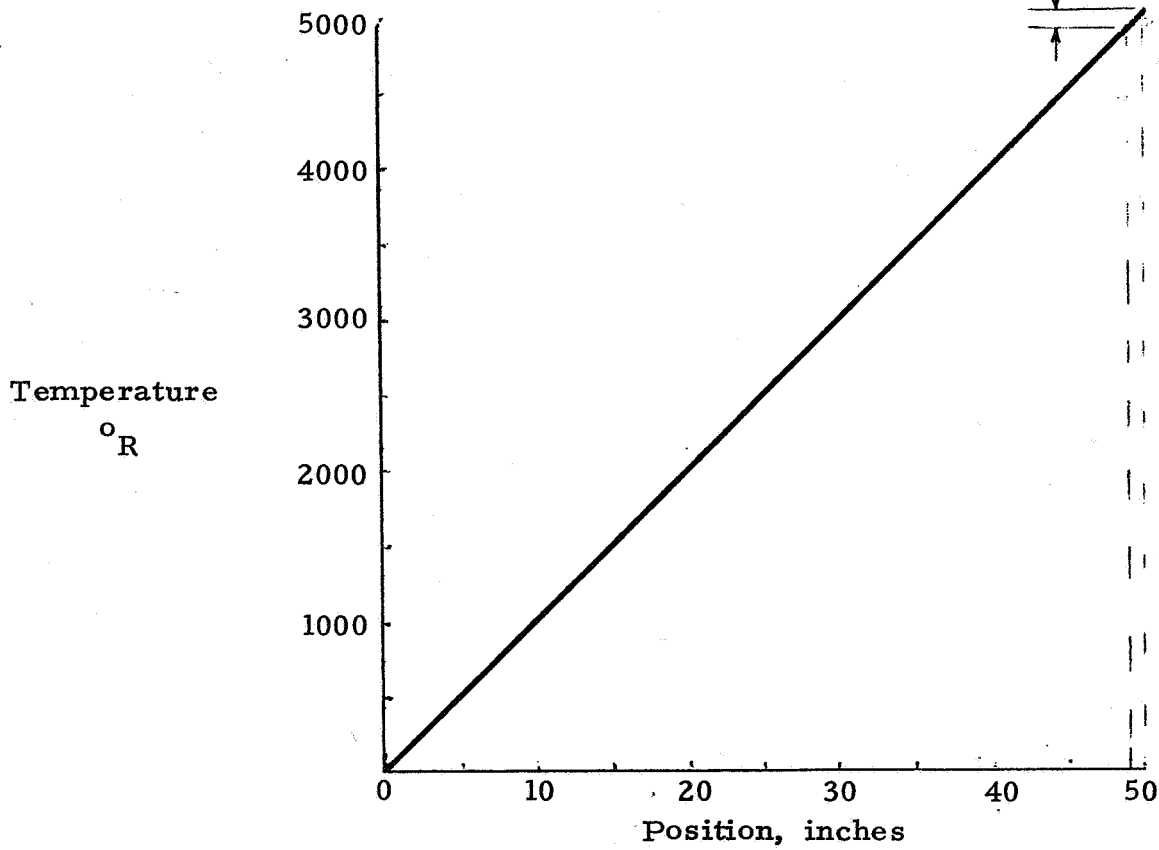
Thus, for a linear temperature distribution (i. e., linear over the distance spanned by the sensors), long overlapping sensors can yield the average temperature over the short differential path defined by the relative positions of the two sensors.

By combining the overlapping lead-ins and the overlapping sensors, several local averages can be obtained.

If we go one step further now, and consider a large number of overlapping sensors, the data obtained would be quite analogous to that obtained in differential path measurements in gases having a temperature gradient. Such measurements have been adequately described in the literature (16, 17, 32) and need not be reiterated here.

The significance of the above may be summarized as follows: first, in a given sensor, the ultrasonic temperature very nearly equals the arithmetic mean temperature, and second, a sequence of differential path measurements can yield the temperature profile, each calculated "point" being localized to a region much smaller than the sensor length itself.

$$T_A = 4900^{\circ}\text{R}$$



\* These readings are predicted assuming (1) a linear temperature distribution  $T = 100x$ , and (2) that  $T_S$  has been corrected and made exactly equal to  $T_A$ .

## APPENDIX II

### METHODS FOR MEASURING ULTRASONIC VELOCITY

Most of the velocity data in this report are normalized to the room temperature velocity  $V_0$ . The reason for presenting  $V/V_0$  rather than  $V$ , as a function of temperature, radiation exposure, etc., is to provide curves applicable to sensors of arbitrary length. This procedure is appropriate provided the delay in transmission through the "kink" or discontinuity between lead-in and sensor is negligibly small ( $< 0.1\%$ ) compared to sensor transit time. Even when the discontinuity delay is not negligible, calibration of a particular length sensor can be made in terms of  $V/V_0$ .

When it is desired to establish  $V_0$  itself, differential path techniques are generally most appropriate. These techniques have been described in the literature (ref. 16, 17, 32; see also footnote, p. 70). Simply stated, changes in transit time are measured for different path lengths. In uniform materials, such measurements yield data as indicated schematically in Fig. 27a.

$V_0$  may be established without destroying the specimen by temporarily coupling an impedance discontinuity to the surface of the specimen. This discontinuity might be in the form of a blade (edge straight or circular) or it may be the edge or corner of a cylindrical member such as a micrometer spindle or extension thereof. A reflection is produced at the point of application of the discontinuity. (The reflection amplitude depends on the material and shape of the reflector, and the coupling between reflector and line.) The reflector may be a spherical or cylindrical member which can be coupled to the specimen in cases where a sharper reflector might mar, scratch or otherwise degrade the surface of the specimen. Longnose pliers have been used for approximate measurements of  $V_0$ .

By moving the discontinuity, or reflector, the source of an ultrasonic reflection moves through the region of interest in the medium. Path length may be changed continuously, or in discrete steps, depending on the accuracy required, time and equipment available for the measurement, etc.

Figs. 27a and b diagrammatically show two methods of continuously varying the path, to test thin wires, rods, strip or tubing for uniformity of velocity, or flaws.

Using the dial indicator, Fig. 27a, or the micrometer, Fig. 27b, as direct reading instruments, displacements from  $\sim 0.0001$  to  $\sim 6$  inches are readily obtained. For greater accuracy in measuring displacement, one may use a linear variable differential transformer. A microwave reflectometer system might be employed to measure distances under ideally favorable circumstances to  $\sim 1 \mu$  inch.

Experimentally, a question arises as to whether one should vary the path  $x$  by an amount corresponding to fiducial marks on the distance-measuring device, and interpolate transit time  $t$ , or vice versa. In some cases it is simpler to vary  $x$  by fixed increments, say 10 mils, 20 mils, etc., and interpolate  $t$  on an oscilloscope. Better accuracy is usually achieved, however, by varying  $x$  until the echo coincides with fiducial marks (calibrated time marks) on the oscilloscope. Then one interpolates to read  $x$ .

If transit times are read on the Pana-Therm Model 5000, it is again convenient to vary the path until the transit time changes by multiples of  $0.1 \mu\text{sec}$ .

The concept of moving reflection points along the wire to establish velocity was applied to the determination of wire uniformity. Here, two reflection points 3 inches apart were obtained by manually squeezing two pairs of  $1/2$  inch diameter dowel pins against opposite sides of refractory wires (Fig. 28). In one case, a tantalum wire exhibited a 7% velocity variation along its length.

### APPENDIX III

#### ULTRASONIC THERMOMETRY BASED ON AMPLITUDE MEASUREMENTS

While the major emphasis in this program is on ultrasonic thermometry based on velocity measurements, it may be of interest to note that measurement of echo amplitudes may in some cases offer alternative approaches.

One of these approaches, demonstrated by Thorne (18), involves observing the presence or absence of echoes associated with the melting or solidification of materials contacting the wire. (This effect might be further emphasized by using shear waves instead of extensional waves.)

Another approach, not yet demonstrated, involves measuring the amplitude reflection coefficient. The amplitude reflection coefficient  $R = (Z_2 - Z_1) / (Z_2 + Z_1)$  where the  $Z$ 's are the acoustic impedances  $\rho VA$  of the first and second materials seen by the extensional wave, and  $\rho$  = density,  $V$  = sound velocity and  $A$  = cross sectional area of the materials ( $A \ll \lambda^2$ ). When  $Z_2 > Z_1$ ,  $R$  is positive. When  $Z_2 < Z_1$ ,  $R$  is negative. When  $Z_2 = Z_1$ ,  $R$  is zero.

For a given material,  $\rho V$  is a function of temperature, and  $\rho VA$  is a function of size. In particular, for a round wire,  $A$  is a function of diameter, namely,  $A = \pi \times \text{diameter}^2 / 4$ .

Figure 29 shows  $\rho VA$  vs temperature for wire materials 1 and 2. Wire 1 is of diameter  $D_1$ , and wire 2, of diameters  $D_2$  and  $D_2'$ . Intersection points correspond to temperatures  $T$  and  $T'$  of zero reflection at the junction of materials 1 and 2 of the diameters indicated. On passing through these "points of no (echo) return" the phase of  $R$  changes sign, going from + to - or - to +. Thus, a positive or negative error signal is readily obtained, when temperature is above or below the set point. The set point is adjusted by choice of wire materials and diameters. The reflection  $R$  can be made zero, or a positive or negative signal at the set point, but zero may generally be the preferred value.

By using a series of connected wires, one can measure temperature distribution, by observing the phases of  $R$  at successive junctions. Furthermore, in the vicinity of a set point, the magnitude of  $R$  is proportional to the temperature deviation from the set point.

Thus, measurement of phase and amplitude of R can, in principle, be used to determine and control temperature, up to the melting or eutectic point of the materials being used.

Elsewhere, we have noted that attenuation may provide a cross-check on temperature. The Dragon Project work suggests that this might be particularly effective at phase changes.

It is to be noted that one of the practical limitations on amplitude-dependent techniques is the nature of the noise present, and the S/N ratio. Also important, the effects of contamination, structural details, feedthroughs, etc., may influence attenuation measurements more than velocity measurements.

## APPENDIX IV

### METHODS OF TEMPERATURE MEASUREMENT

In this program, six methods of temperature measurement were considered relative to calibrating the sensor:

1. Pyrometer
2. Thermocouple
3. Resistivity
4. Melting Point/Eutectic Point/Phase Change
5. Sound velocity in gas:  $V = \sqrt{\gamma RT/M}$
6. Sound velocity in calibrated, adjacent sensor

Mostly, methods 1 and 2 were used, generally in routine fashion.

Resistivity data are available for most metals. For the refractory metals, including rhenium, resistivity vs temperature is known in most cases to  $\sim 5000^{\circ}\text{R}$  or higher (37).

Calibration (of thermocouples) via melting point indications has been reported up to the melting point of tantalum (38). To extend this method to acoustic sensor calibration, a thin wire of a pure metal whose melting point is well known would be strung across the sensor and its melting observed either optically, or, if it exerts a sufficient surface pressure, through the sudden disappearance of its acoustic reflection. The temperature recorded in this case should be properly corrected for alloying effects. It has been reported that platinum and molybdenum give clear, reproducible melting point indications when strung across tungsten. Additionally, some metals and metal alloy sensors have built-in check points in the sense that they will exhibit sharp velocity changes at eutectic points or points of phase changes whose temperatures are generally well established.

Another way of measuring high temperatures is through the well known dependence of acoustic velocity on the absolute temperature of a perfect gas:  $V = \sqrt{\gamma RT/M}$ . The specific heats and the molecular weight of an inert monatomic gas, such as helium, at low densities, are very insensitive to temperature even up to  $10,000^{\circ}\text{R}$ . This method is therefore viewed as a potential primary temperature standard. The

method has already been exploited at cryogenic temperatures by Plumb and Cataland (39) at NBS, while we have demonstrated high temperature measurements of sound velocity up to  $\sim 30,000^{\circ}\text{R}$  (32).

Finally, if an unknown wire sensor is placed alongside a known wire sensor, previously calibrated, and the two are heated inside a cavity (e. g., a long tube) then the velocity/temperature curve for the unknown may be established.

## APPENDIX V

### RADIATION TEST CAPSULE DESIGNS

The following capsule designs are presented because of their possible interest in related studies. Note that none of these designs were tested in a radiation environment in the present program.\*

#### Unheated, Acoustically Monitored Capsule

This capsule would permit wire samples to be acoustically monitored continually during irradiation, but would not provide any heating. Access would be through a thin welded diaphragm.

#### Heated, Monitored Capsule

This capsule would permit acoustic monitoring of wire samples, and in addition, would permit temperature to be controlled up to 5000°R. One can use gamma heating to achieve an elevated temperature of several thousand °R, and use supplementary electrical heating which may be required for further annealing at temperatures up to 5000°R.

#### Gamma Plus Electrical Heating

The reasons for choosing gamma plus electrical heating over either heating type alone are as follows. If gamma heating were used alone, it would be difficult to control or adjust the temperature distribution and maximum temperature. Assuming thorium or uranium gamma heaters, temperature increase in the B & W test reactor of about 2000°R can be expected at the axis, for an outside wall temperature of 500°R. Thus, these heaters could not achieve 5000°R. Also one could not easily determine the minimum temperature at which adequate annealing occurs. To study different wires, different gamma heated capsule constructions would be required, probably one per wire type. Temperatures can be lowered to some degree by flowing cold He gas through the capsule. Possibly, higher temperatures could be attained with composite gamma heaters, for example, a tungsten center, surrounded by a dense, insulating ceramic.

On the other extreme, if electrical heating were used alone, the entire heating burden falls on one, or possibly two or three,

---

\* The designs were analyzed and in a few cases were mocked up to determine construction and assembly feasibility with relation to the Babcock & Wilcox test reactor.

electrical elements. Should a heater open up, the remaining heaters might not be able to sustain the required temperatures.

By taking advantage of the high gamma flux available, one can establish some intermediate temperature, several thousand  $^{\circ}\text{R}$ , for example, and then raise this temperature as required by energizing the electrical heater(s). Thus, by using both gamma and electrical heating, a more reliable, more easily regulated high temperature capsule is achieved.

A proposed design of heated capsule is shown schematically in Fig. 34. A coiled refractory metal foil serves as a dual purpose heater (i. e., gamma plus electrical heater). Foil thickness is about 0.001 inch. Between turns, a refractory insulator in the form of a powder is uniformly dispersed, and this insulator also serves more than one purpose. First, it reduces the thermal conductivity in the radial direction. Second, it electrically insulates the turns from one another, so that a hot resistance, of the order of ten ohms, can be developed between the innermost and outermost layers of the coiled heater. This resistance is easily heated by using a Variac, and current levels of 10 to 20 amp. Third, the refractory insulator is also a gamma heater.

The current path through the coil is seen to spiral through the entire length of the coil. The power generated in any turn is proportional to the resistance of that turn. Since the resistivity of metals generally increases nearly linearly with temperature, electric power dissipation will follow the temperature distribution very closely.

In a given volume, to achieve more gamma heating, one chooses a greater proportion of dense metal, and a lesser portion of insulator. (In the present case, the outside diameter of the capsule is limited to  $\sim 1\text{-}3/4$  inch.)

The use of coiled refractory metal for thermal radiation shielding has been demonstrated at NASA-Lewis by Ebihara and Kaczmarek (41). Ebihara and Kaczmarek\* typically use about 3 turns

---

\* Private communications (Oct. 14, 1965).

of 0.001 inch thick tungsten foil, with turns separated by "tungsten wool," as a thermal radiation shield around a thicker tungsten cup susceptor (2 inch diameter x 3 inches high x  $\sim 0.050$  inches thick) inductively heated at 10 kHz. In their work susceptor temperatures of 5000 to 6000 $^{\circ}$ R were achieved routinely.

To optimize the Fig. 34 capsule design with respect to coil and insulation proportions, calculations and experiments can be performed for several cases. In one limiting case, for example, about 100 feet of 0.001 inch foil would be heated, and the insulating particles would separate the turns by about 0.002 inches. Spacing is limited by the availability of fine mesh refractory powder. It appears that thorium, for example, is presently commercially available in particles no finer than 0.0017 inches diameter.

To electrically simulate gamma heating, one should dissipate heat throughout the heater in a manner that duplicates the absorption of the gamma rays in question: more intense at surface, less intense in the interior. However, electrical heating, dc or 60 cycle, leads to more concentrated  $I^2R$  heating near the center of the coiled foil capsule heater, where temperatures and resistivity are highest. One can partly offset this tendency, if required, by insulating only between every second or third turn (or  $n$ th turn, in general) in the hotter portions. Thus, the increased cross sectional area of shunted turns would offset the increased resistivity at elevated temperature. (Another approach would be to use a solid susceptor and an rf frequency such that the skin depth approximates the "half-value" layer thickness for the gammas.)

Babcock and Wilcox, Lynchburg, Va., suggested another approach to a gamma heated plus electrically heated capsule. In this design, the gamma heated portion is surrounded by a concentric electrically heated tube. This tube need be heated only to a moderately elevated temperature, according to the Babcock and Wilcox suggestion, to substantially reduce radial heat loss out of the gamma heated portion. If the gamma portion is well insulated, the hottest parts of the capsule could theoretically reach temperatures well above the temperature of the electrically heated tube (for example, temperature rise of  $\sim 2000^{\circ}$ R for thorium or uranium tubular gamma heater). This design, however, would exhibit low thermal diffusivity, and so the hot zone temperature could not be changed quickly. Nevertheless, one experiment was planned, Fig. 35, in which one would measure the electrical

power  $P_1$  required to maintain particular hot zone temperatures  $T_1$ , as a function of nichrome temperature  $T_2$ .  $P_1$  would be dissipated in a coiled wire (e.g., Mo).  $P_1$  is intended to simulate the power that would have to be generated by gamma ray absorption in the insulation in the absence of the (Mo) wire. Departing slightly from the Babcock and Wilcox suggestion, two electrical elements could be used. For example, the nichrome tube and the (Mo) coil could be connected in parallel. Nichrome's resistivity increases very slightly with temperature,  $\sim 7\%$  on heating from 500 to 2500 $^{\circ}$ R, whereas the resistivity of Mo increases by more than an order of magnitude (5.7 to 80  $\mu\Omega$ -cm; see Ref. 40, p. A-4) on heating from 500 to 5000 $^{\circ}$ R. Through suitable proportioning of the two heaters, one can arrange the elements so that at low temperatures Mo would draw most of the power. As temperature increased, Mo would dissipate a smaller fraction of the total electrical power. Thus, paradoxically, Mo would govern the lower temperatures, and nichrome would govern the higher temperatures. This arrangement should afford faster heating and better control of the hot-zone temperature, than the use of the nichrome tube as the only electrical heater.

## APPENDIX VI

### ATTENUATION MEASUREMENTS

A material attenuates ultrasonic waves by various mechanisms. One of the more common means of describing the attenuation is the logarithmic decrement  $\delta$ . This is the natural logarithm of the ratio of amplitudes one period of vibration apart in time, or one wavelength apart in space, and is written as:

$$\delta = \ln \frac{A_n}{A_{n+1}} = \frac{A_n - A_{n+1}}{A_{n+1}} = \pi Q^{-1}$$

where  $Q^{-1}$  represents the tangent of the phase angle between stress and strain. Attenuation may also be measured by observing the decrease in amplitude of a travelling wave as it passes through a body. It is appropriate to relate the amplitude at some point  $A_x$  to the initial amplitude  $A_0$  through the relation  $A_x = A_0 e^{-\alpha x}$ ,  $\alpha$  being the attenuation coefficient. The attenuation coefficient,  $\alpha$ , and the logarithmic decrement,  $\delta$ , are related by the following expression:

$$\alpha (\text{db}/\mu\text{sec}) = 8.686 \times 10^{-6} f (\text{sec}^{-1}) \delta (\text{nepers})$$

where  $f$  is the frequency.

Several of the more important attenuation mechanisms are: scattering from grains, effects of dislocations, thermal conductivity of the material, thermoelastic effect, and effects due to heat exchange between electrons and phonons in the solid (44). The mechanism or mechanisms which contribute to the attenuation will be dependent upon the material being examined, frequency, vibration modes, and the environment, especially temperature. In this program, ultrasonic attenuation larger than  $\sim 1$  db/ft has been measured for the first time in refractory wires for frequencies ranging up to 300 kHz, and for temperatures beyond 4500°R (Fig. 44). These preliminary measurements have been made on molybdenum, tungsten, rhenium, and tungsten-

rhenum wires. Preliminary attenuation determinations indicate a relatively sudden increase in attenuation beyond a particular temperature for each metal, possibly corresponding to the recrystallization temperature.

There are various experimental procedures that are generally used to measure attenuation, the most important being the resonance technique, multiple pulse echo, and the differential path technique. Damping measurements can be made with the resonance technique by making the specimen oscillate at its own resonant frequency and then observing the rate at which these oscillations decrease in amplitude once the driving force has stopped. This method has been found useful for frequencies up to the low ultrasonic range. Shown in Fig. 45a is a schematic of a method for the measurement of attenuation for a freely decaying vibration.

With the multiple pulse echo technique the attenuation is obtained by measuring the relative amplitudes of successive reflections within the specimen. On an oscilloscope, a number of equally spaced peaks of decreasing height, each representing a consecutive reflection, will be observed. In the first approximation, at least, the peak height theoretically decreases exponentially with distance and the absorption coefficient is obtained from the logarithmic decrement of the peaks, or the time constant of the envelope's decay. This method is usually used in the frequency range from  $\sim 3$  to 100 MHz or higher. Shown in Fig. 45b is the exponential decay of the peaks. This method might not be very satisfactory when working with several wires that are welded together, end-to-end, due to the uncertainty in the reflection coefficient and due to the poor signal to noise ratio for the signals following the second reflection.

The differential path length technique (16, 32) uses the pulse echo and/or the through transmission method, but it also varies the length of the specimen that is being investigated. With this method one measures the amplitude of the ultrasonic wave for at least two different acoustic path lengths. (One of these paths,  $x_1$ , may be so short that  $e^{-\alpha x_1} \approx 0$ .) Then, one calculates the attenuation coefficient (Fig. 45c). At a given temperature, when the length of the sensor is changed, the end echo height will change and then the attenuation coefficient can be determined. If the pulse echo technique is used, it is possible to ignore the uncertainties in the value of the reflection and transmission coefficients, and the ratio of the signal to noise generally

will be larger than if multiple echoes in the wire were used. The differential path method appears applicable to wires in the frequency range 20 kHz to 3 MHz. We used this method\* for refractory wires ~ 2 inches to ~ 2 feet long, at temperatures ranging up to 5000°R. Oscillograms obtained with this method are given in Fig. 46.

---

\* The differential path method has also been applied in determining plate (~ Lamb) wave attenuation at room temperature by L. Niklas, "Plattenwellen," *Materialprüfung* 4 (1) 12-20 (1962). Niklas tested an aluminum sheet 1.5 m long x 1 m wide x 1 mm thick at a frequency of 2 MHz. Using sheet metal shears, strips of about 25 mm width were cut off the sheet (perpendicular to beam) and the increase in echo amplitude was measured as a function of path length, in the far field. Niklas demonstrates how one separates the decrease in intensity due to beam divergence (power law) from the decrease due to absorption and scattering (exponential law). See also R. Frielinghaus and J. Koppelman, "Genaue Schallschwächungsmessungen mit handelsüblichen Ultraschall-Impulsecho-Geräten" (Accurate measurements of ultrasonic attenuation by means of commercial ultrasonic pulse-echo devices), *Materialprüfung* 6 (10), 337-342 (Oct. 1964). This latter paper deals with coupling losses.

## ACKNOWLEDGMENTS

The authors gratefully acknowledge the contributions of the following personnel who assisted in the experiments at Panametrics: S. L. Klaidman, R. N. Lawson, T. Lynch, L. J. Remington, Jr. and B. J. Spencer. S. S. Fam and M. S. McDonough contributed to this report, especially to the appendixes on temperature distribution and attenuation, respectively. The authors are also indebted to Professor J. F. W. Bell of the Royal Naval College, Greenwich, and T. A. J. Jaques and E. A. Thorne of the A.E.E., Winfrith, for personally communicating the detailed background and art of their thin wire ultrasonic thermometry. E. A. Thorne was kind enough to visit us and help set up some of the experiments early in the program. His able assistance, and the cooperation of the A.E.E. which made his visit possible, are sincerely appreciated. Particular thanks are also due M. O. Dustin of NASA-Lewis, for continued guidance and support during the conduct of this program. Finally, we acknowledge the cooperation of personnel at Westinghouse Astronuclear Laboratory, especially G. Remley and G. J. Zellner.

## REFERENCES

- (1) Mayer, A. M., "On An Acoustic Pyrometer," Phil. Mag., 45 (1873), p. 18. Background information on acoustic techniques and applications at elevated temperatures is given by Carnevale, E. H., pp.73-103 in Mannella, G. G. (ed.), NASA SP-132, Aerospace Measurement Techniques for sale by Supt. of Doc., U.S. Govt. Printing Office, Wash., D. C. 20402 (\$1.00) (1967).
- (2) Anderson, J. A. and Smith, Sinclair, "General Characteristics of Electrically Exploded Wires," Astrophys. J., 64 (1926), pp. 295-314.
- (3) Sherratt, G. G. and Griffiths, E., "The Determination of the Specific Heat of Gases at High Temperatures by the Sound Velocity Method I-Carbon Monoxide," Proc. Roy. Soc., A147 (1934), p. 292.
- (4) Apfel, J. H., "Acoustic Thermometry," Rev. Sci. Instr., 33 (1962), pp. 428-430. U.S. Patent No. 3,214,977 (Nov. 2, 1965).
- (5) Suits, C. G., "The Determination of Arc Temperature From Sound Velocity Measurements," Physics, 6 (1935), p. 190.
- (6) Livengood, J. C., Rona, T. P. and Baruch, J. J., "Ultrasonic Temperature Measurement in Internal Combustion Engine Chamber," J. Acoust. Soc. Am., 26 (1954), p. 824.
- (7) Carnevale, E. H., Poss, H. L. and Yos, J. M., Temperature-Its Measurement and Control in Science and Industry, Reinhold Publishing Corp., New York, N. Y., (1962), Vol. 3, Part 2, pp. 959-967.
- (8) Bell, J. F. W., Hub, D. R. and Smith, S. G., "Elastic Properties of Graphite," Dragon Project Rpt 5, A.E.E. Winfrith (Oct. 1960). (See preface.)
- (9) Bell, J. F. W., "The Velocity of Sound in Metals at High Temperatures," Phil. Mag., 2 (8) (1957), pp. 1113-1120. (Origin of "notched wire" technique.)

## REFERENCES (Cont'd)

- (10) Bell, J. F. W., "Some Acoustic Effects at Phase Changes," Paper J52, Proceedings of the Fourth International Congress on Acoustics, Copenhagen (1962) (Organization Committee of the 4th ICA and Harlang and Toksvig, Copenhagen, 1963), Pt. I.
- (11) Bell, J. F. W., Doyle, B. P., Smith, B. S., "An Instrument for the Measurement of Acoustic Pulse Velocity and Attenuation in a Solid Probe," J. Sci. Instrum., 43 (1) (1966), pp. 28-31.
- (12) Frederick, J. R., A Study of the Elastic Properties of Various Solids by Means of Ultrasonic Pulse Techniques, Ph.D. thesis, Univ. of Mich. (1947). (Origin of "notched bar" technique); Frederick, J. R., "Ultrasonic Measurement of the Elastic Properties of Polycrystalline Materials at High and Low Temperatures," J. Acoust. Soc. Amer., 20 (1948), p. 586(A).
- (13) Lynnworth, L. C. and Carnevale, E. H., "Ultrasonic Thermometry and Flaw Detection in Steel Above 2000°F," Abstract Materials Eval. 22 (9) (Sept. 1964), p. 423, presented at Society for Nondestructive Testing 24th National Convention, Philadelphia, Pa. (Oct. 19-23, 1964).
- (14) Lynnworth, L. C. and Carnevale, E. H., "Ultrasonic Testing of Solids at Elevated Temperatures," Proc. Fifth Int. Conf. on Nondestructive Testing, Montreal (21-26 May 1967).
- (15) Carnevale, E. H., Lynnworth, L. C. and Larson, G. S., High Temperature Measuring Device, NASA CR-54339 (Feb. 1, 1965); Lynnworth, L. C. and Carnevale, E. H., Techniques for Mounting an Ultrasonic Temperature Device, NASA CR-54979 (Feb. 1966).
- (16) Carnevale, E. H., Lynnworth, L. C. and Larson, G. S., "Ultrasonic Determination of Transport Properties of Monatomic Gases at High Temperatures," J. Chem. Phys. 46 (8) 3040-3047 (15 April 1967); Carnevale, E. H., Carey, C. and Larson, G., "Ultrasonic Determination of Rotational Collision Numbers and Vibrational Relaxation Times of Polyatomic Gases at High Temperatures," J. Chem. Phys. 47, (8) 2829-2835 (15 Oct. 1967).

## REFERENCES (Cont'd)

- (17) Lynnworth, L. C., Carnevale, E. H. and Carey, C. A., "Hot-Gas Measurements with Ultrasonics," Space/Aeronautics 48 (4) 121-128 (Sept. 1967); "Ultrasonic Thermometry in Solids and Gases at Elevated Temperatures," paper III-B, in Proc. Fifth Temperature Measurements Society Conf. and Exhibit, Hawthorne, Calif. (March 14, 15, 1967).
- (18) Thorne, E. A., "The Measurement of High Temperatures by the Determination of the Velocity of Sound Waves in Materials," Paper P23, Proc. of the Fourth International Congress on Acoustics, Copenhagen (1962).
- (19) In circumferentially magnetized wires, a torsional wave may be launched, according to the Wiedemann effect. See, for example, Tzannes, N. S., Wiedemann Sonic Delay Line, Ph.D. Thesis, Johns Hopkins Univ., (1966); "Joule and Wiedemann Effects - The Simultaneous Generation of Longitudinal and Torsional Stress Pulses in Magnetostrictive Materials," IEEE Trans. on Sonics and Ultrasonics, SU-13 (2) 33-41 (July 1966). See also Brockelsby, C. F., et al, Ultrasonic Delay Lines, Iliffe Books, Ltd., London (1963), Chapter 6 and Davidson, S., "Wire and Strip Delay Lines," Ultrasonics 3 (3) 136-146 (July-Sept. 1965).
- (20) Mason, W. P., Piezoelectric Crystals and Their Application to Ultrasonics, Van Nostrand, Princeton, N.J., 508 pp. (1950).
- (21) Materials Engineering 66 (2) 19 (Aug. 1967).
- (22) Faris, F. E., Green, L., Jr., and Smith, C. A., "The Thermal Dependence of the Elastic Moduli of Polycrystalline Graphite," J. Applied Physics 23, p. 89 (Jan. 1952).
- (23) Johnson, S. O. and Dull, R. B., WADD TR 61-72, Vol. 23 (April 1963).
- (24) Armstrong, P. E. and Brown, H. L., "Dynamic Young's Modulus Measurements Above 1000°C on Some Pure Polycrystalline Metals and Commercial Graphites," Trans. Met. Soc. AIME, 230 (Aug. 1964), pp. 962-966. See also Kalugin, B. A. and Mikhailov, I. G., Akust. Z. 12 (1) 114-116 (1966); Sov. Phys.-Acoust., 12 (1) 91-92 (July-Sept. 1966).

## REFERENCES (Cont'd)

- (25) Brown, H. L. and Armstrong, P. E., "Young's Modulus Measurements above 2000°C," Rev. Sci. Instrum. 34 (6) 636-639 (June 1963).
- (26) Shaffer, P. T. B., High-Temperature Materials, No. 1, Materials Index, Plenum Press, New York (1964).
- (27) Köster, W. and Rauscher, W., Z. f. Metallkunde 39, 111-120 (1948).
- (28) Schwarzkopf, P. and Kieffer, R., p. 156, Refractory Hard Metals-Borides, Carbides, Nitrides and Silicides, Macmillan, New York (1953).
- (29) Touloukian, Y. S., (ed.) Thermophysical Properties Research Literature Retrieval Guide, Plenum Press, New York (1967).
- (30) Gonser, B. W., Rhenium, pp. 108-109, Elsevier Publishing Co., Amsterdam, New York (1962); J. E. Hughes, Assoc. Elec. Ind. Rpt. No. A497 (Nov. 1955).
- (31) Rose, F. K. and Metcalfe, A. G., Advanced Method to Test Thin Gage Materials, AFML-TR-66-318, 84-91 (Feb. 1967).
- (32) Carnevale, E. H., Larson, G. S., Lynnworth, L. C., Carey, C. A., Panaro, M. and Marshall, T., Experimental Determination of the Transport Properties of High Temperature Gases, NASA CR-789 (June 1967); Carnevale, E. H., et al, Phys. Fluids 10 (7) 1459-1467 (July 1967).
- (33) Pears, C. D., A Progress Report on a 6500°F Furnace for Thermophysical Property Studies, presented at the Thermal Cond. Conf. Gatlinburg, Tenn., (Oct. 1963); Pears, C. D., Digesu, F. J. and Woodward, J. D., The True Stress-Strain Properties of Brittle Materials to Very High Temperatures, Final Rept. to AEC, 1963-1964, under contract No. AT-(40-1)-2964 (Oct. 30, 1964); Research/Development 15 (8), cover, 9 (Aug. 1964).

## REFERENCES (Cont'd)

- (34) Ferris, J. R., Malarky, J. T. and Zellner, G. J., TME 1585, High Temperature Thermocouple Qualification Test Facility-Design Verification and Shakedown Testing (June 30, 1967), Confidential (NE-2469).
  
- (35) Jain, S. C. and Krishnan, K. S., "The Distribution of Temperature Along a Thin Rod Electrically Heated in Vacuo - I. Theoretical," Proc. of the Royal Soc., A, Vol. 222, pp. 167-180 (1954); II. "Theoretical (continued)," A, Vol. 225, pp. 1-7 (1954); III. "Experimental," A, Vol. 225, pp. 7-18 (1954); IV. "Many Useful Empirical Formulae Verified," A, Vol. 225, pp. 19-32 (1954); V. "Time Lag," A, Vol. 227, pp. 141-154 (1955); VI. "End-losses," A, Vol. 229, pp. 439-445 (1955); Krishnan, K. S. and Jain, S. C., "Determination of Thermal Conductivities at High Temperatures," British Journal of Applied Physics, Vol. 5, pp. 426-430 (Dec. 1954).
  
- (36) DMIC Rpt. 191, Engineering Properties of Tungsten and Tungsten Alloys, Battelle (Sept. 27, 1963).
  
- (37) Rudkin, R. L., Parker, W. J. and Jenkins, R. J., "Measurements of the Thermal Properties of Metals at Elevated Temperatures," pp. 523-534, in Herzfeld, C. M. and Dahl, A. I. (ed.), Temperature - Its Measurement and Control in Science and Industry, Vol. 3, Part 2, Reinhold, New York (1962).
  
- (38) Kocherzhinskiy, Yu. A., Kobzenko, G. F., et al, "Calibration of the V'R-5/20 (W-5% Re and W-20% Re) Thermocouple to Critical Points up to 3000°C. Determination of the Melting Points of Vanadium and Niobium of High Purity," AN UKRSSR. Institut Metalafiziki, Spornik Nauchnykh Rabot, (No. 17) 209-210 (1963), Foreign Techn. Div., AF Systems Command Translation FTD-TT-65-1888/1+2+4 (17 March 1966).
  
- (39) Plumb, H. H. and Cataland, G., Science, 150 (Oct. 8, 1965) pp. 155-161.
  
- (40) Schmidt, F. F. and Ogden, H. R., The Engineering Properties of Molybdenum and Molybdenum Alloys, DMIC Rpt. 190, Battelle Memorial Institute, pp. A-4 to A-6 (Sept. 20, 1963).

## REFERENCES (Cont'd)

- (41) Ebihara, B. T., NASA Tech Brief 65-10188 (June 1965).
- (42) Vines, R. F., The Platinum Metals and Their Alloys, The International Nickel Co., Inc., New York (1941).
- (43) Nadler, M. R. and Kempter, C. P., Rev. Sci. Instr. 32 43-47 (Jan. 1961); J. Chem. Phys. 64 1468-1471 (Oct. 1960).
- (44) Bhatia, A. B., Ultrasonic Absorption, Clarendon Press, Oxford (1967).
- (45) Hall, B. F., Jr., and Spooner, N. F., Study of High Temperature Thermocouples, AFCRL 65-251 (March 1965) (AD 619 038); "Temperature Measurement in a Graphite Environment from 1600 to 2500°C," ISA Preprint No. 16. 13-3-64 (Oct. 12-15, 1964).
- (46) Brown, E. A., Goodier, B. G., Perry, J. E., Jr., Petty, R. L., Prince, W. R. and Tallman, C. R., "Thermocouple Development for Project Rover," Section 31 (discusses shunt effects and sheath integrity) in High Temperature Thermometry, Wash-1067 (TID-4500) (March 1966), AEC Seminar, Wash., D. C., held Feb. 24-26, 1965.
- (47) Asamoto, R. R. and Novak, P. E., "A Survey for a High-Temperature Sensor for SEFOR," G. E. Atomic Power Eqpt. Dept. Rpt. GEAP-4903 (July 1965) under AT(04-3)-540, 2539-T10-2, 230-TM-7/65, Rev. Sci. Instrum. 38 1047-1052 (Aug. 1967); A 67-36515.
- (48) Brooks, E. J. and Kramer, W. C., Tungsten-Rhenium Alloy Thermocouples and Their Use in a UO<sub>2</sub>-Fueled Reactor; Argonne Nat'l. Lab Rpt. ANL-6981 (Nov. 1965).
- (49) Walker, R. F., "High Temperature Measurements and Standards," pp. 7-38 in International Union of Pure and Applied Chemistry, Commission on High Temperatures and Refractories, "High Temperature Technology," Proc. of an Int. Sym. on High Temp. Tech., organized and directed by Stanford Research Inst., Pacific Grove, Calif. (8-11 Sept. 1963), Butterworths, London (1964).

## REFERENCES (Cont'd)

- (50) Murray, T. P., Rev. Sci. Instrum. 38 (6) 791-798 (June 1967).
- (51) Gardner, A. R., Prod. Eng. 38 (20) 111-113 (Sept. 25, 1967).
- (52) Buckley, J. D. and Braski, D. N., "Dynamic Modulus of Stabilized Zirconia," presented at the 68th Annual Meeting of The American Ceramic Society, Wash., D. C. (May 7-12, 1966). Available from NASA Langley.
- (53) Gitzen, W. H., Alumina Ceramics, WPAFB AFML-TR-66-13 (Jan. 1966). AD 480064.
- (54) Soga, N., Schreiber, E. and Anderson, O. L., "Estimation of Bulk Modulus and Sound Velocities of Oxides at Very High Temperatures," J. Geophys. Res. 71 (22) 5315-5320 (Nov. 15, 1966).
- (55) Garofalo, F., J. Basic Eng. 82 867-881 (Dec. 1960); ASME paper 59-A-112.
- (56) Kyros, W., Gibbs, T. W. and Theberge, C. L., "A Resistance Heating Facility for Determination of Tensile Properties of Alloys for Aircraft and Missiles," Proc. ASTM, Phila. Pa., 63 1160-1184 (1963).

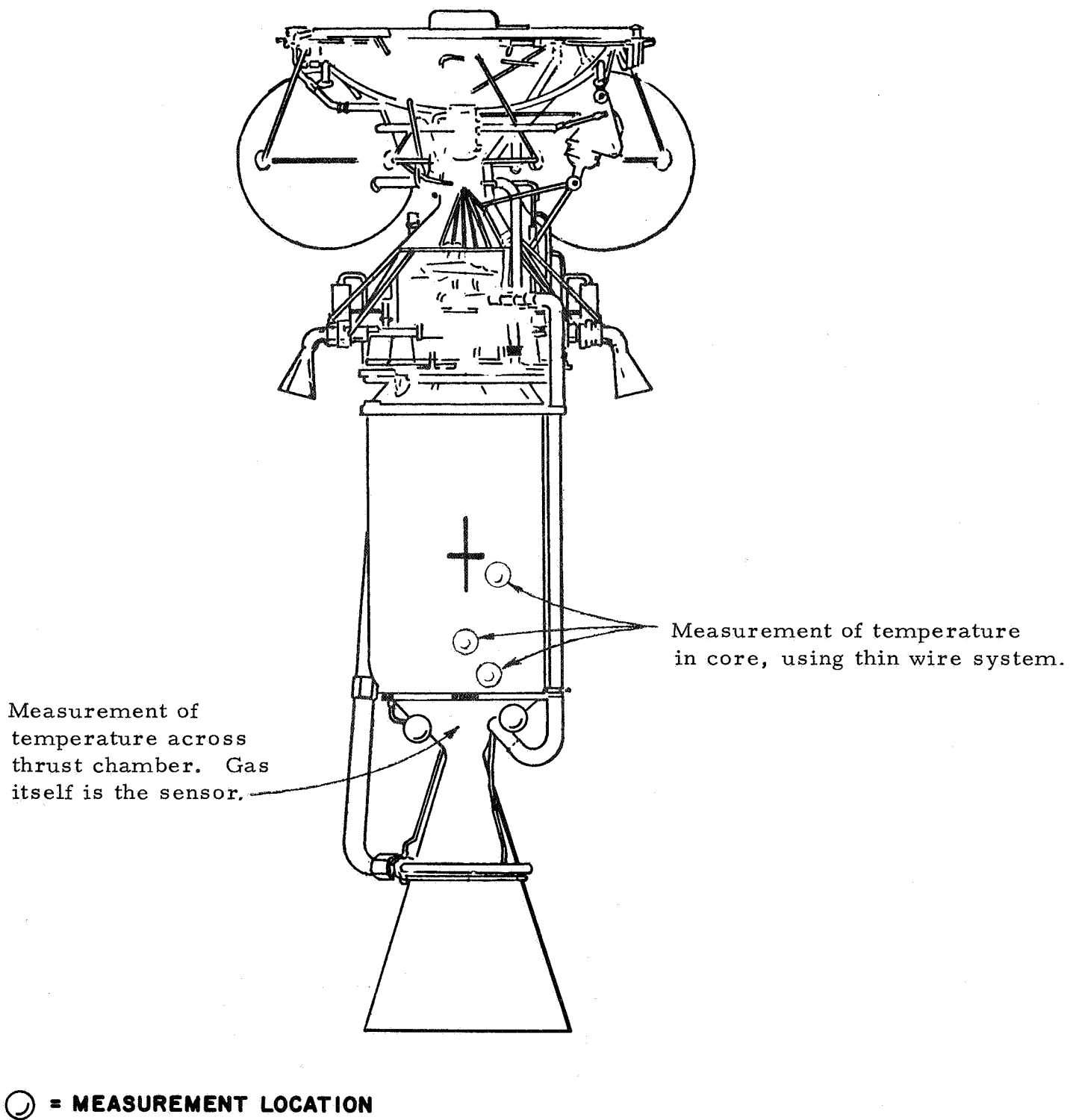


Figure 1. Nuclear rocket engine.

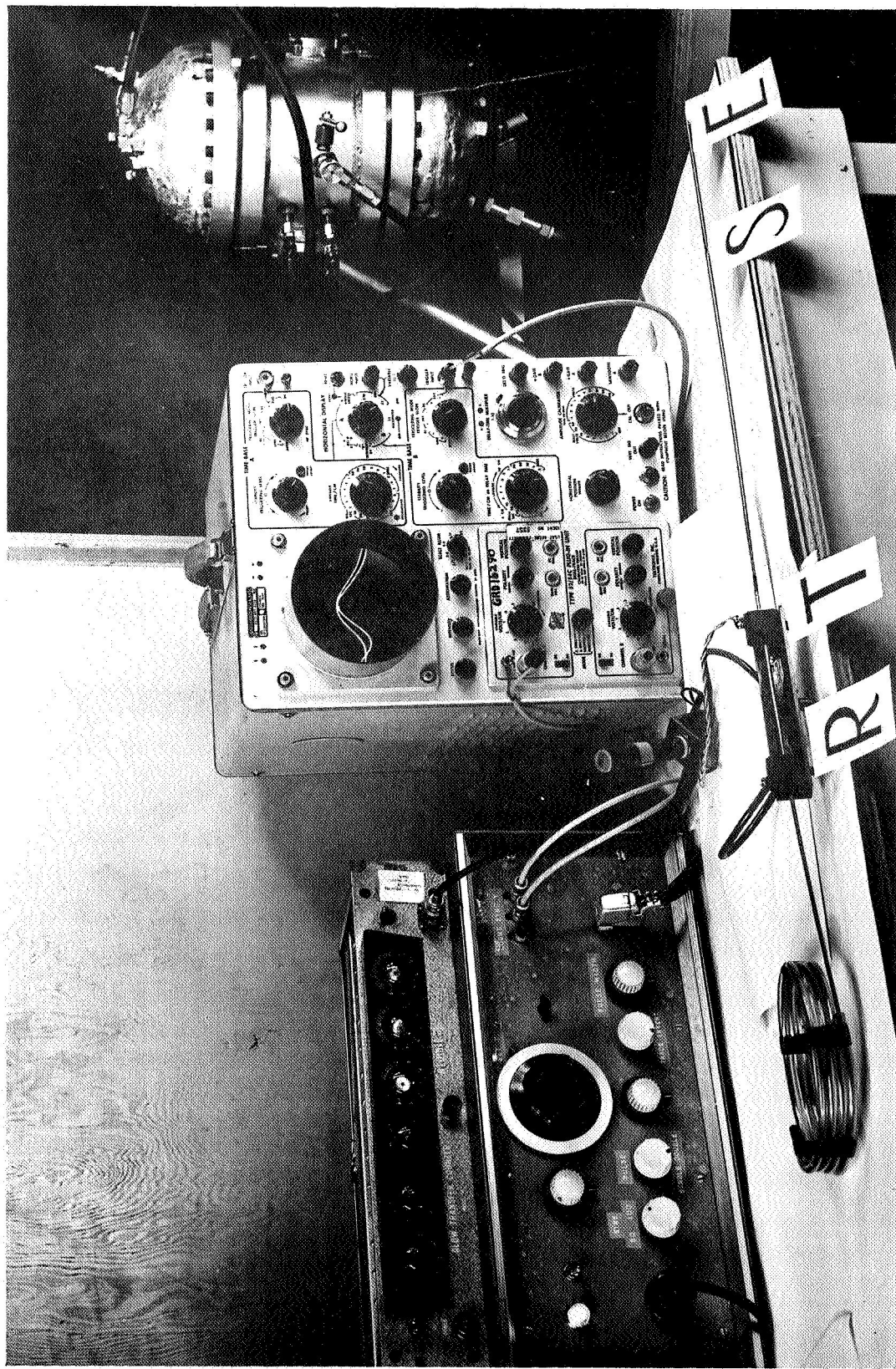


Figure 2. Ultrasonic thermometry system developed by Bell (8-11), Thorne (18) et al in Dragon Project. The ultrasonic line shown includes transmitter coil T, receiver coil R, shoulder S and end E. Electronics includes double pulser, oscilloscope for observing echoes, and counter. In the early part of the present program, this system was used at Panametrics to measure velocity in wires tested in the SRI oven.

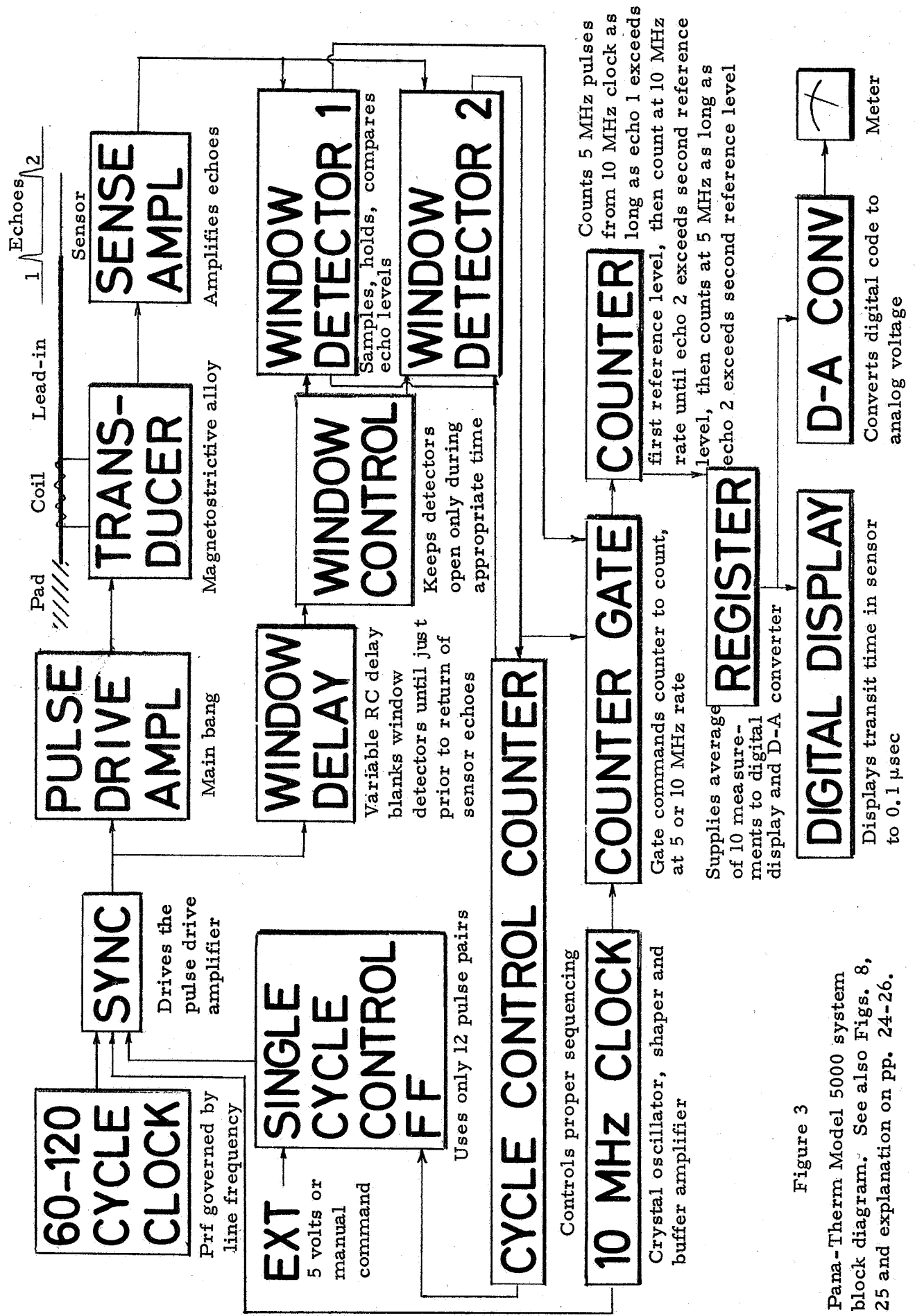


Figure 3

Pana-Therm Model 5000 system block diagram. See also Figs. 8, 25 and explanation on pp. 24-26.

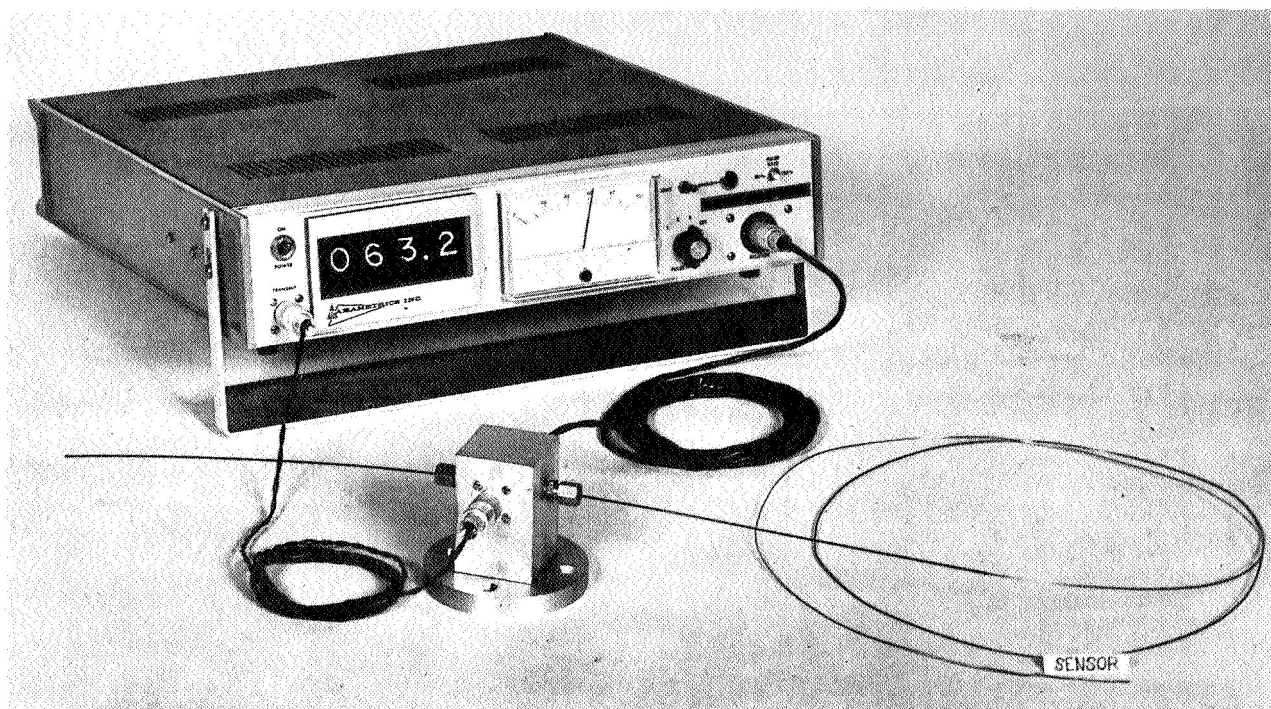


Figure 4. Pana-Therm Model 5000 automatically measures transit time in sensor, from which temperature is determined. The ultrasonic temperature measuring system illustrated here consists of the transmitter/receiver and readout instrument, transducer, lead-in wire and sensor.

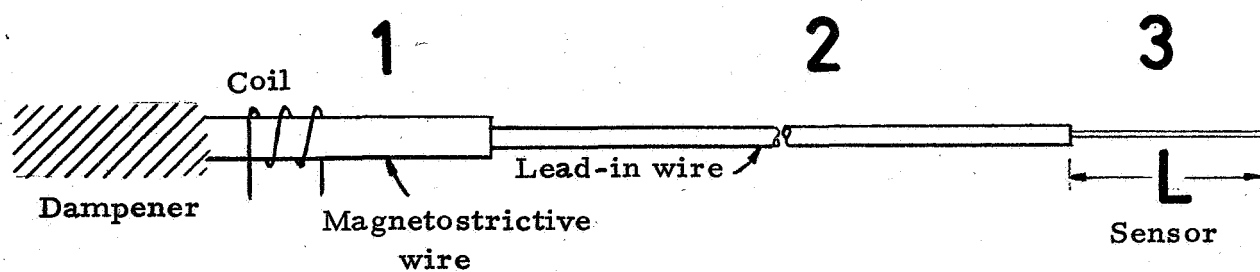


Figure 5a. Typical ultrasonic line.

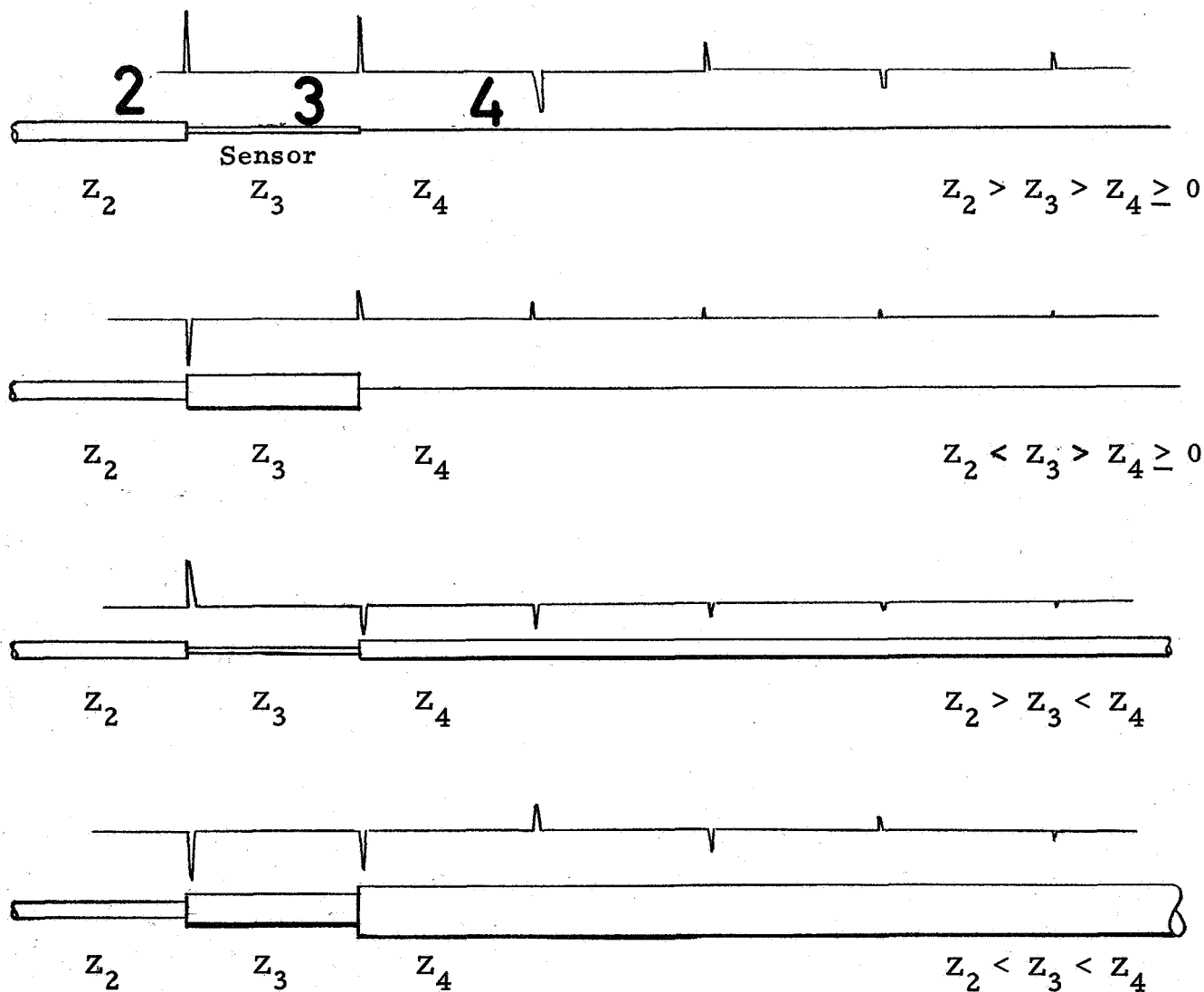


Figure 5b. Polarity of echoes for different ratios among  $Z_2$ ,  $Z_3$  and  $Z_4$ . As the pulse reverberates in the sensor, its relative polarity at any time depends on the number of reverberations, and the magnitudes of  $Z_2$  and  $Z_4$  relative to  $Z_3$ . (Amplitudes not drawn to scale.) (See also Fig. 14.) If the positive echoes are assumed to correspond to compression pulses, then the negative echoes correspond to rarefaction pulses. Polarities actually observed on an oscilloscope would depend on electronics, sense of coil(s) and magnetic bias(es).

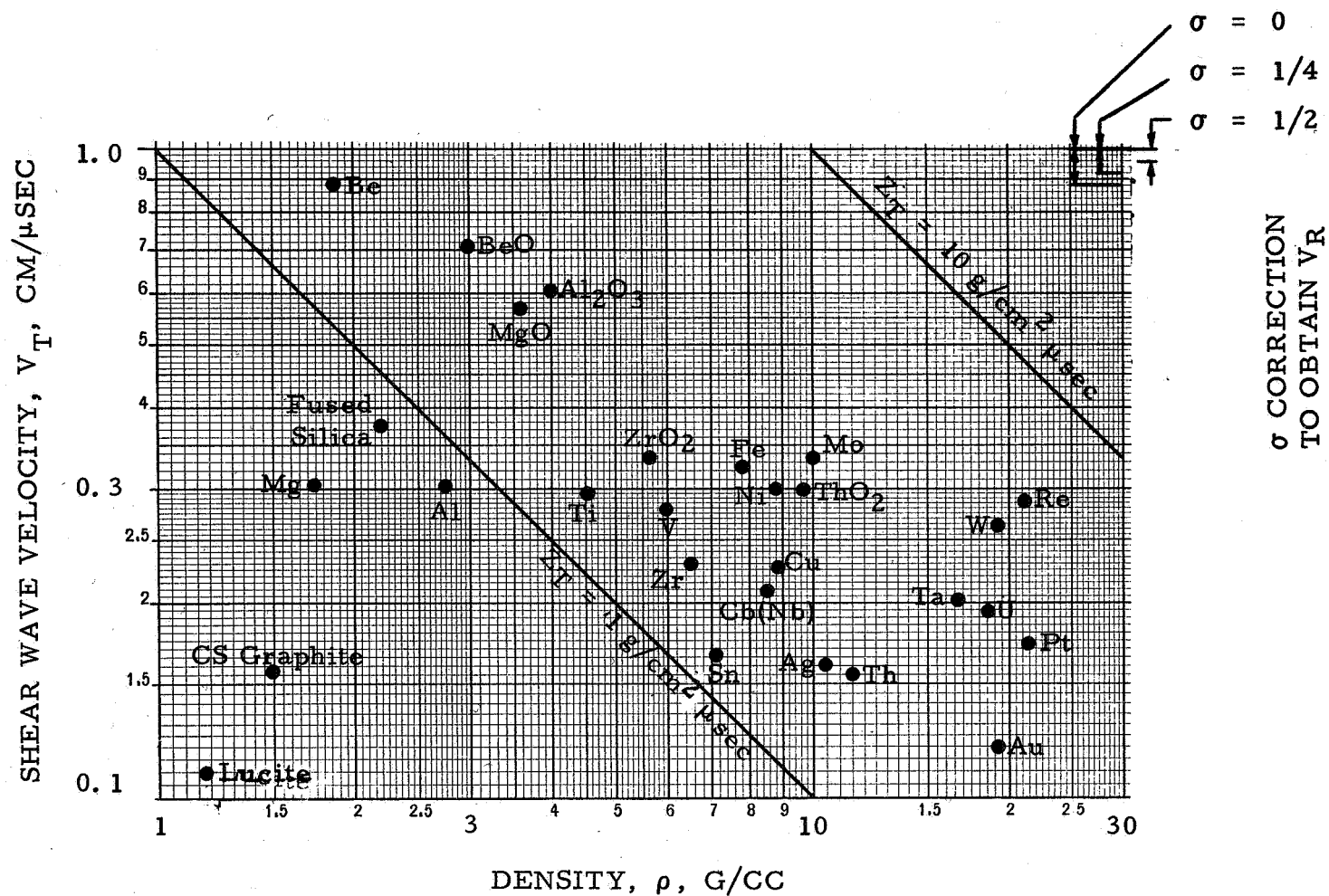


Figure 6. Shear wave characteristic impedance nomogram.  $Z_T = \rho V_T$  impedance values are used in calculating shear wave reflection and transmission coefficients. Room temperature data principally from ref. 20. Note: Some data are only approximations, the appropriate value depending on method of specimen preparation, working, heat treatment and test frequency. In scale at upper right,  $\sigma$  = Poisson's ratio, and  $V_R$  = Rayleigh (surface) wave velocity.

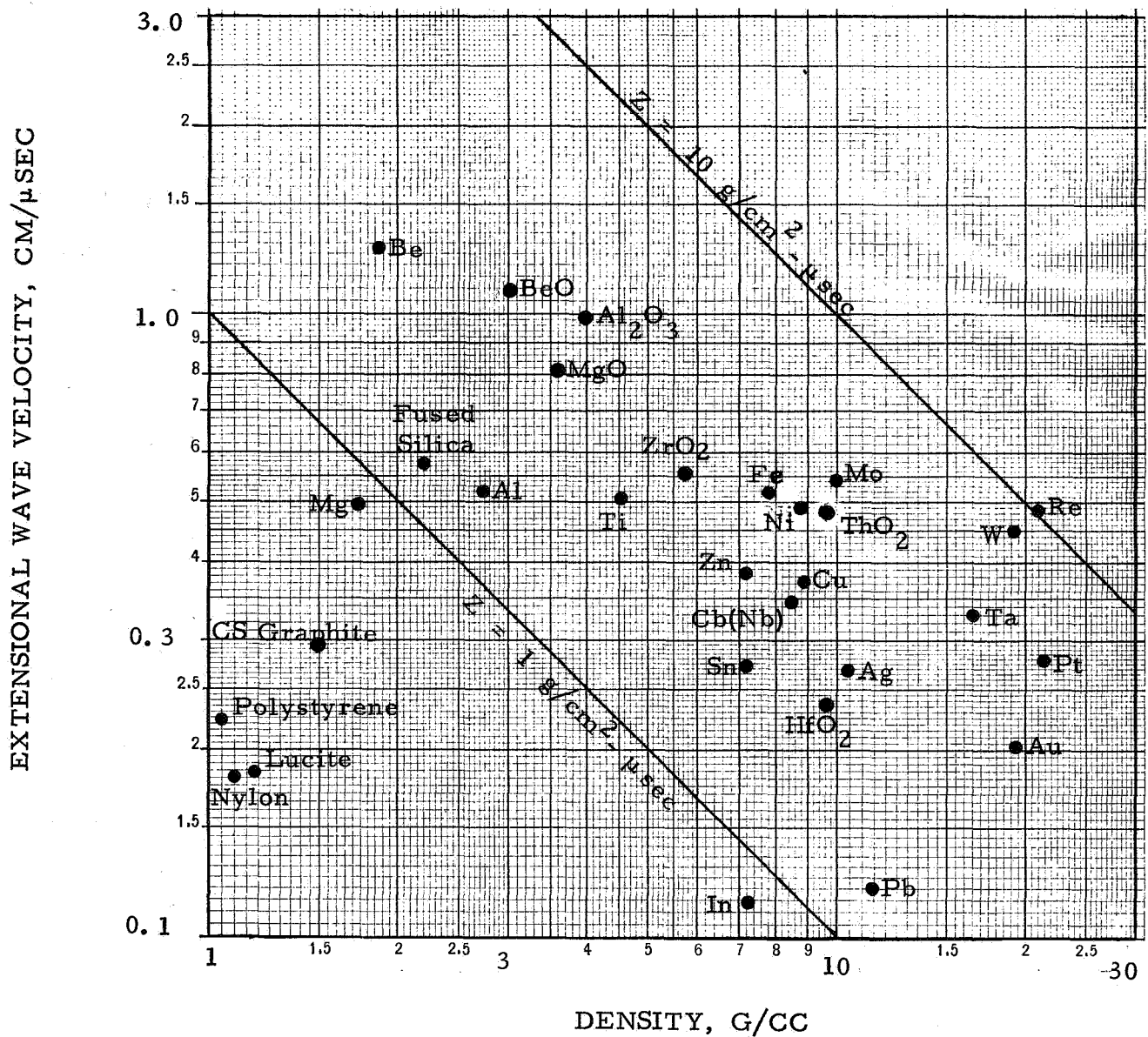


Figure 7. Extensional wave characteristic impedance nomogram.  $Z = \rho V_o$  impedance values are used in calculating extensional wave reflection and transmission coefficients. Room temperature data principally from ref. 20. Note: Some data are only approximations, the appropriate value depending on method of specimen preparation, working, heat treatment and test frequency.

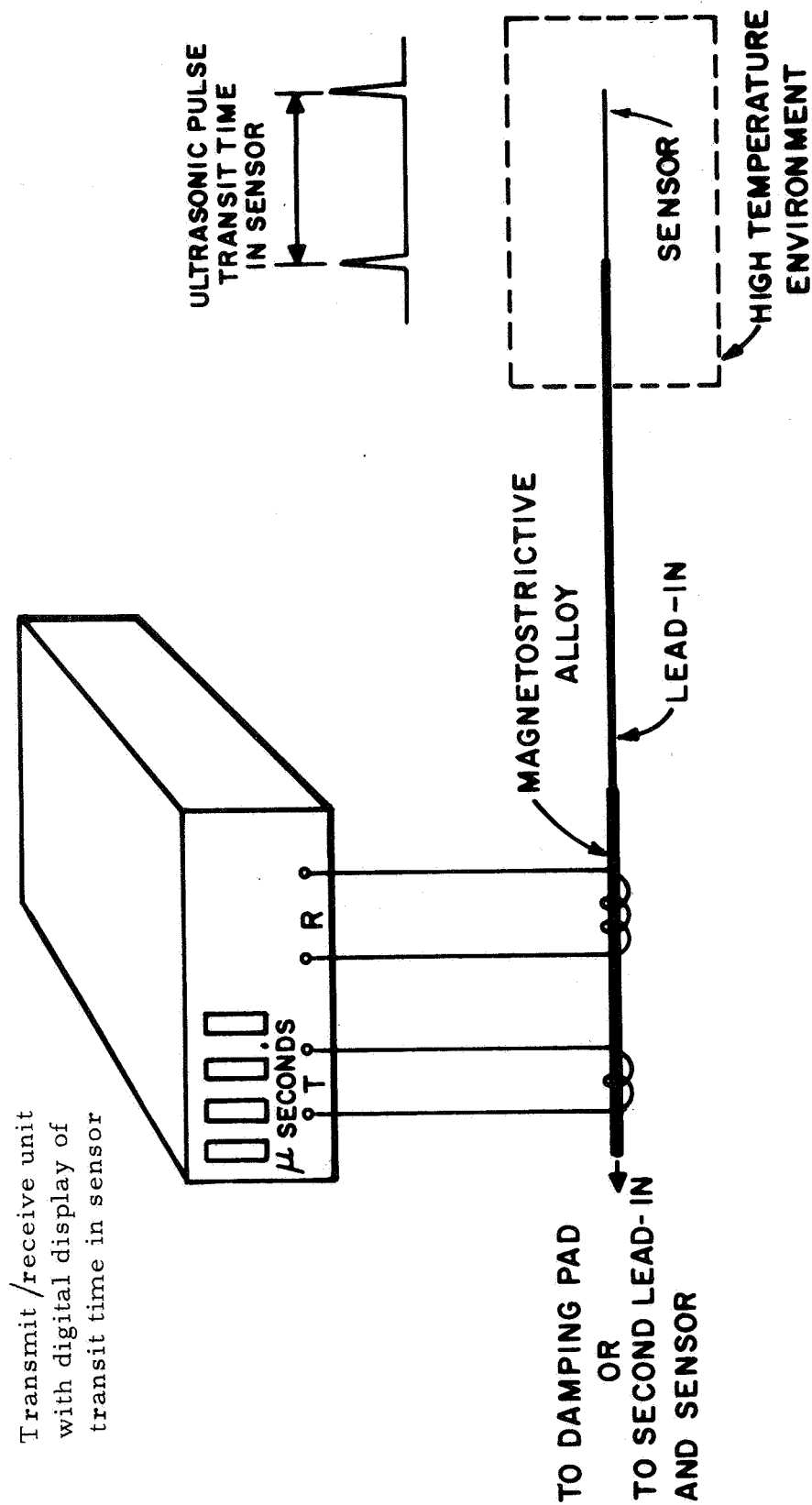


Figure 8. Schematic of automatic measurement of pulse transit time in sensor, using Pana-Therm Model 5000 (see also Figs. 3, 4, 25).

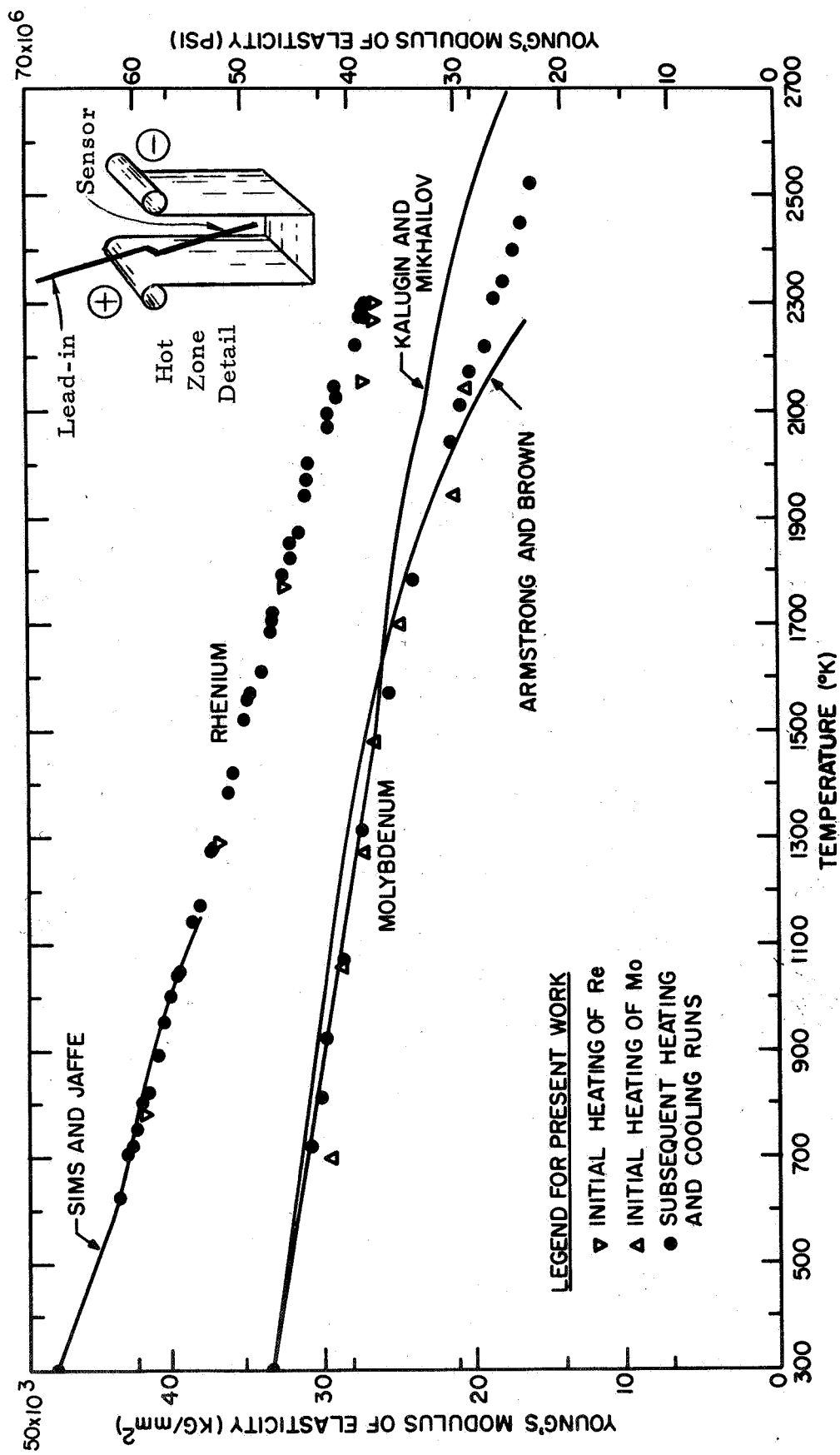
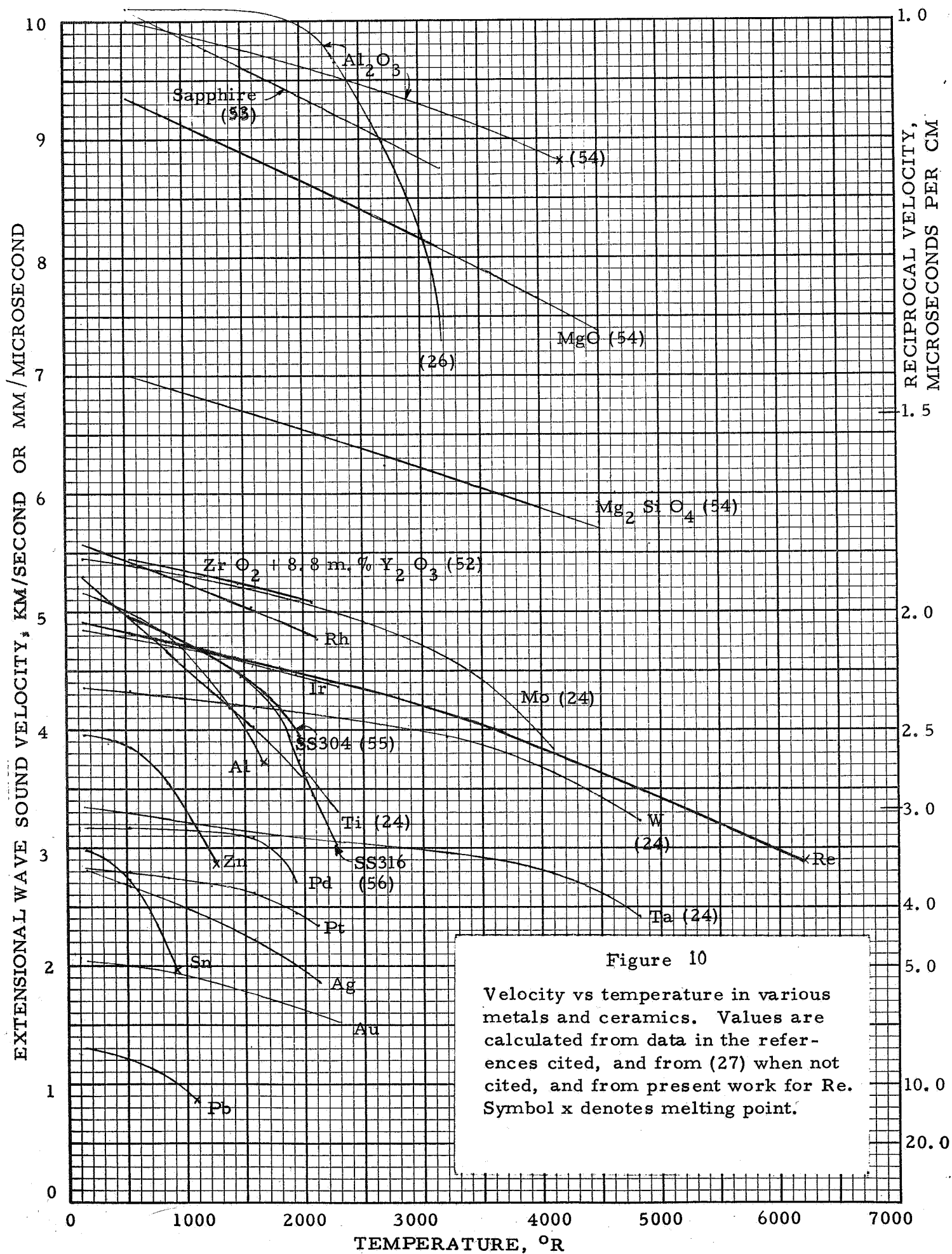


Figure 9. Young's modulus of elasticity vs temperature in Mo and Re. Experimental data points shown were obtained using Pana-Therm Model 5000 of Figure 4. Wire specimens were heated in vacuum by three-sided tungsten element as shown (Abar oven - see also Figs. 31a and b). Solid curves, from independent investigators (ref. 24, 30).



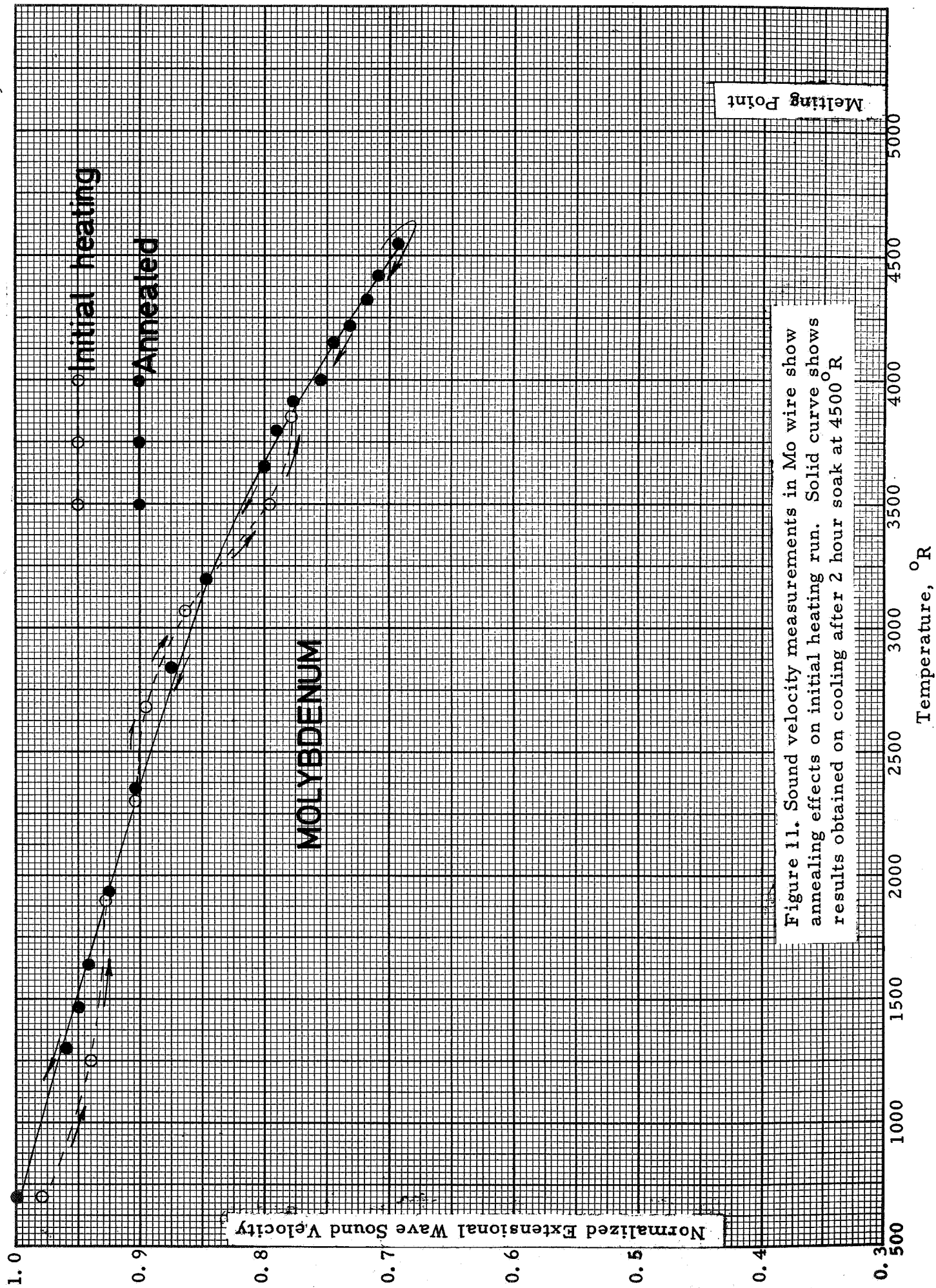
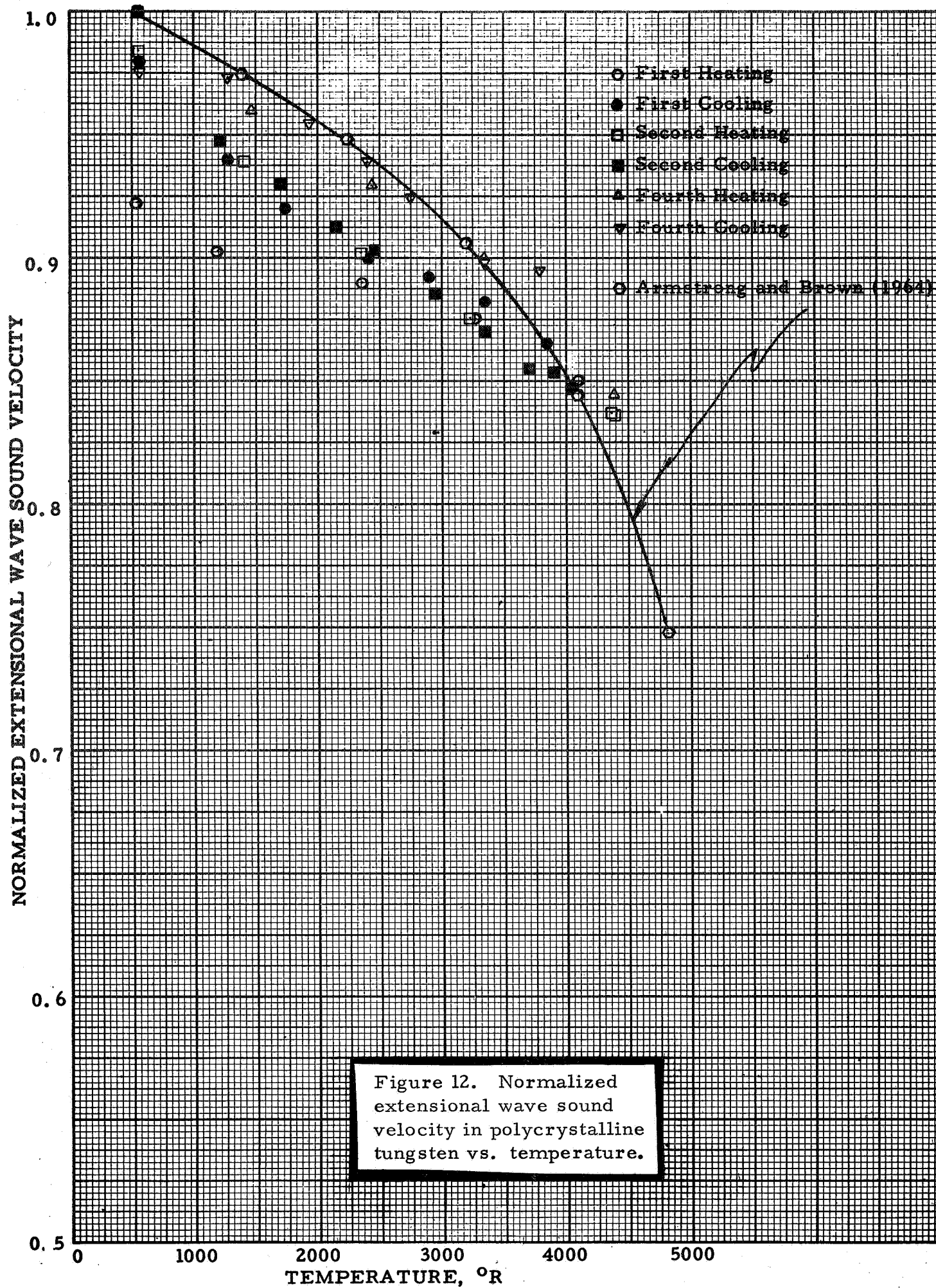


Figure 11. Sound velocity measurements in Mo wire show annealing effects on initial heating run. Solid curve shows results obtained on cooling after 2 hour soak at 4500°R



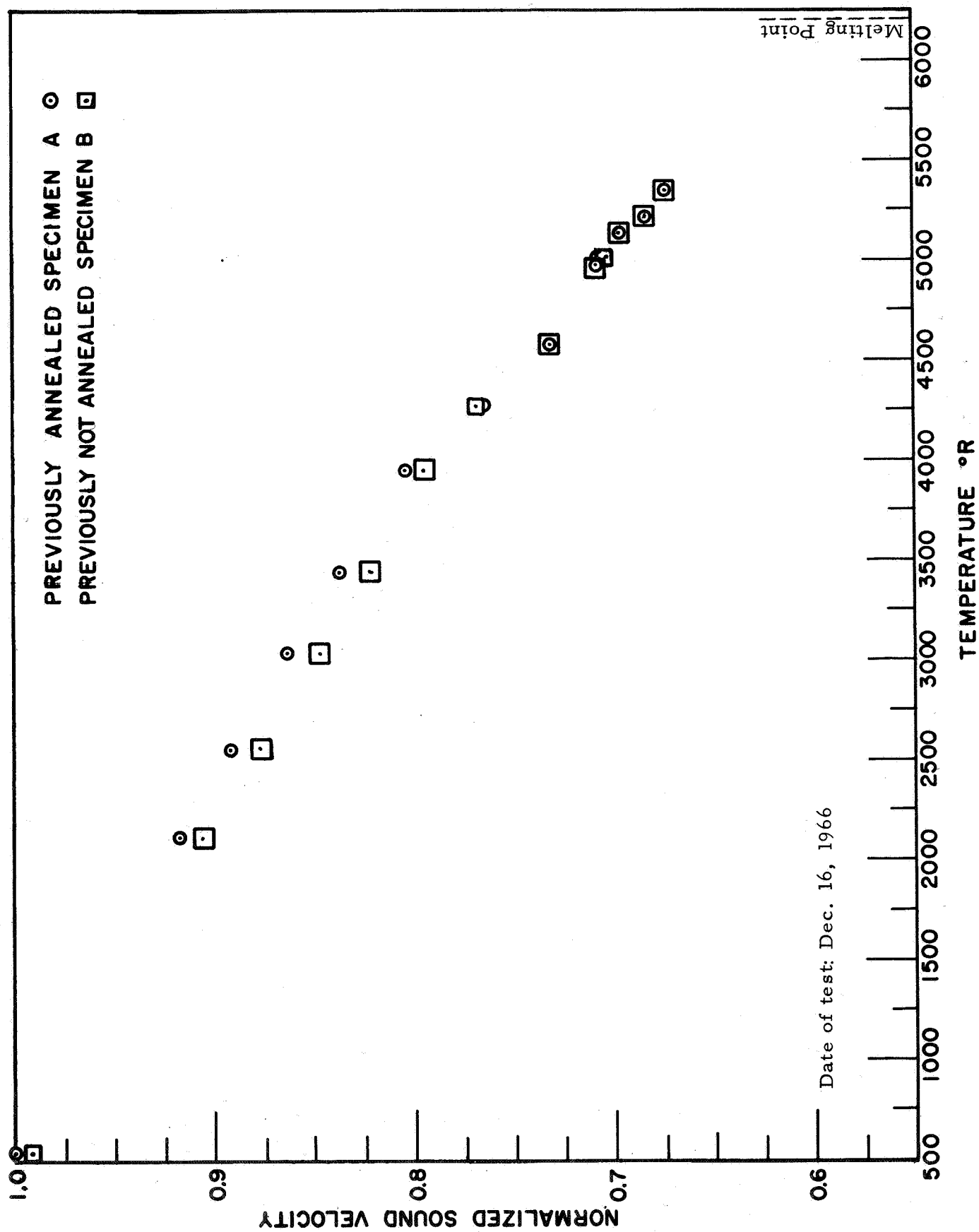


Figure 13. Normalized velocity vs temperature in two nonirradiated rhenium specimens.

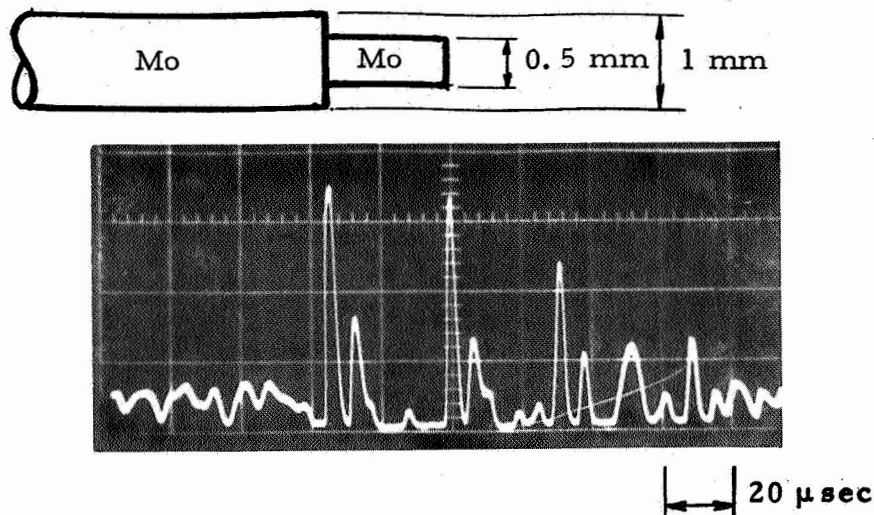


Figure 14. Room temperature echoes obtained with Pana-Therm Model 5000 from front and rear of 0.5 mm dia molybdenum sensor, flash butt welded to 1 mm dia molybdenum lead-in wire. Vertical sensitivity, 2 v/cm. (Note that transit time for first round trip traverse of the sensor is about 36  $\mu$  sec, but for second traverse it appears to be only about 32  $\mu$  sec. This apparent discrepancy is due to the rectification of the video triplet pulse. The true position of the echo for two traverses would be a negative spike (not shown, due to rectification) approximately midway between the two positive spikes observed about 32 and 38  $\mu$  sec after the centerline. See also Fig. 5b, for clarification of echo polarities due to multiple reflections within sensor.)

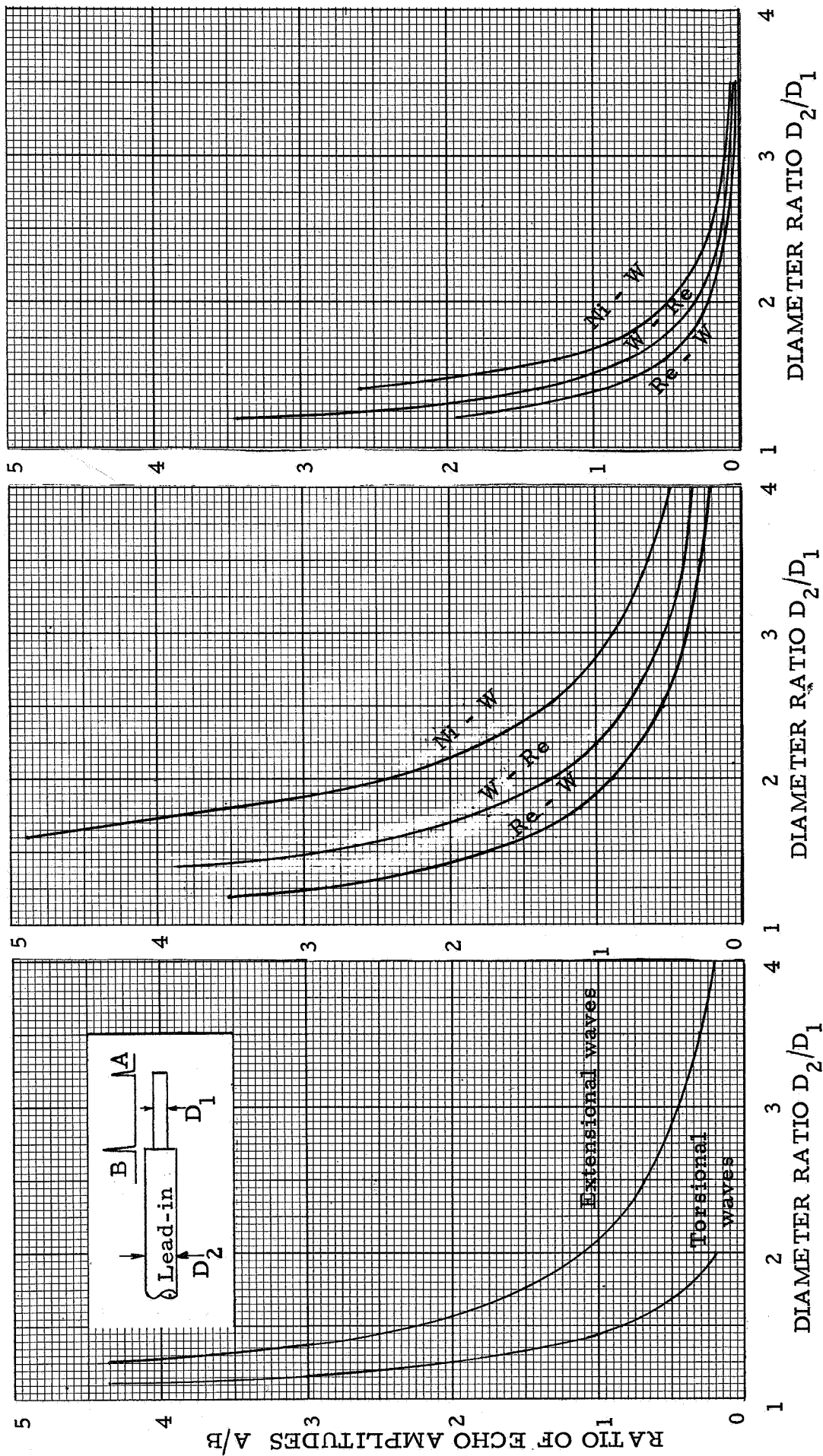


Figure 15a. Calculated echo amplitude ratio vs diameter ratio, for lead-in and sensor of same material.

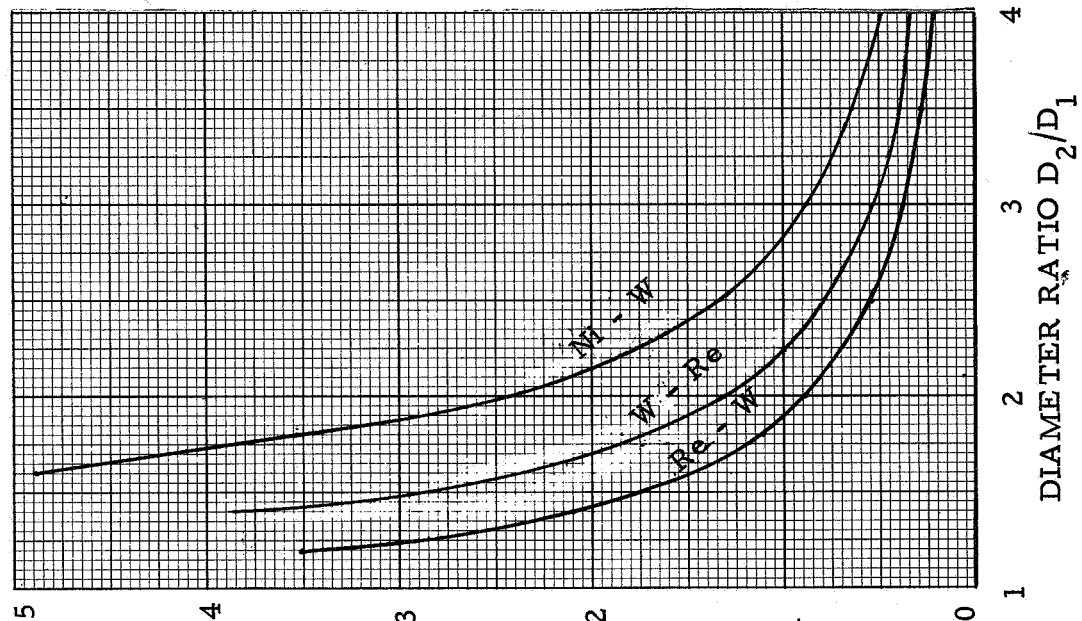


Figure 15b. Calculated extensional wave echo ratio, for Ni-W, W-Re, and Re-W. First material is lead-in, second is sensor.

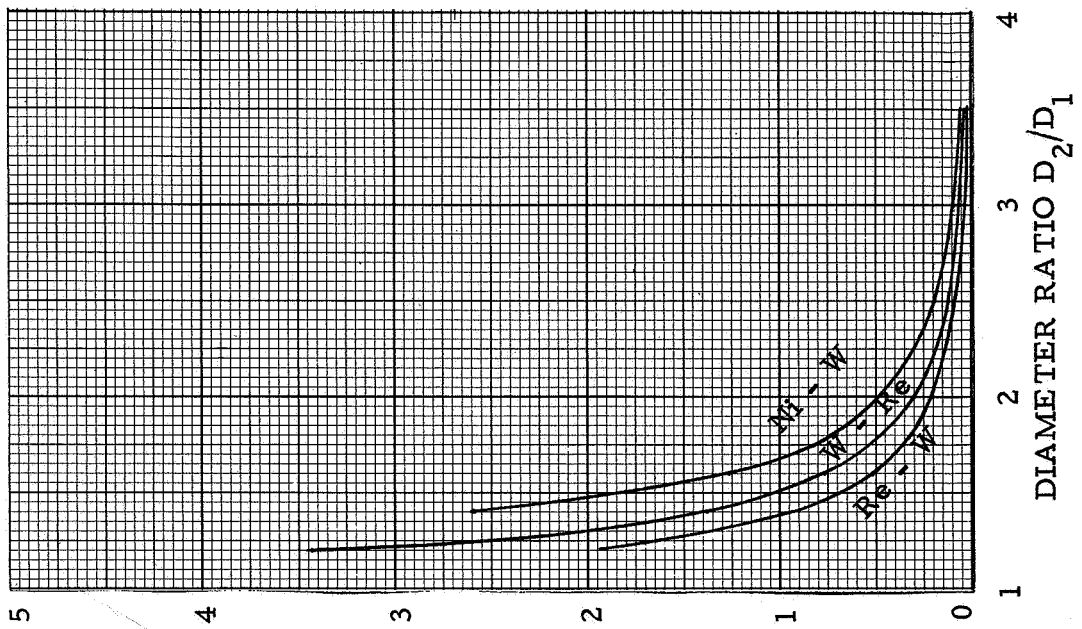


Figure 15c. Calculated torsional wave echo ratio, for Ni-W, W-Re, and Re-W.

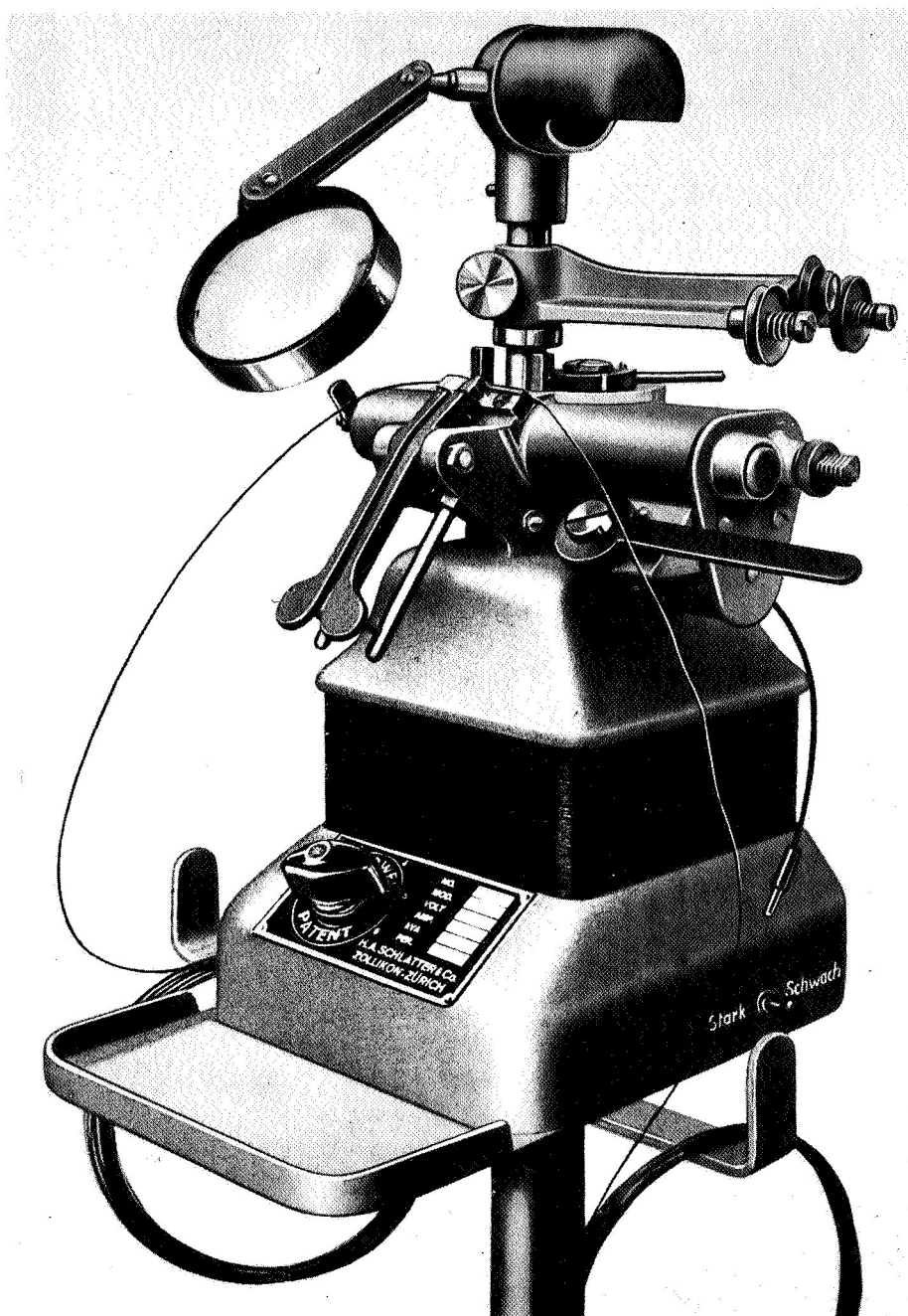


Figure 15d. Flash butt welder for joining refractory metal wires, strip, etc.

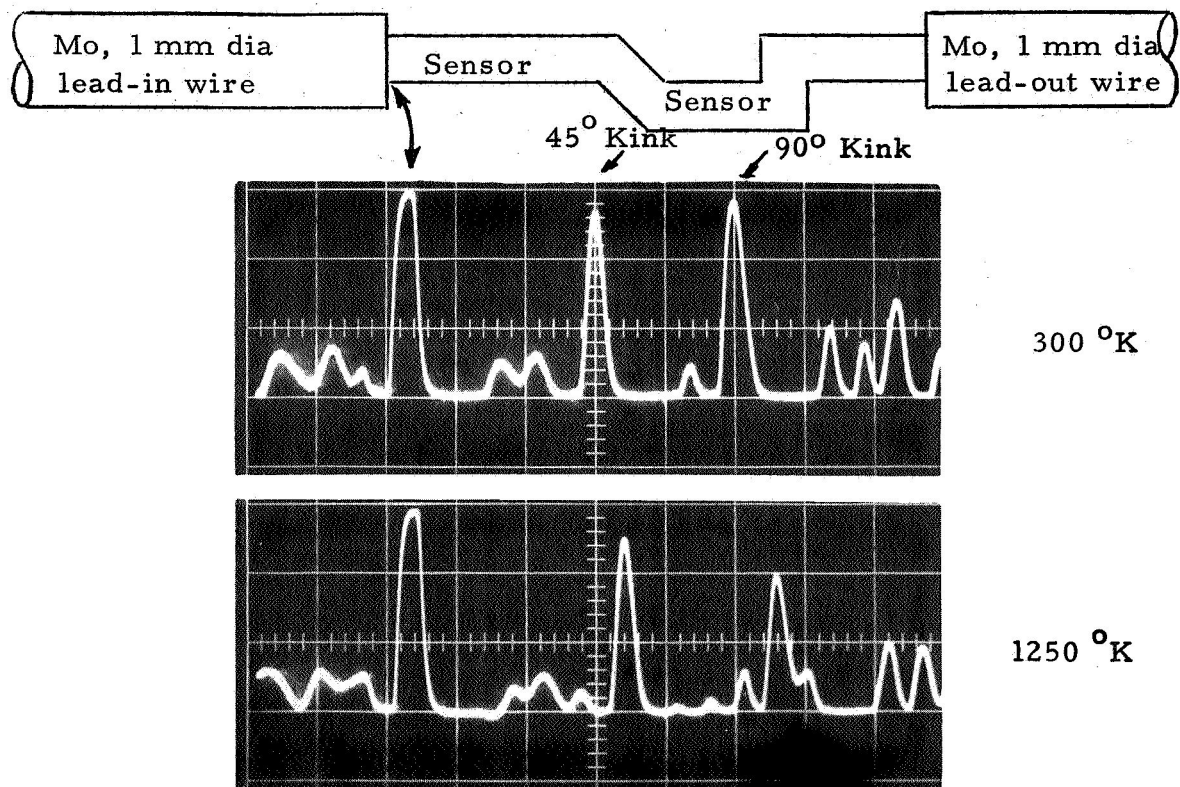


Figure 16. Oscillograms show echo patterns from two adjacent 0.5 mm dia molybdenum sensors. Left sensor, approximately 75 mm long; right sensor, approximately 50 mm long. Lead-out wire was used to facilitate Joule heating of the sensors. Sweep, 10  $\mu$ sec/cm. Wires not drawn to scale.

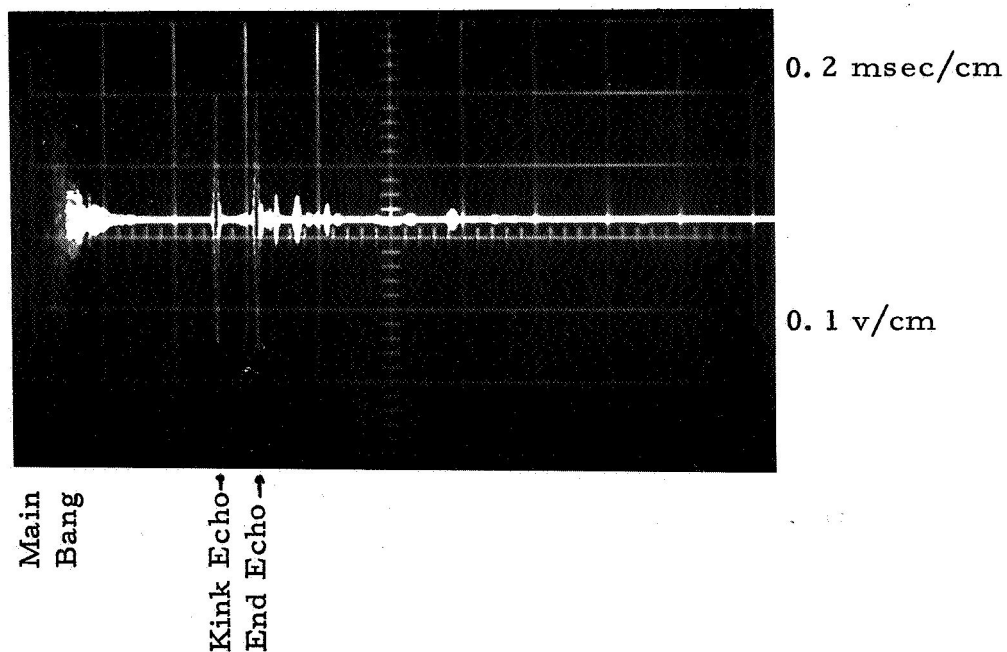
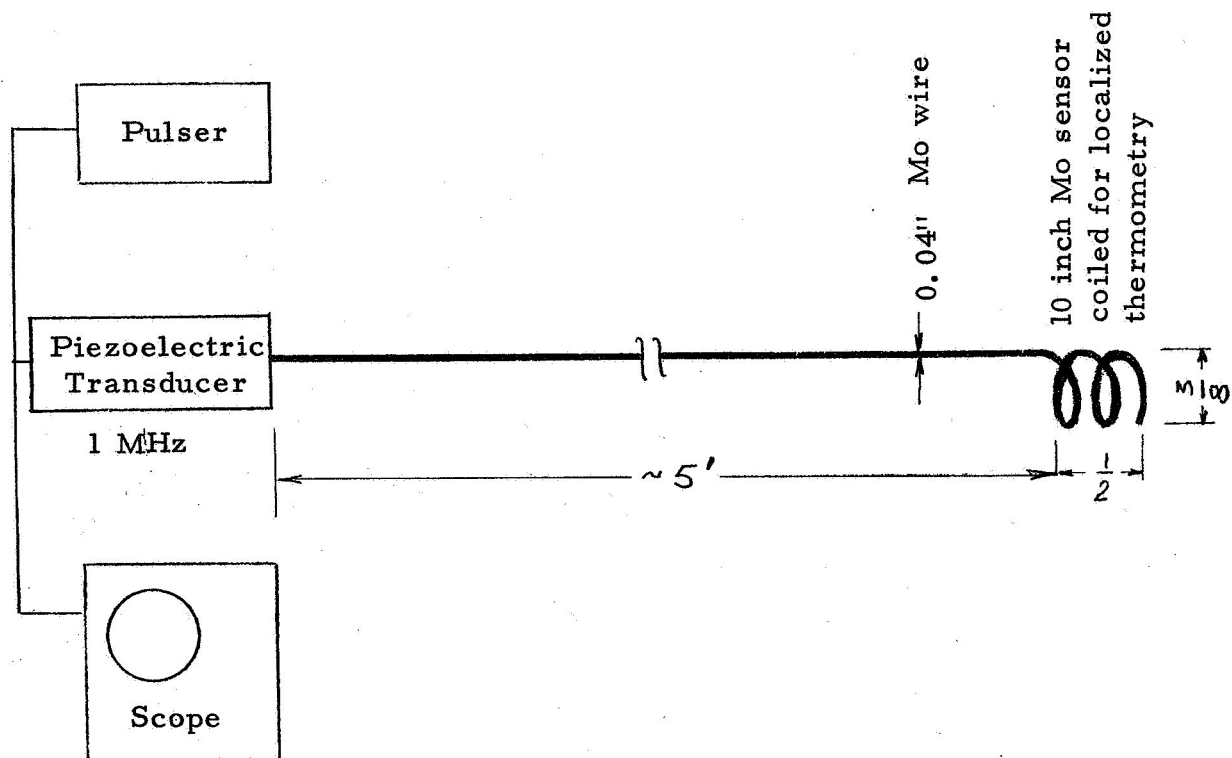
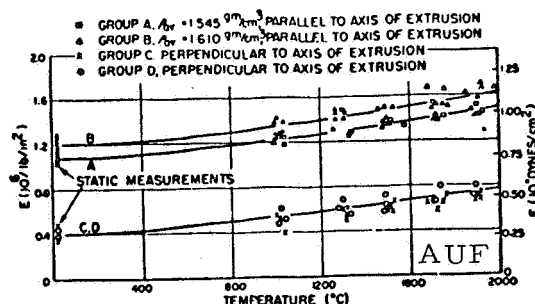
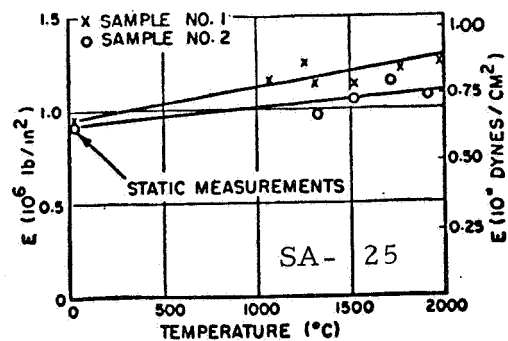


Figure 17. Pulse echo experiment in Mo wire at 1 MHz. Small coil diameter ( $3/8''$ ) requires relatively high frequency, e.g., 1 MHz. This frequency, in turn, is more conveniently obtained with a piezoelectric transducer rather than with magnetostrictive transducer.



(a) Temperature variation of Young's modulus for AUF graphite.



(b) Temperature variation of Young's modulus for SA-25 graphite.

Figure 18. Modulus vs temperature in AUF and SA-25 graphites, after Faris, Green and Smith, J. Appl. Phys. 23 89-95 (1952).

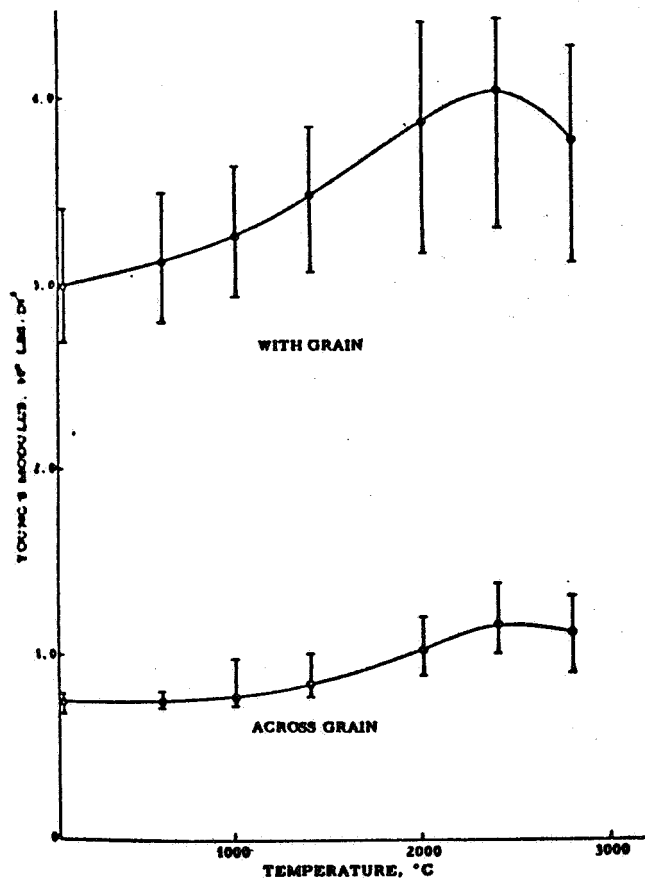


Figure 19. Young's modulus vs temperature in a highly anisotropic graphite, after Johnson and Dull, WADD TR 61-72 (1963).

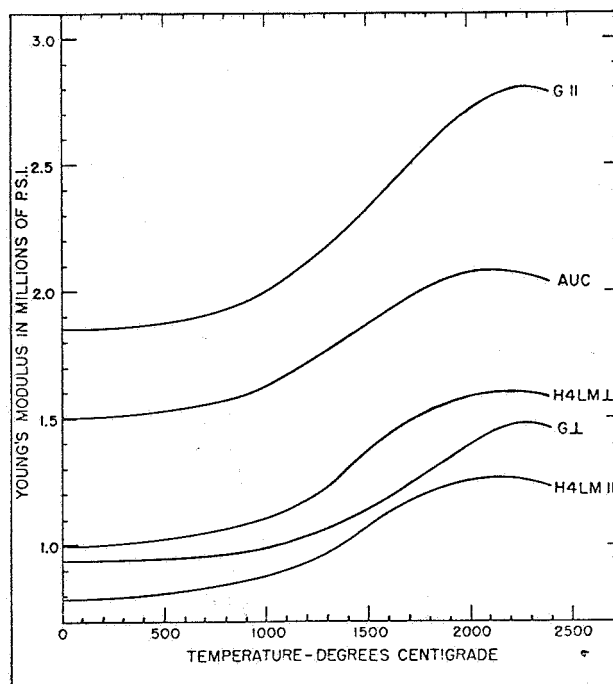


Figure 20. Young's modulus vs temperature for representative commercial graphites, after Armstrong and Brown (1964).

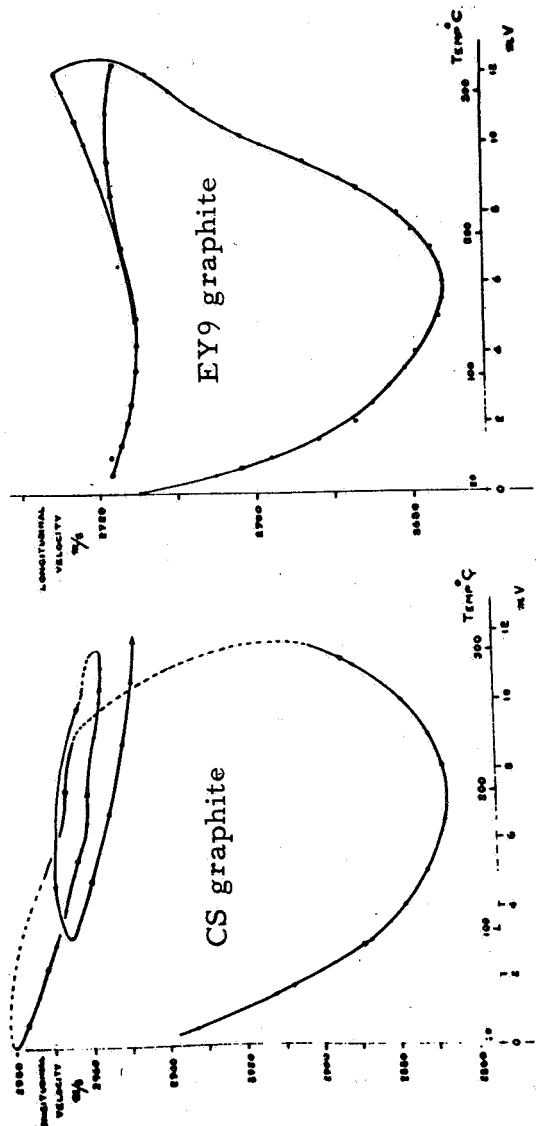


Figure 21

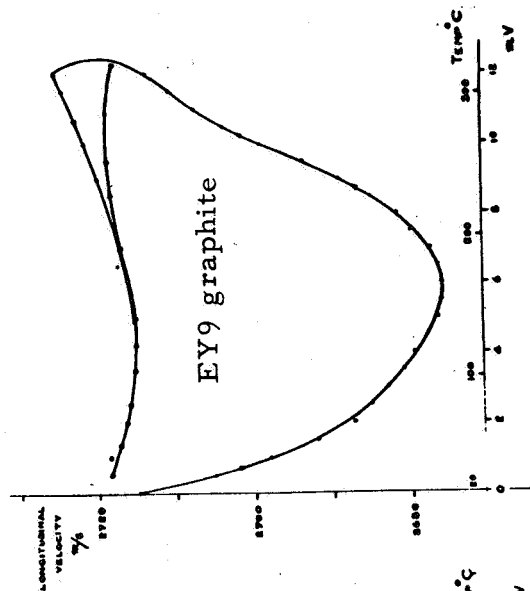


Figure 22

Extensional wave velocity in CS and EY9 graphites, after Bell, Hub and Smith (1960). See also J. F. W. Bell, "An Ultrasonic Thermometer," presented at Ultrasonics for Industry 1967 Conference, London (31 Oct. 1967), abstract in Ultrasonics 5, 265 (Oct. 1967).

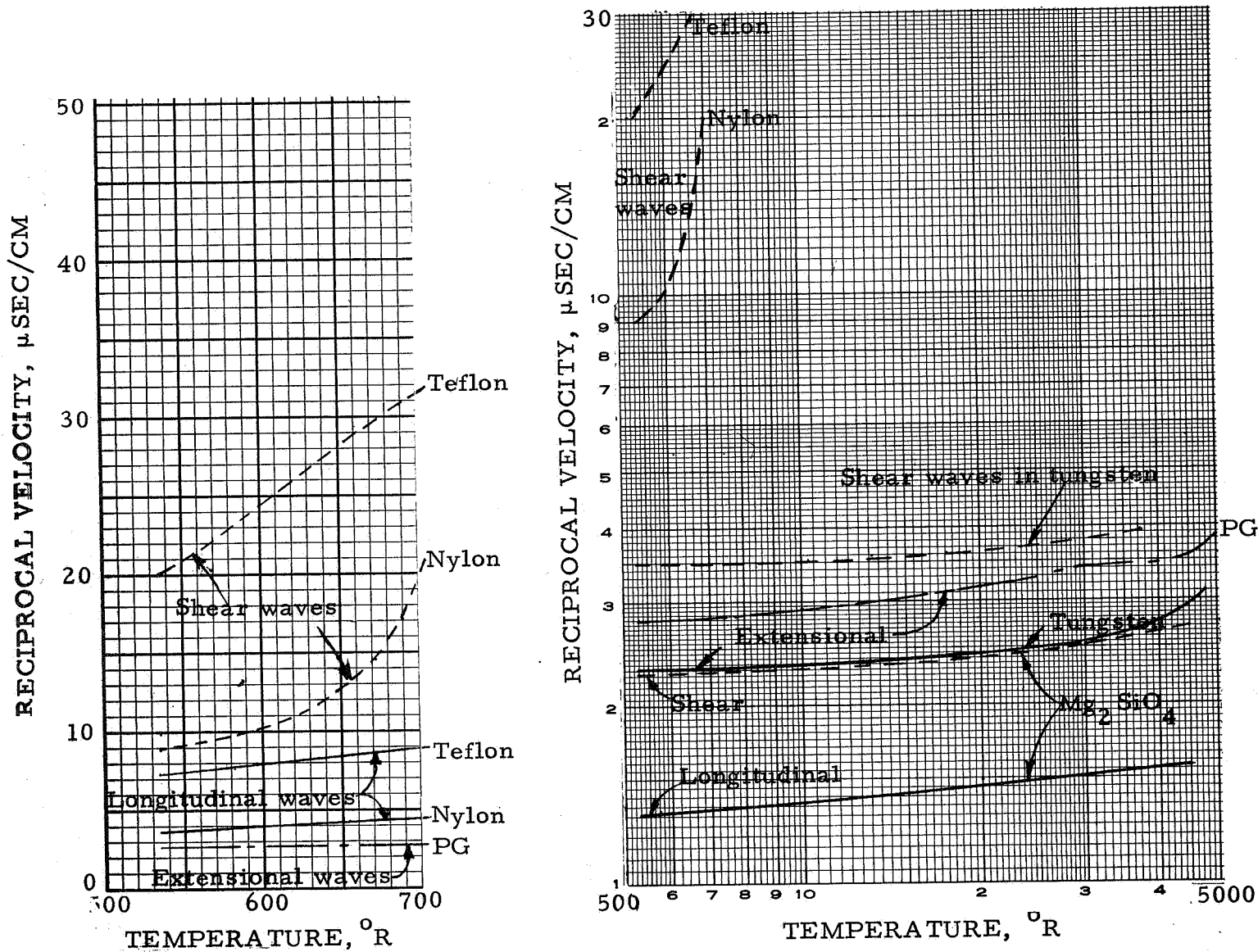
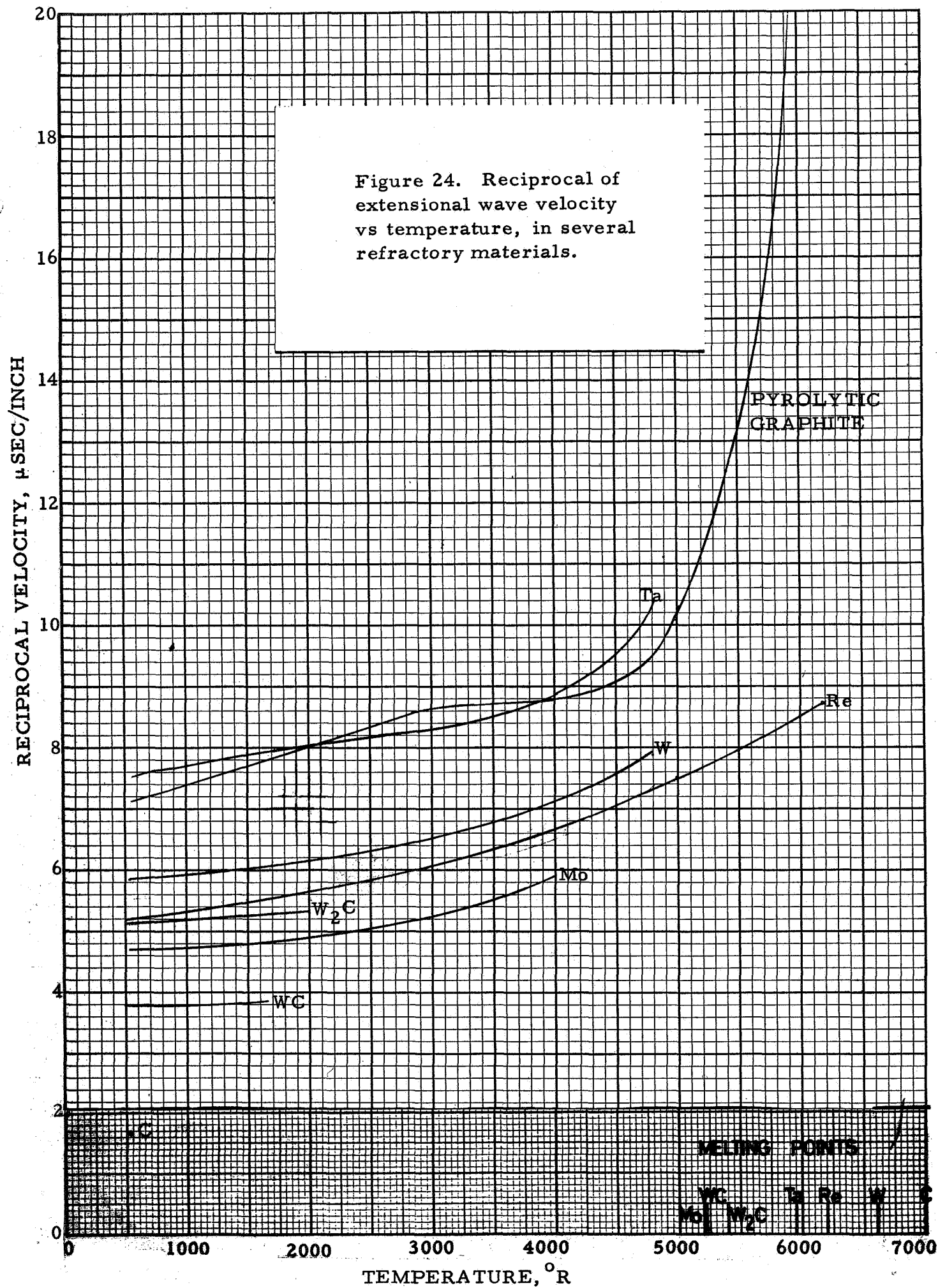


Figure 23. Reciprocal velocity vs temperature in several non-metallic materials. Graph at left compares plastics with pyrolytic graphite (PG) near room temperature. Graph at right compares plastics [data from Asay and Guenther, J. Appl. Polymer Sci. 11, 1087-1100 (1967)], PG; and a ceramic ( $\text{Mg}_2\text{SiO}_4$  data from ref. 54). Polycrystalline tungsten data are also plotted for extensional waves (ref. 24) and shear waves [Lowrie and Gonas, Union Carbide Tech. Rpt. C-27 (Jan. 1965)] for comparison purposes.



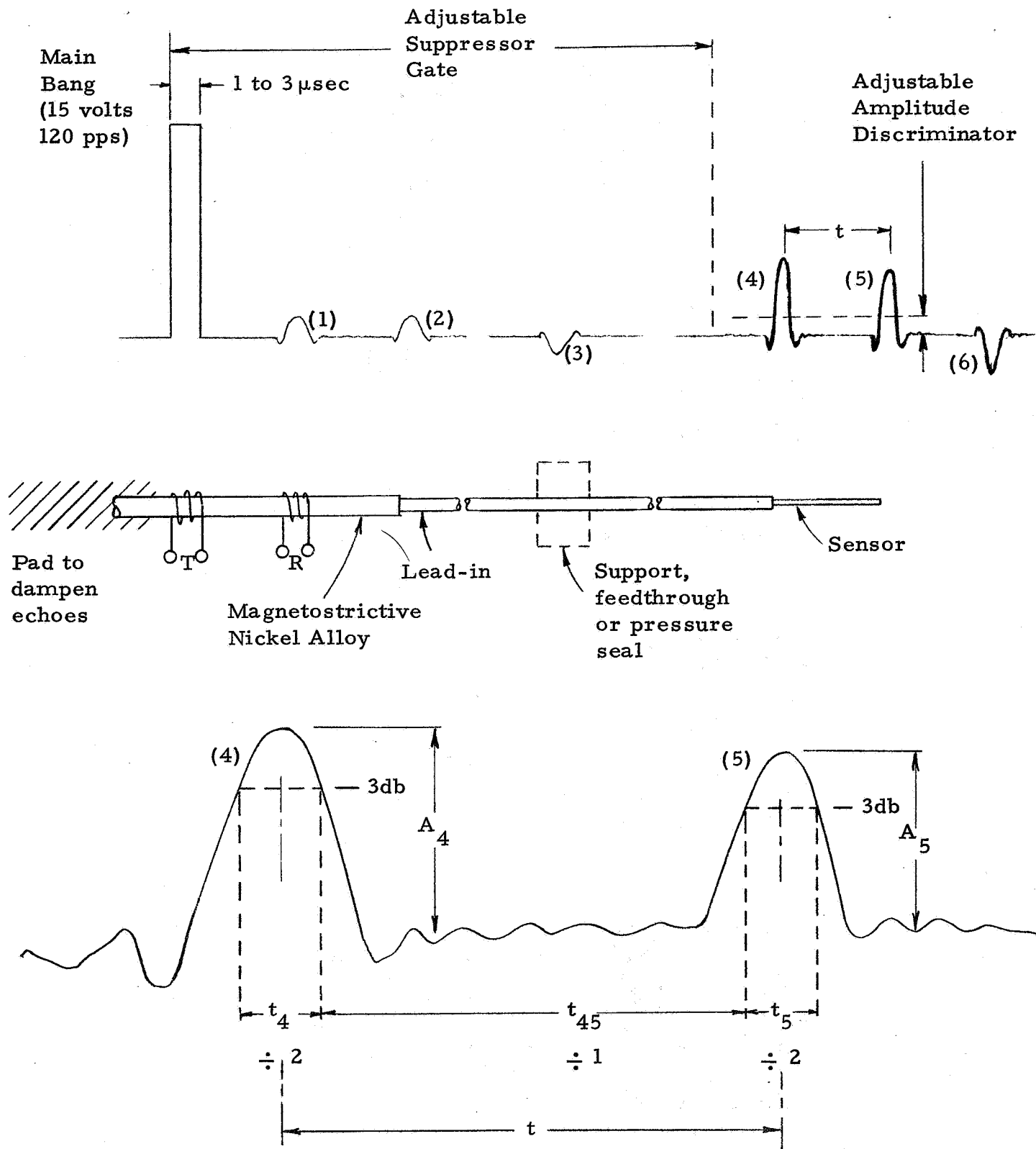
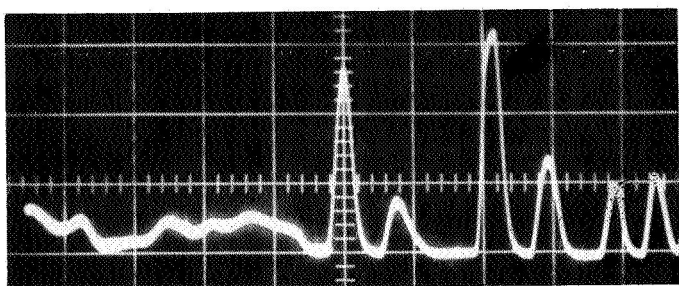
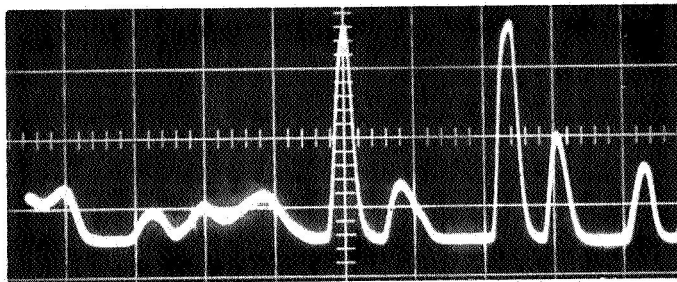


Figure 25. Schematic of waveforms on ultrasonic line.

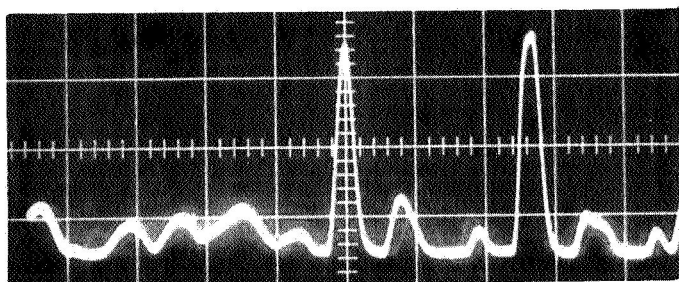
Lead-in sensor



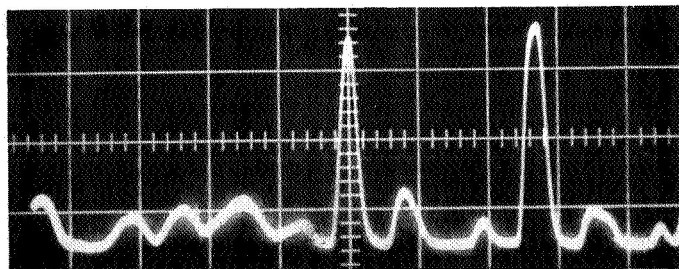
300°K



1340°K



1920°K



2360°K

Figure 26. Oscillograms for rhenium sensor of dimensions 0.5 mm diameter x 50 mm long. Sensor heated in Abar oven (Fig. 31). Sweep speed,  $10 \mu \text{ sec/cm}$ .

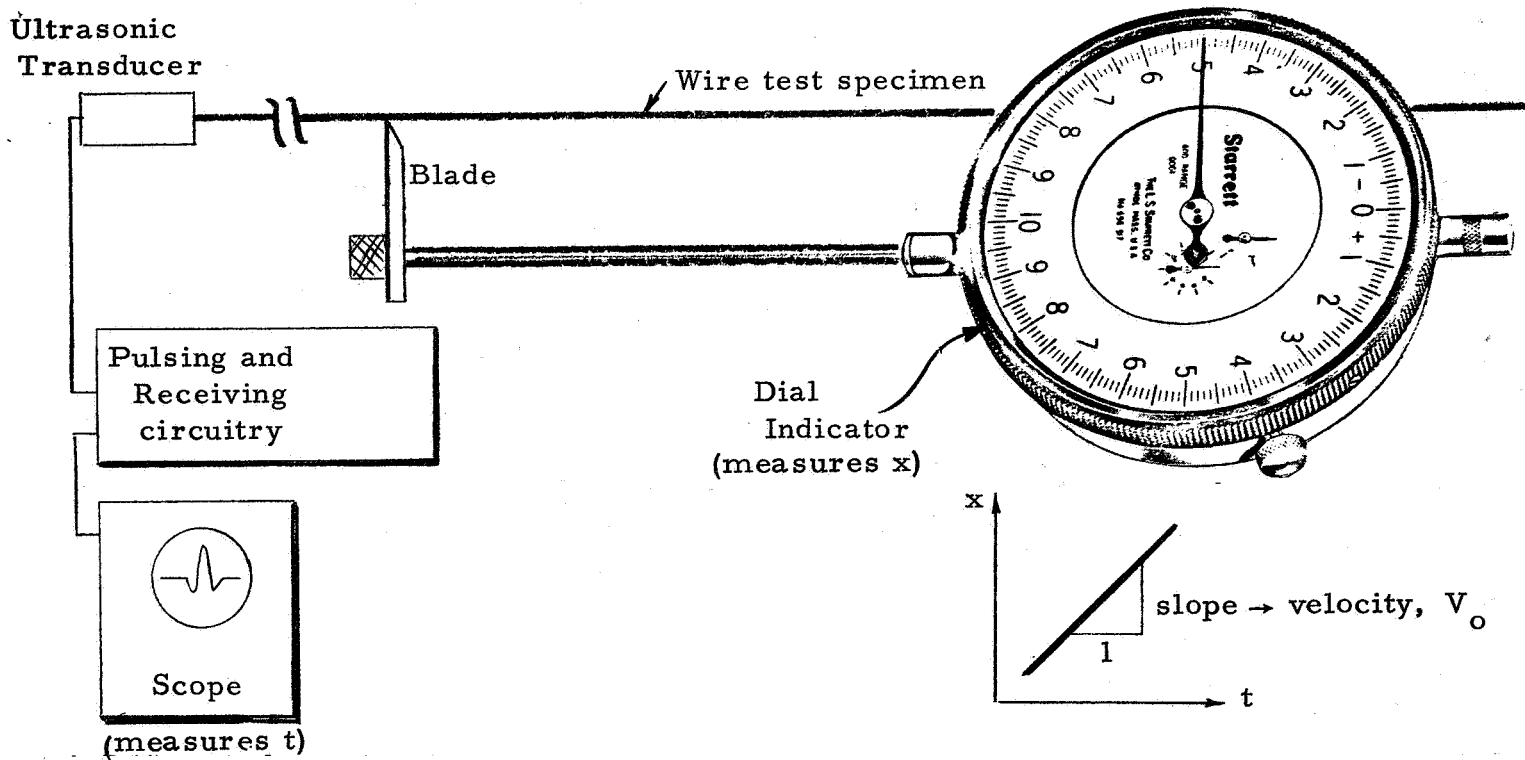


Figure 27a. Schematic of movable reflector using dial indicator.

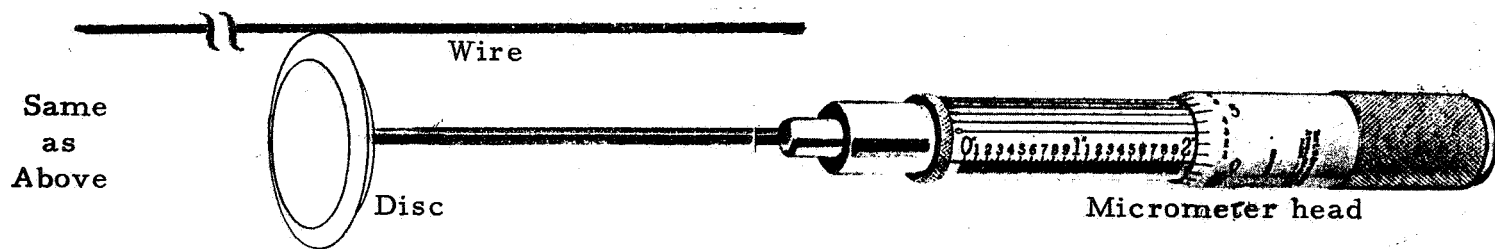


Figure 27b. Schematic of movable reflector using micrometer spindle.

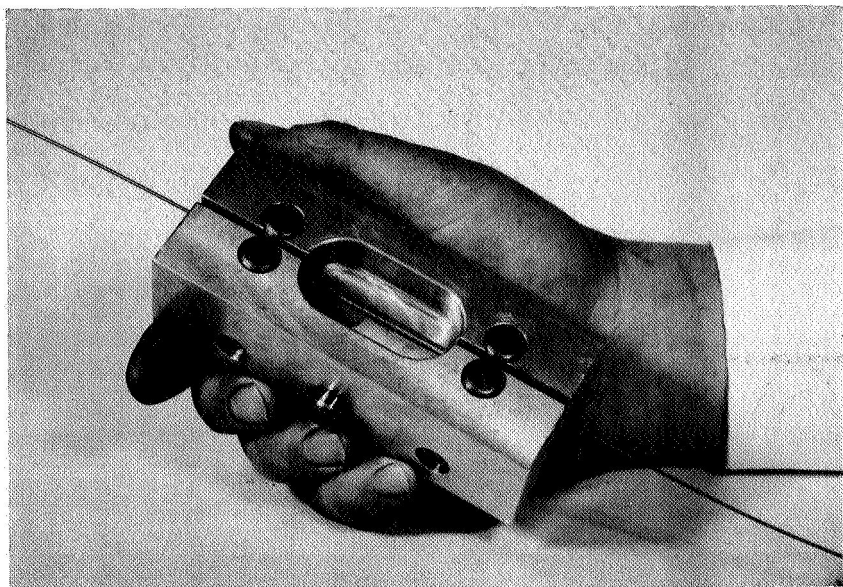
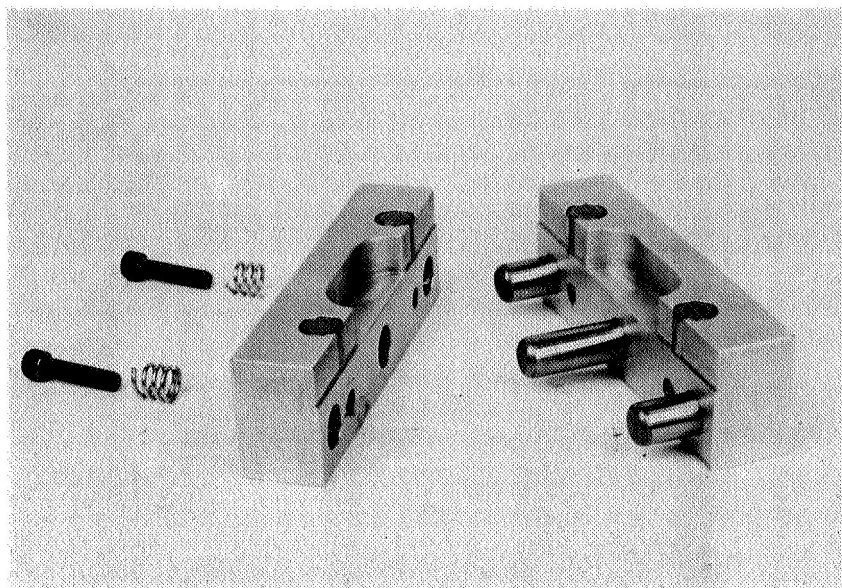


Figure 28. Two-point reflector for monitoring uniformity and quality of wire.

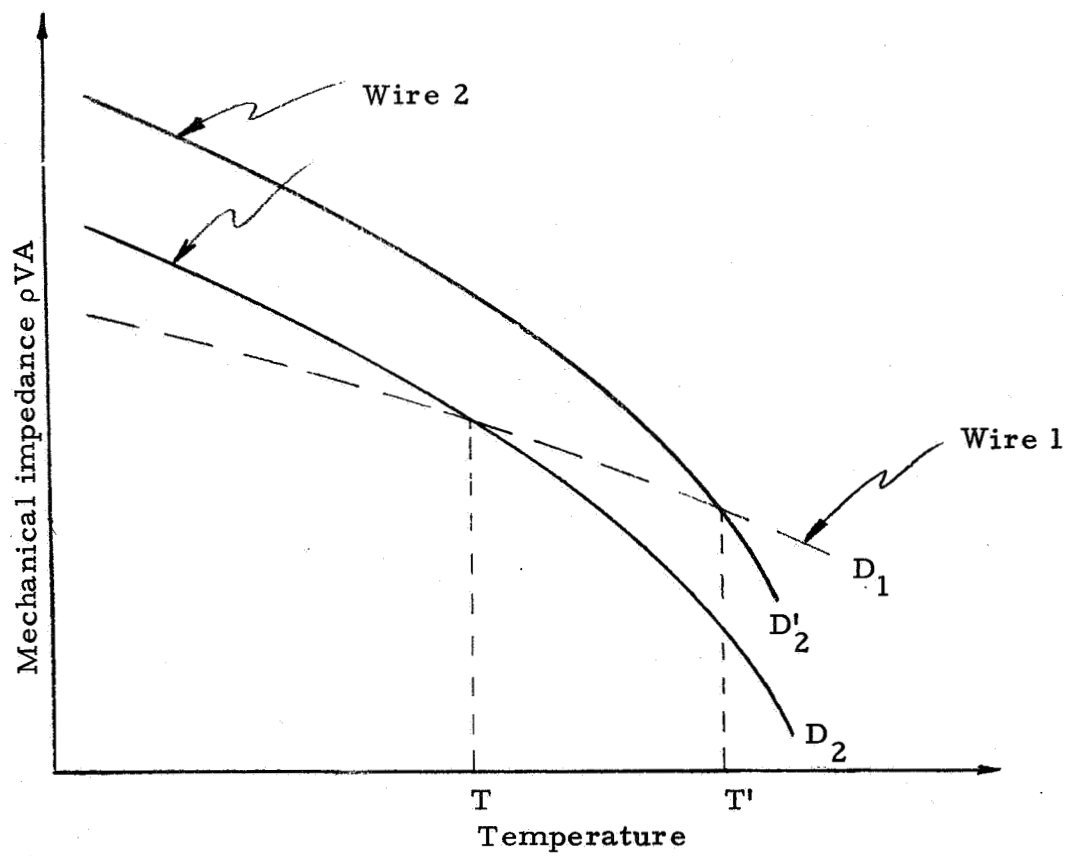


Figure 29. Impedance vs temperature for wire 1, diameter  $D_1$ , and wire 2, diameters  $D_2$  and  $D'_2$ .

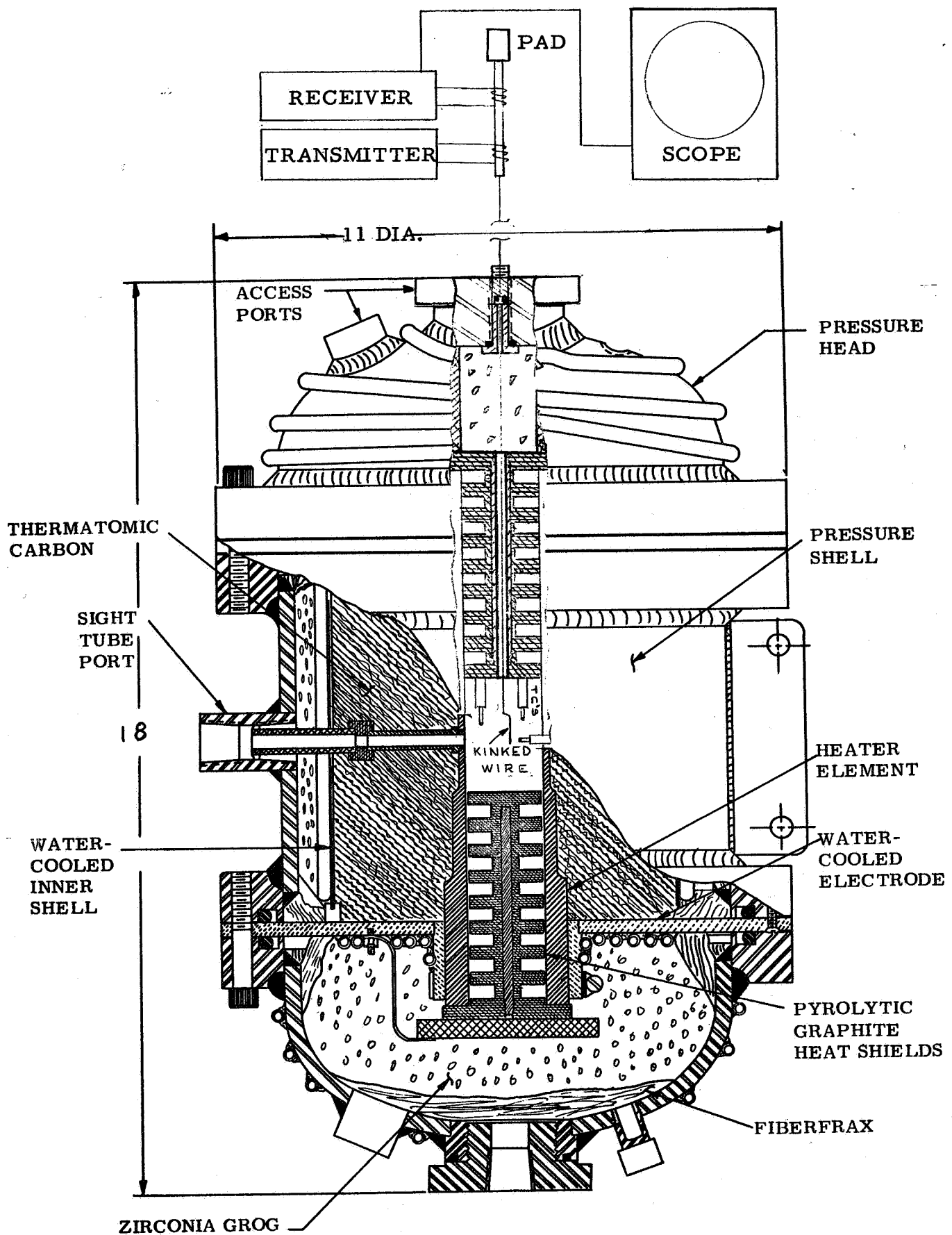
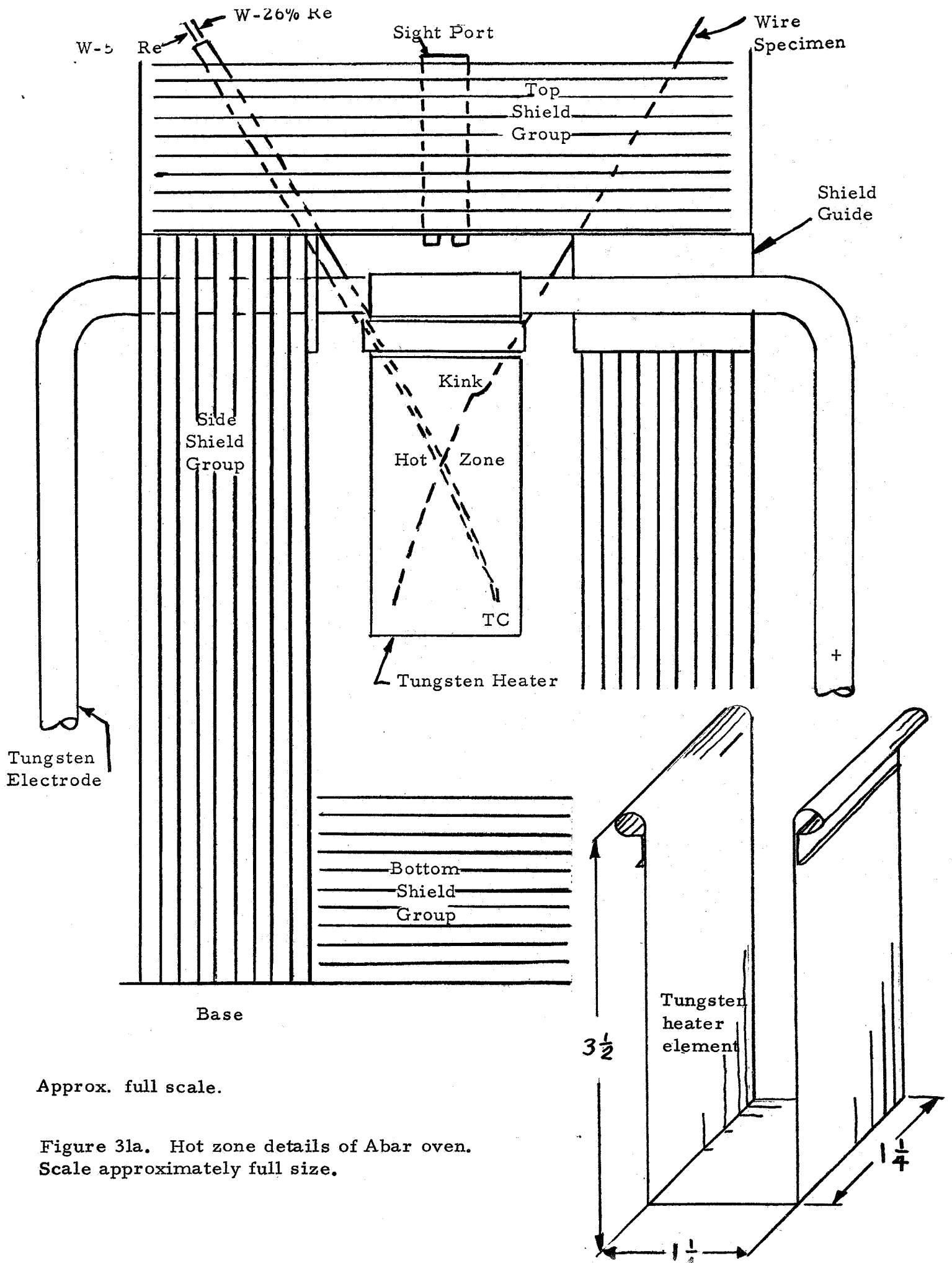


Figure 30. Schematic of the 7000° R radiant heating source for testing thin wire ultrasonic thermometer in graphite environment (SRI oven).



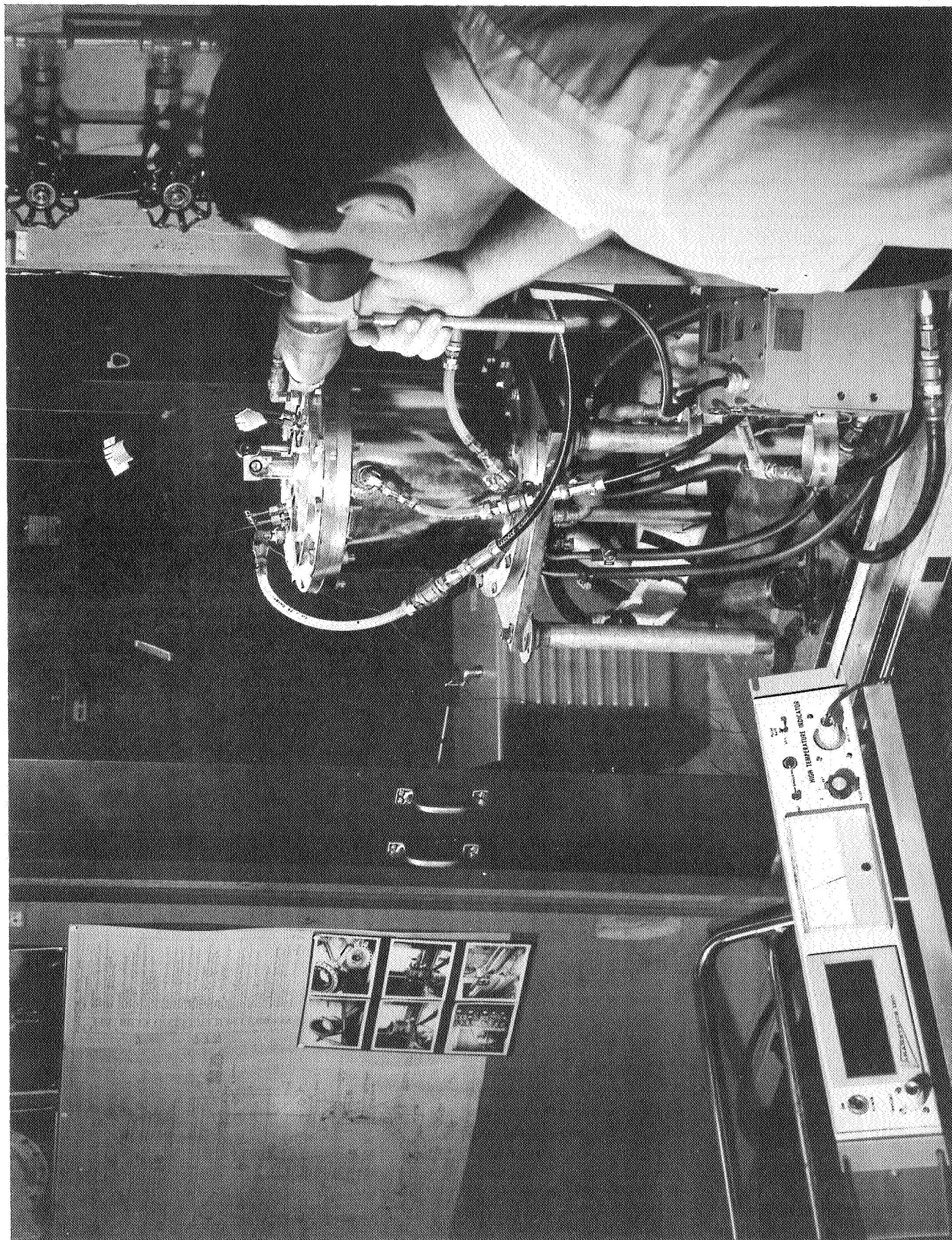


Figure 31b. Ultrasonic, thermocouple and pyrometric temperature measurements in Abar oven.

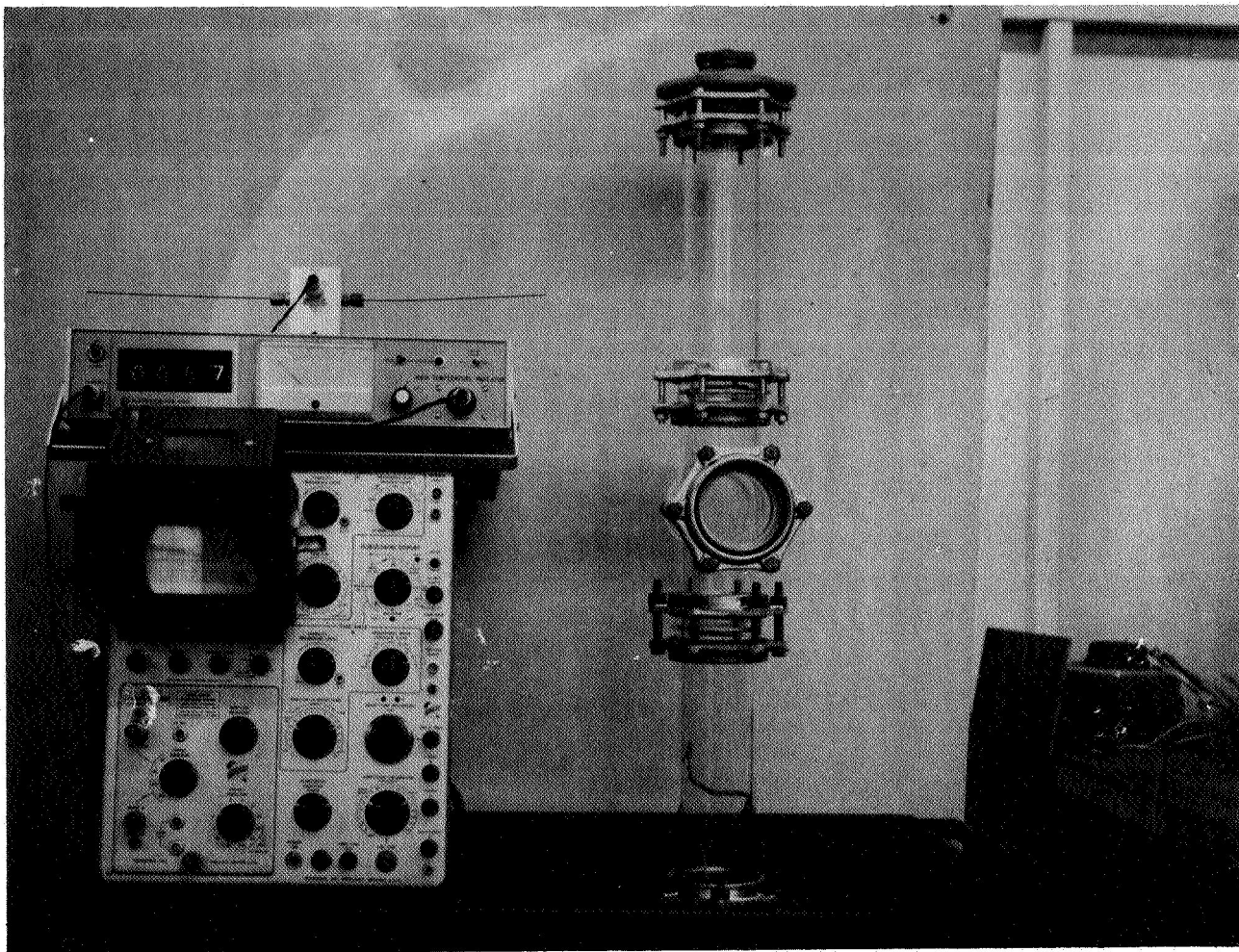
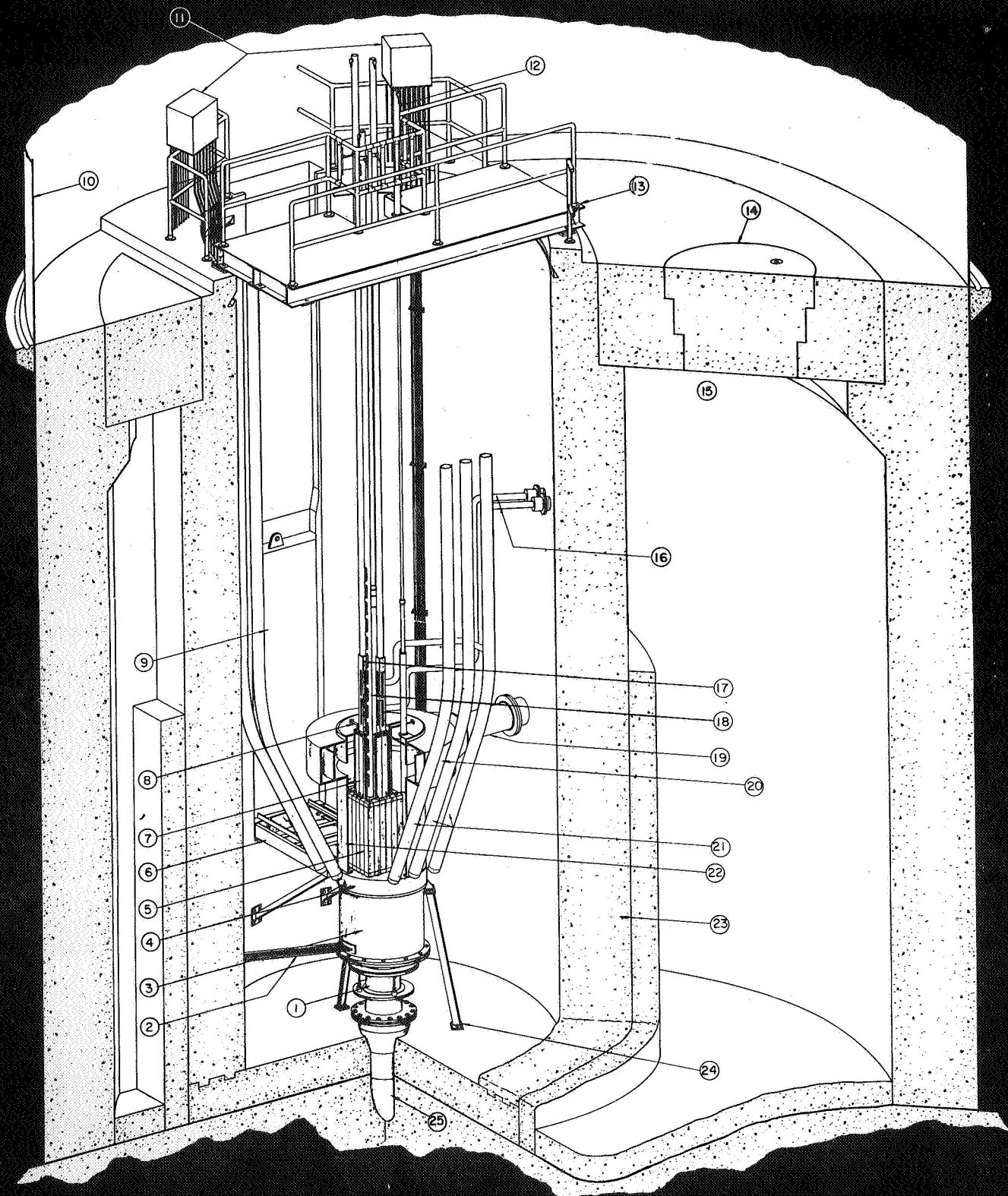


Figure 32. Photograph of lab set up for ultrasonically testing self-heated wires.  
See also Fig. 42.



1. PRIMARY OUTLET HEADER
2. SHIM ROD DRIVE CABLE CONDUIT
3. LOWER SHROUD
4. GRID PLATE
5. REACTOR CORE
6. TRANSFER CAR BRIDGE
7. SHIM ROD GUIDE
8. SHIM ROD GUIDE SUPPORT

9. POOL GATE
10. CONTAINMENT SHELL
11. SHIM ROD DRIVES
12. FISSION CHAMBER DRIVE
13. BRIDGE
14. ACCESS PLUG
15. OUT-PILE EQUIPMENT SPACE
16. HIGH PRESSURE LOOP INLET & OUTLET

17. SAFETY ROD DRIVE
18. REGULATING ROD DRIVE
19. PRIMARY WATER INLET
20. PRIMARY INLET PLENUM
21. ION CHAMBER CONTAINERS
22. UPPER SHROUD
23. POOL WALL
24. CORE SUPPORT LEGS
25. PRIMARY PIPING

Figure 33. Trimetric view of Babcock & Wilcox test reactor, Lynchburg, Va.

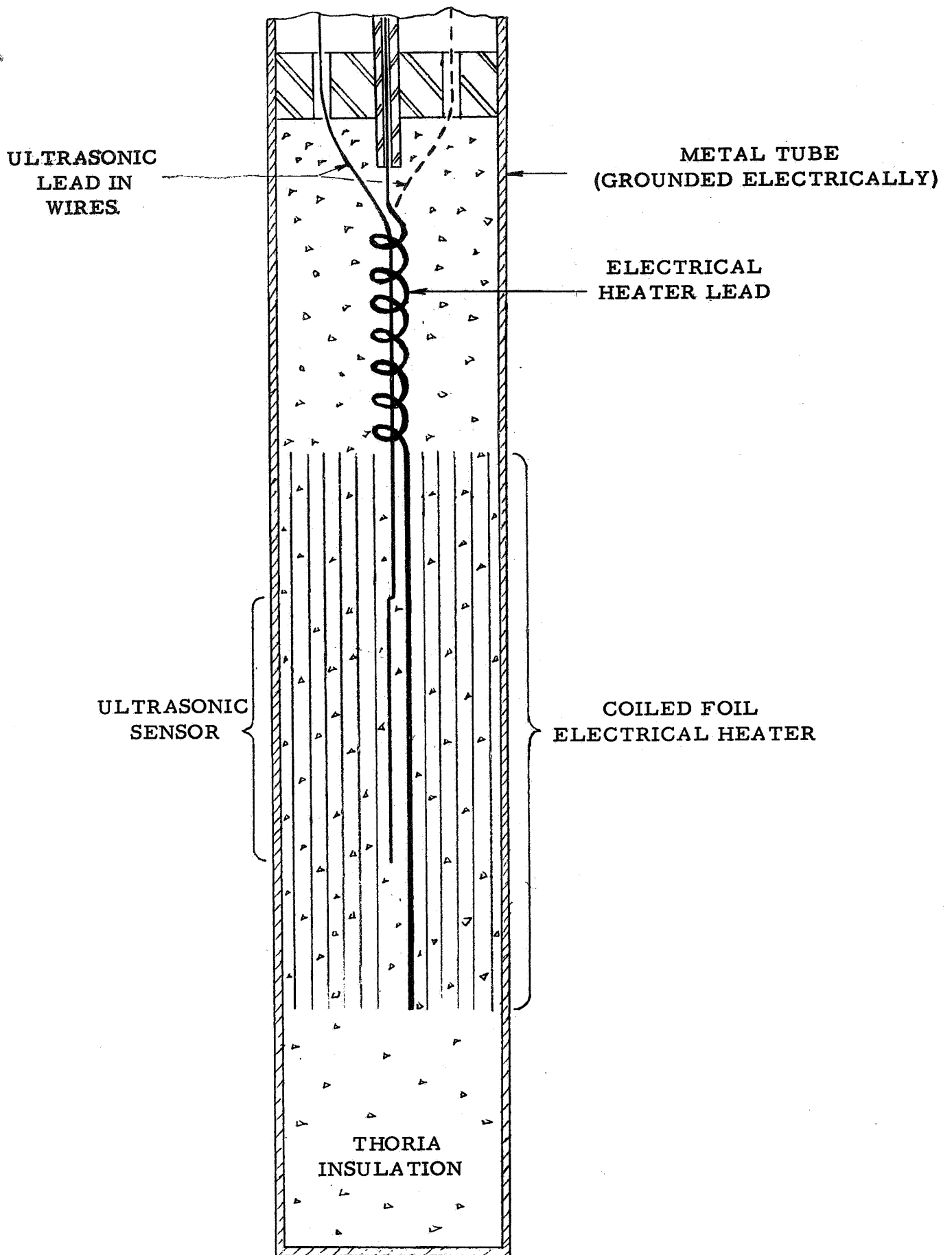


Figure 34. Schematic of capsule with coiled foil for studying radiation effects at elevated temperatures. Capsule employs coiled foil electrical heater and thoria gamma heater.

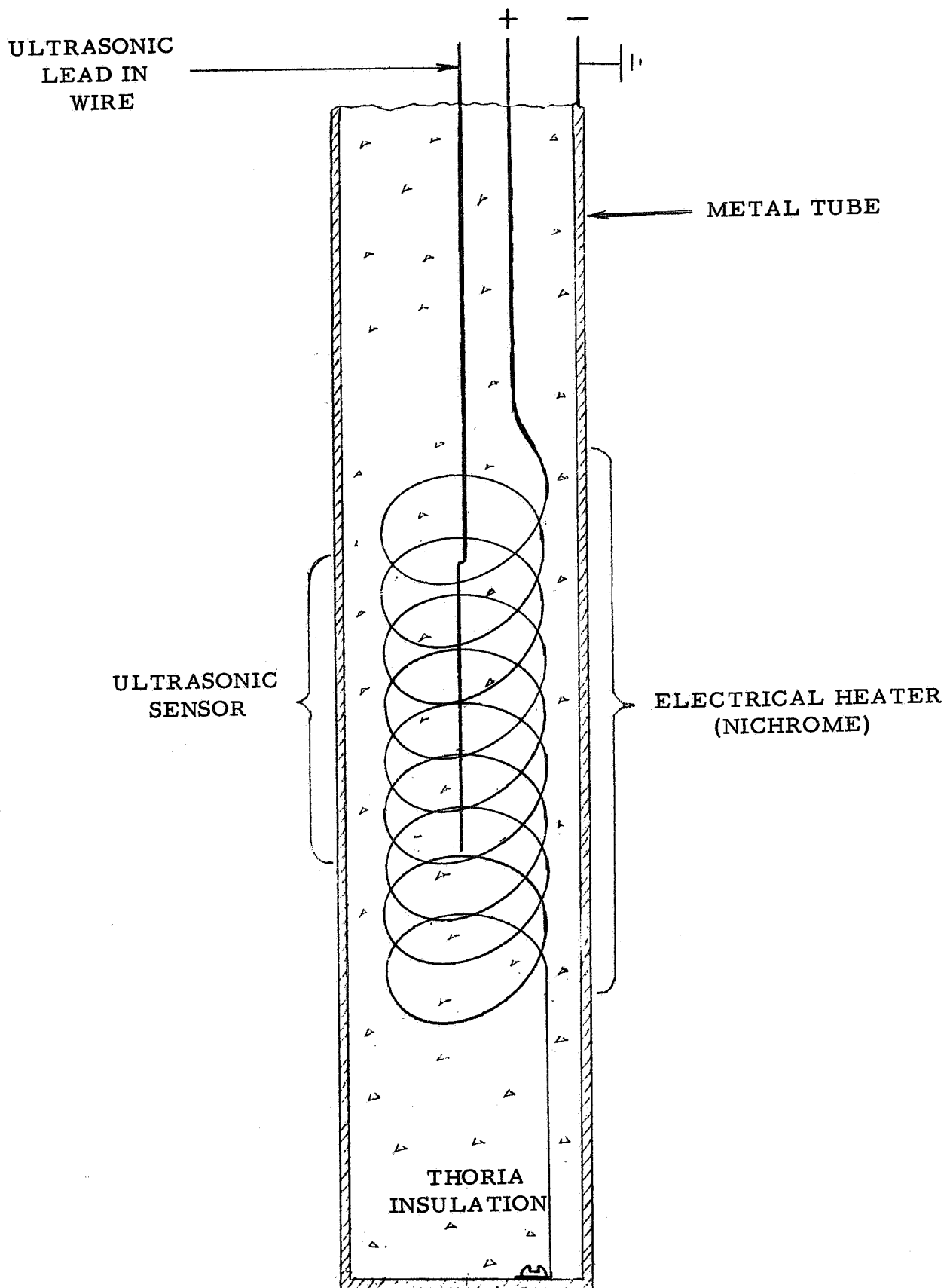
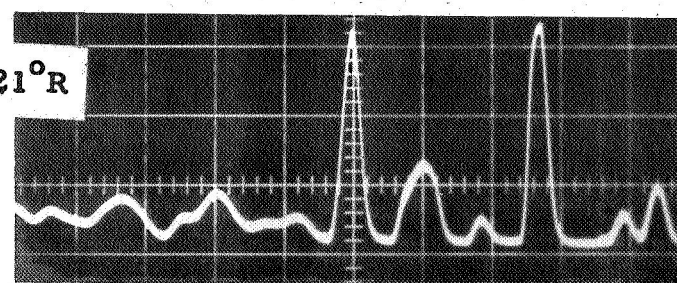
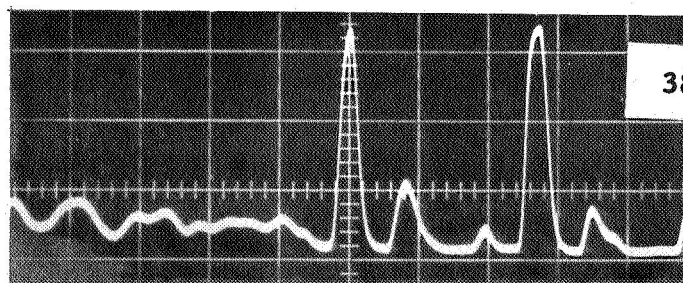
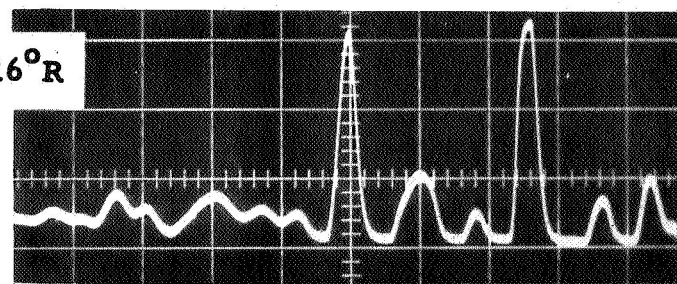
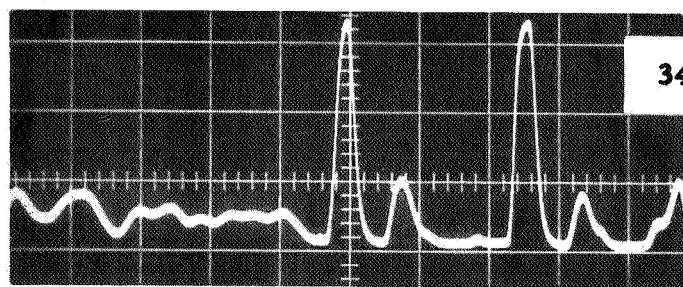
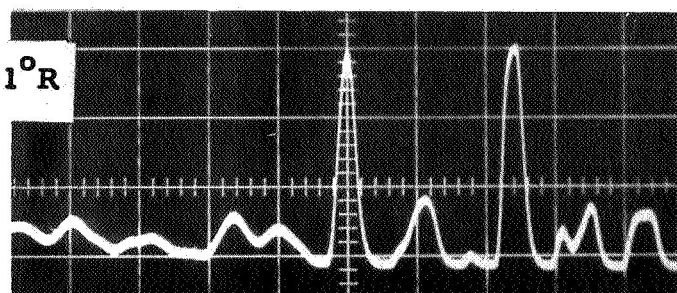
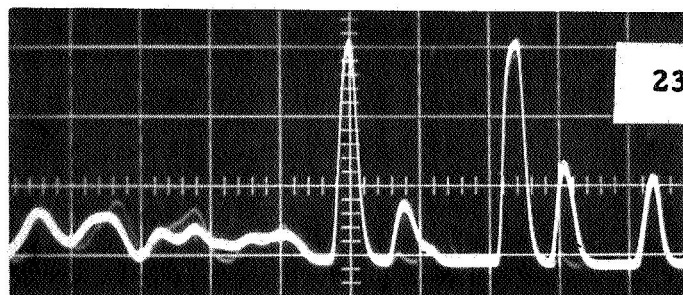
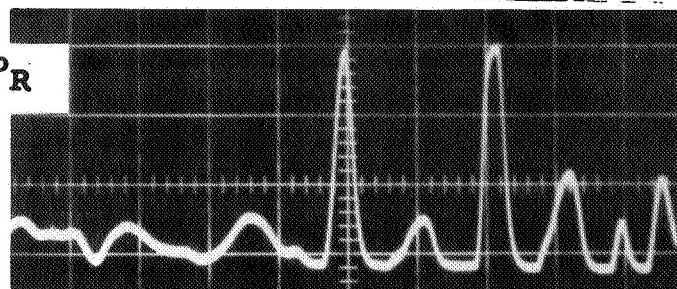
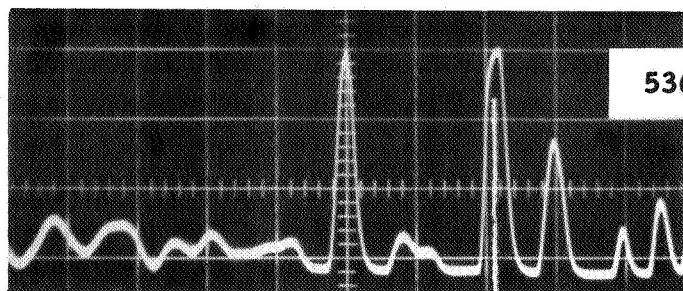


Figure 35. Schematic of capsule for studying radiation effects at elevated temperatures. Center of capsule may be several thousand °R hotter than electrical heater, due to gamma heating.

lead-in sensor

lead-in sensor



CONTROL WIRE

IRRADIATED WIRE

Figure 36. Representative oscillograms show echoes from front and rear of control and irradiated rhenium sensors. Sweep speed,  $10\mu\text{s}/\text{cm}$ . Sensor dimensions:  $0.02''$  ( $0.5\text{ mm}$ ) dia  $\times$   $2''$  ( $50\text{ mm}$ ) long. Date of test: December 12, 1966.

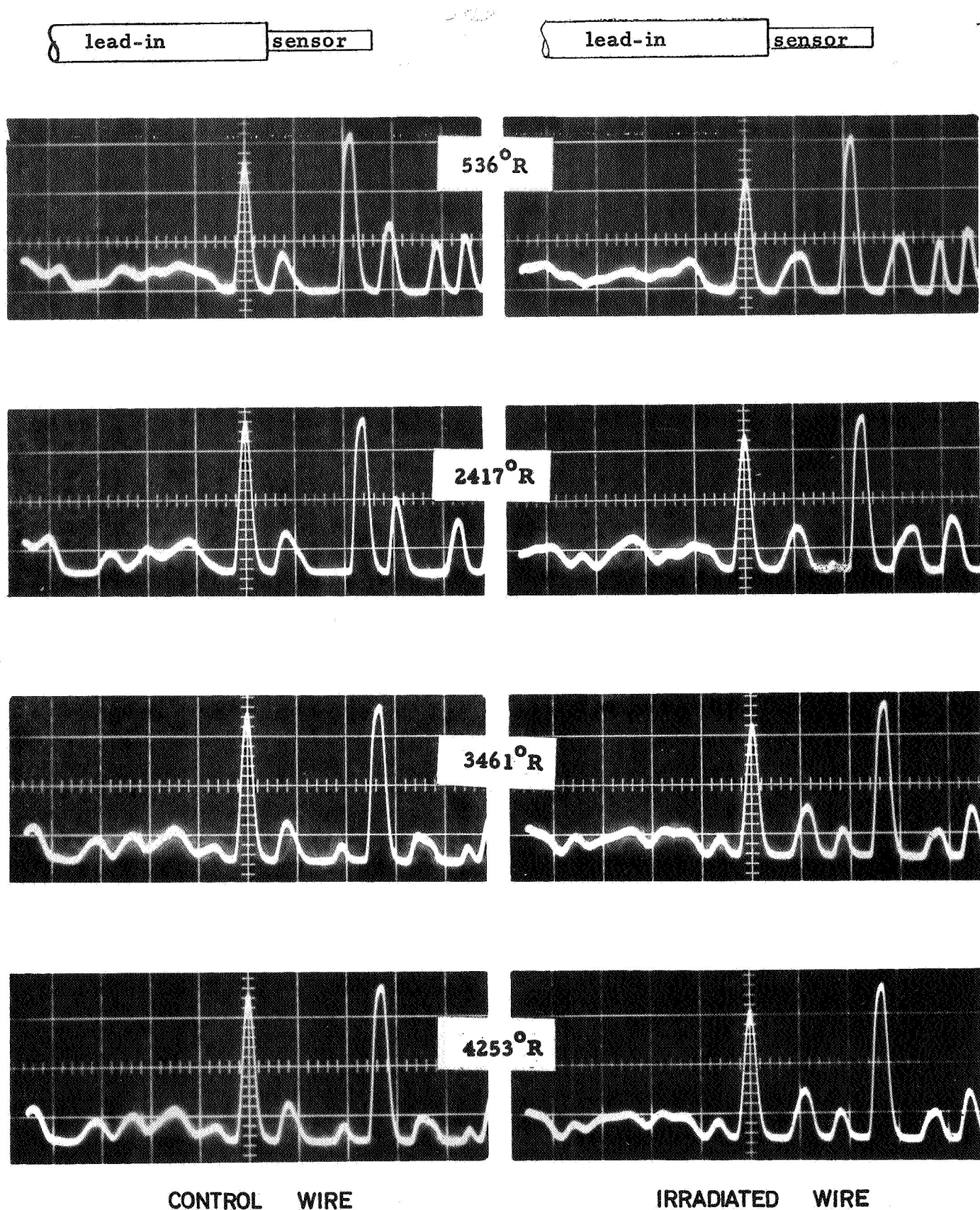


Figure 37. Confirming tests in second pair of control and irradiated rhenium sensors show reproducibility obtained in ultrasonic experiment. Sweep speed,  $10 \mu\text{s}/\text{cm}$ . Sensor dimensions: 0.02" (0.5 mm) dia x 2" (50 mm) long. Date of test: December 15, 1966.

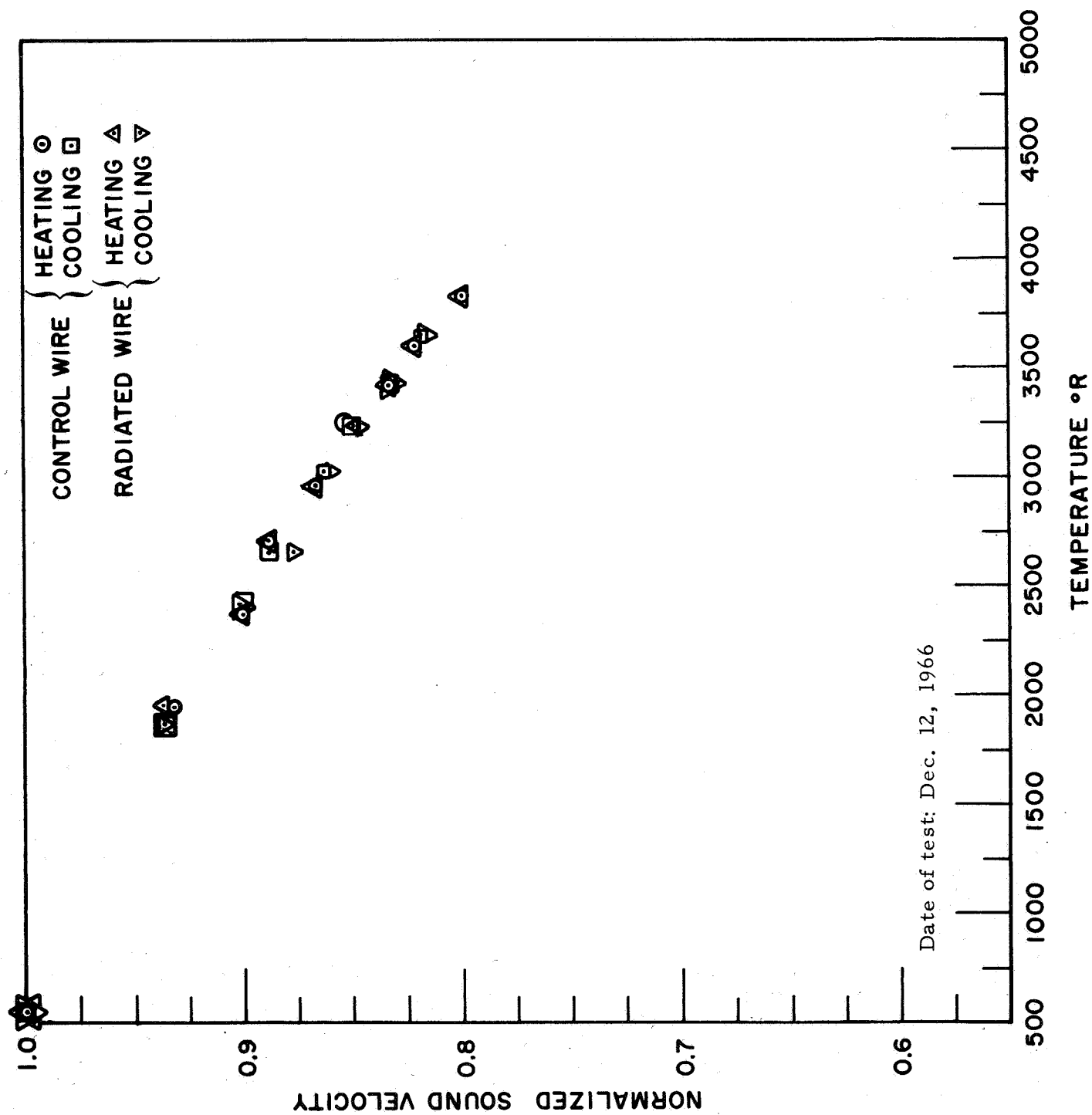


Figure 38. Normalized velocity vs temperature in control and irradiated rhenium specimens.

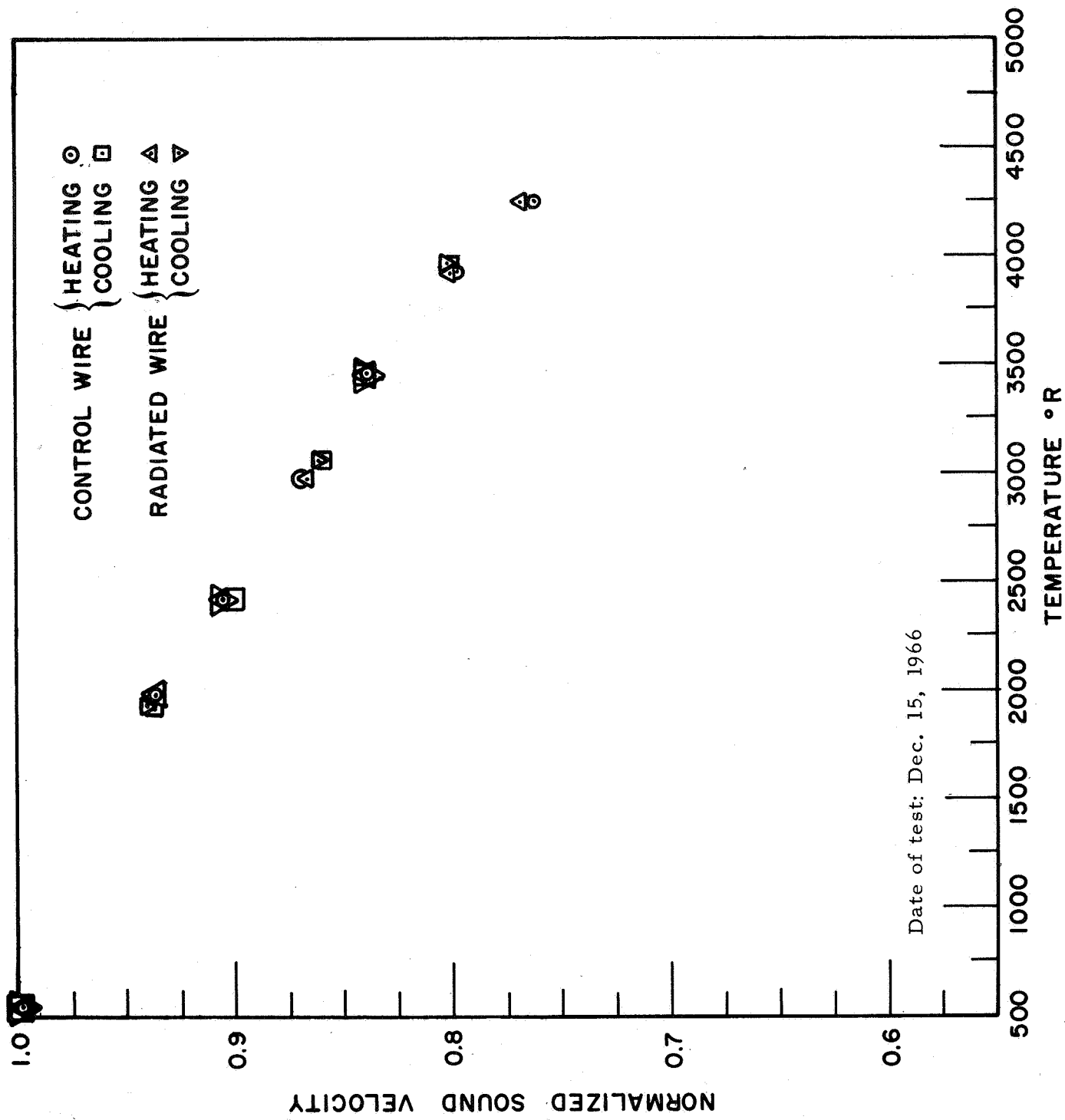


Figure 39. Normalized velocity vs temperature in control and irradiated rhenium specimens.

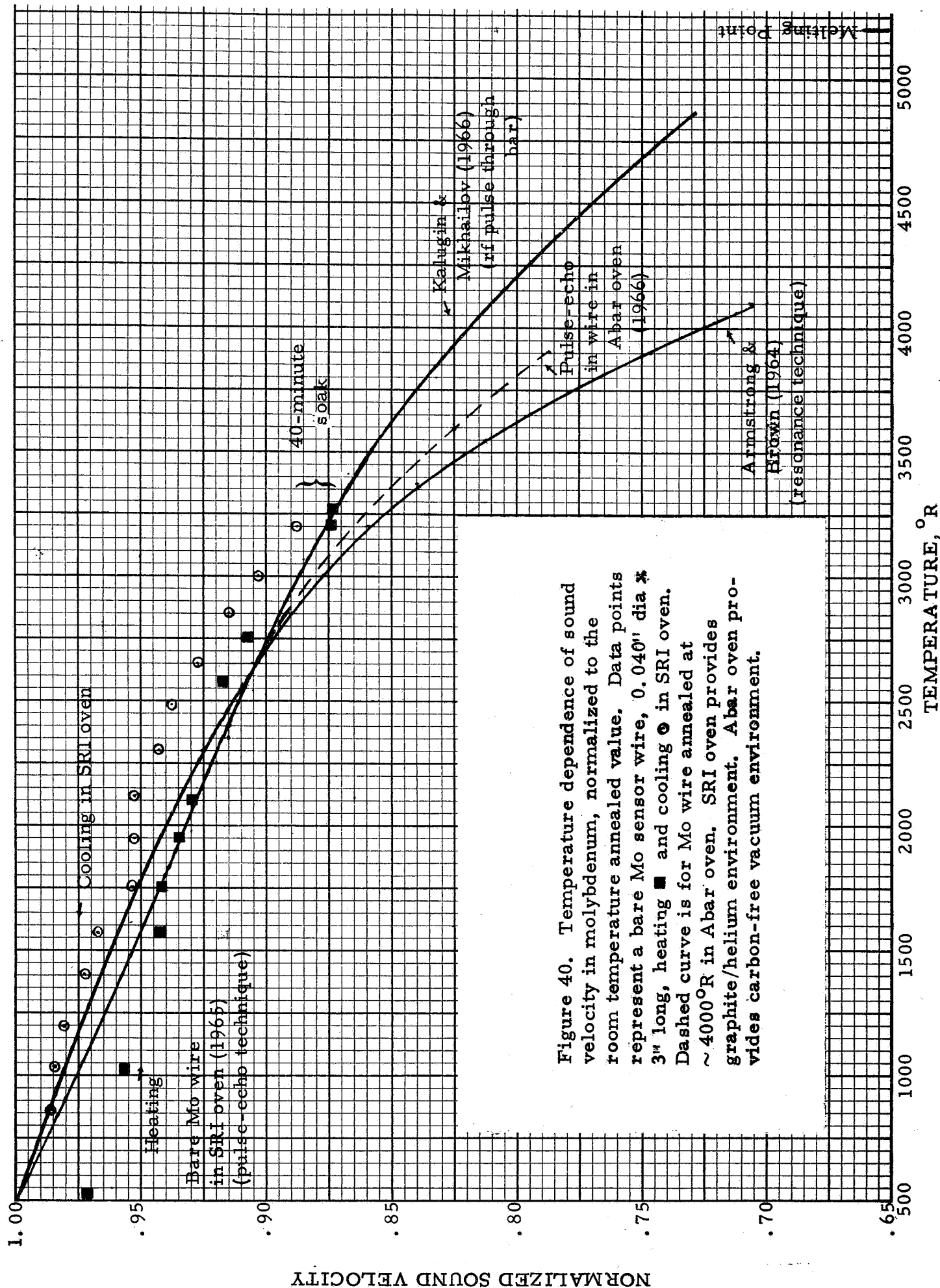


Figure 40. Temperature dependence of sound velocity in molybdenum, normalized to the room temperature annealed value. Data points represent a bare Mo sensor wire, 0.040" dia x 3" long, heating ■ and cooling ○ in SRI oven. Dashed curve is for Mo wire annealed at ~4000°R in Abar oven. SRI oven provides graphite/helium environment. Abar oven provides carbon-free vacuum environment.

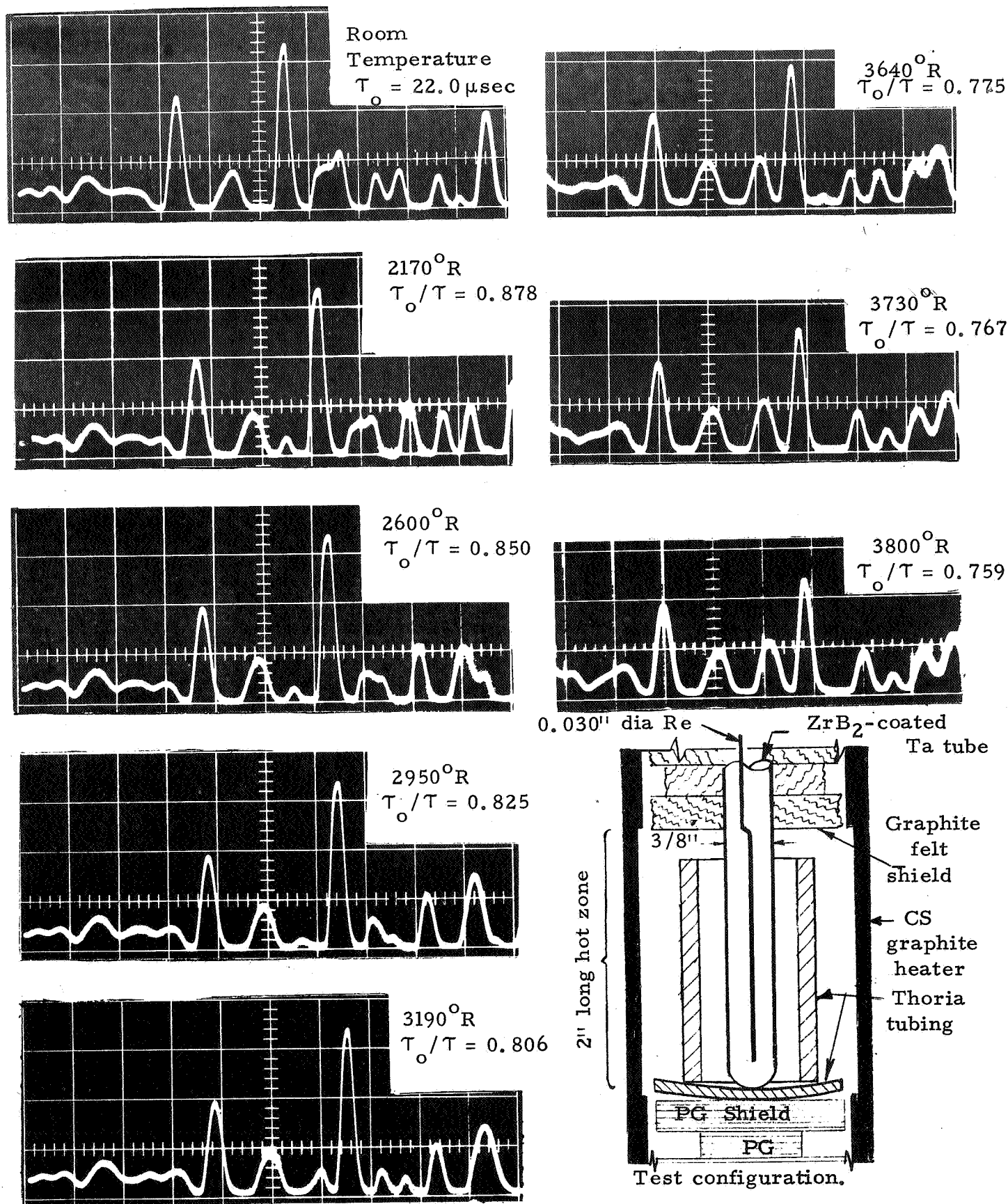


Figure 41. Tests on kinked rhenium wire in zirconium diboride coated tantalum sheath, heated in SRI oven. Oscillograms: 10μsec/cm, 2 v/cm. Date of Test: Oct. 4, 1966. Temperatures measured with L&N pyrometer. Transit times measured automatically with Pana-Therm Model 5000. Test terminated because of sheath failure, and attenuation, which may have been due to the sensor pressing against that sheath.

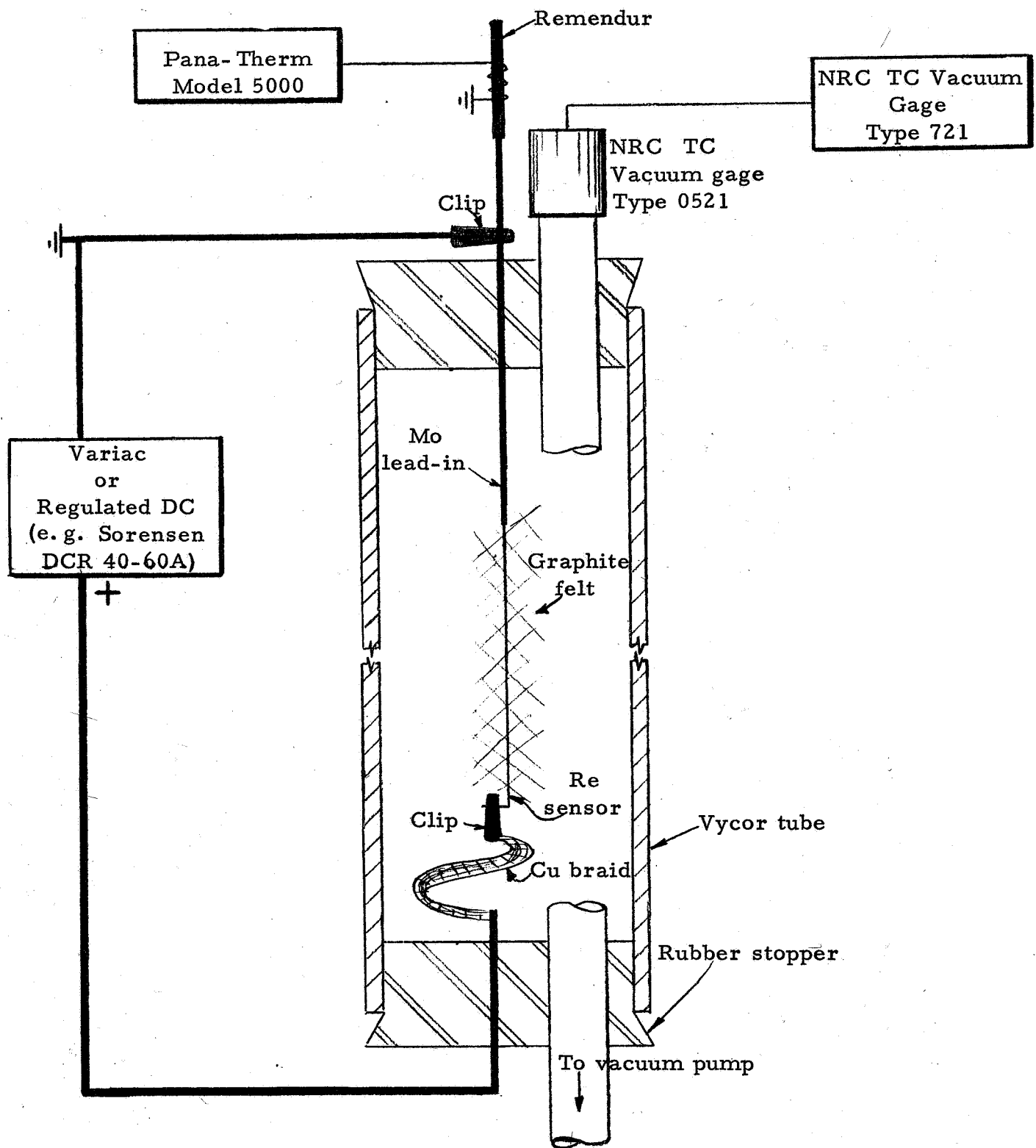
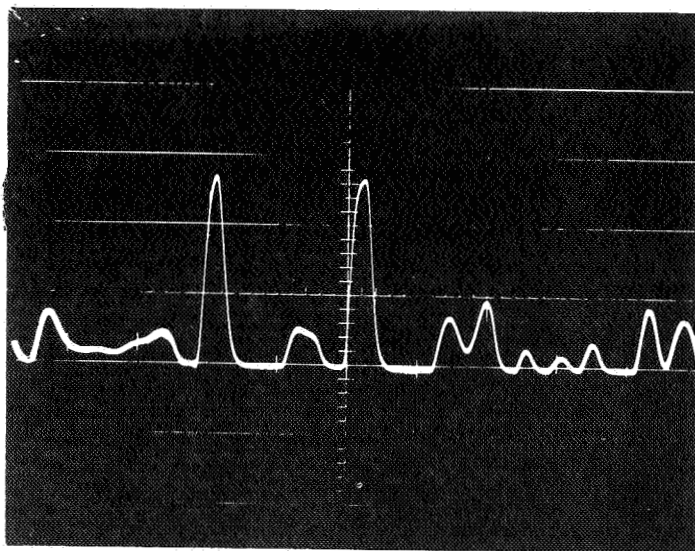
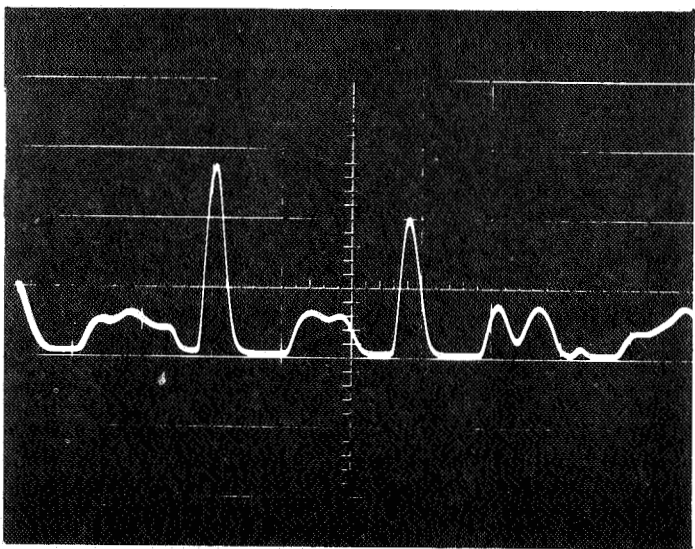


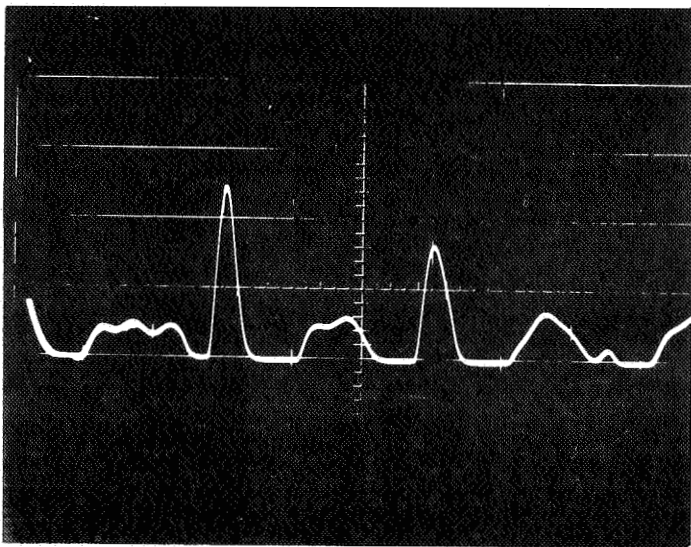
Figure 42. Self-heating apparatus to test survival of rhenium sensor in graphite felt. See also Fig. 32.



(a)  $V/V_o = 1$ ;  $T \approx 530^\circ\text{R}$

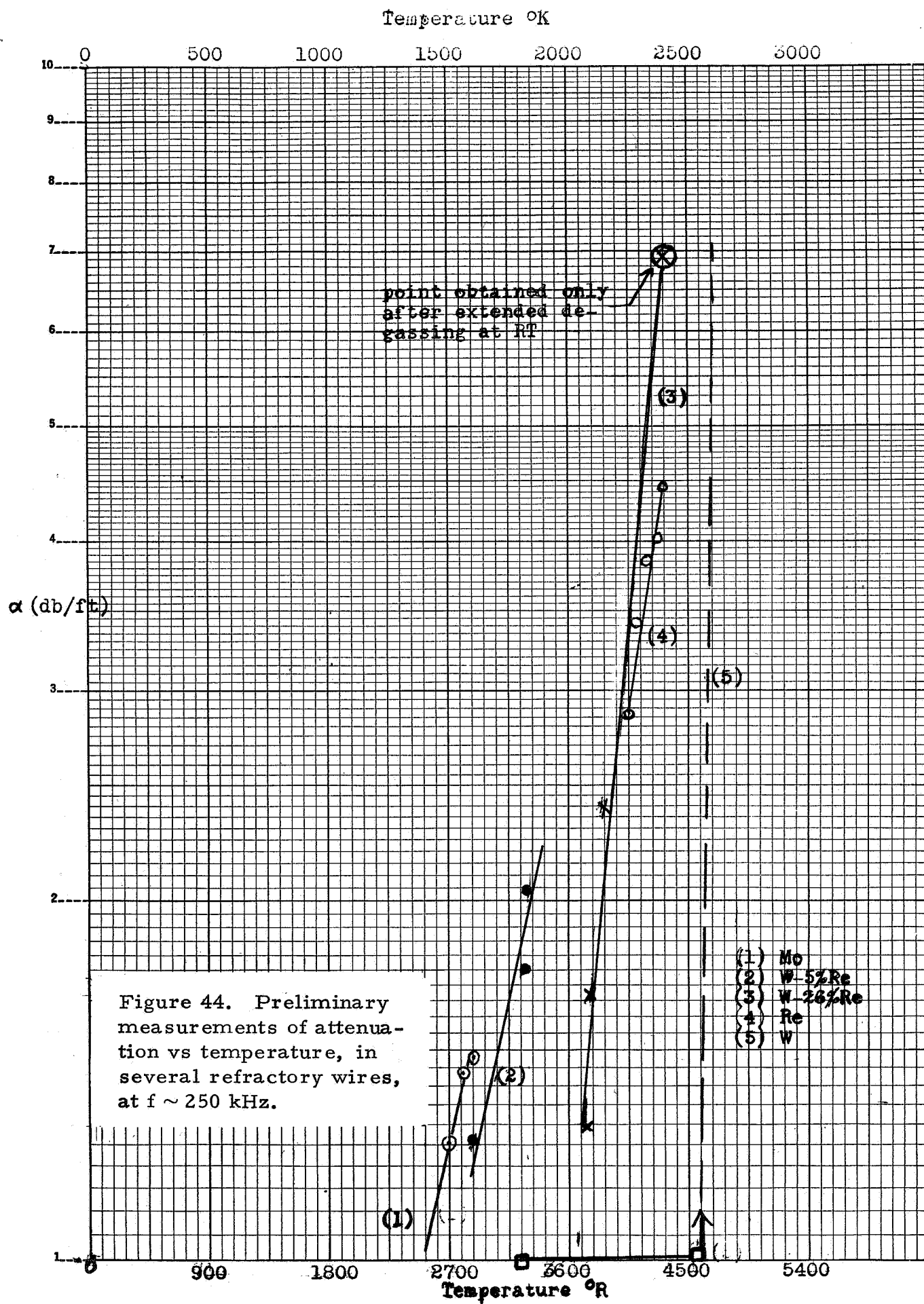


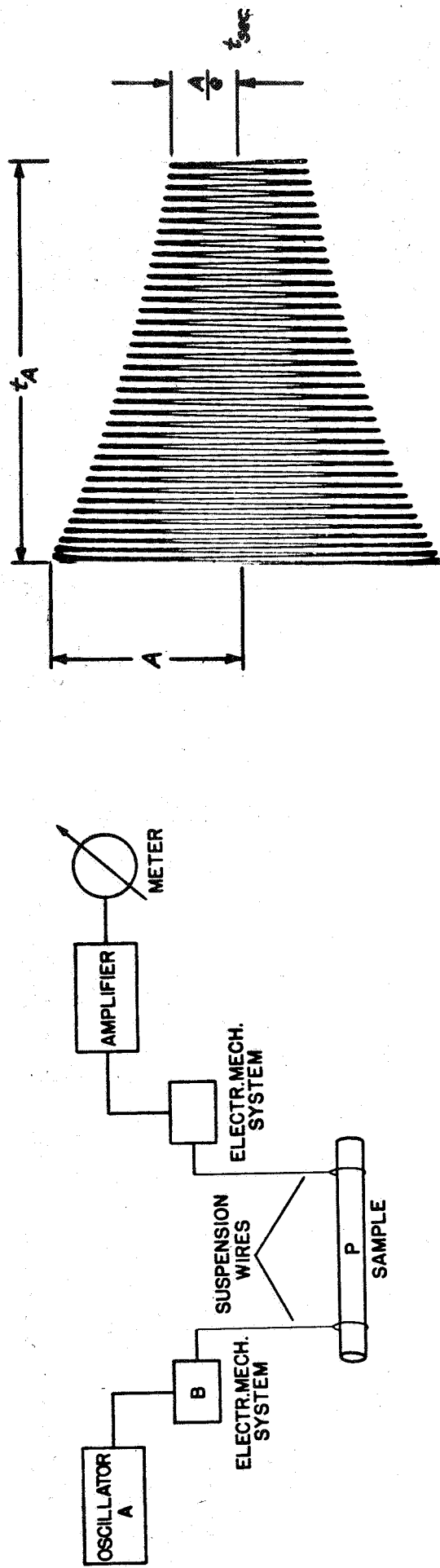
(b)  $V/V_o = 0.762$ ;  $T \approx 4400^\circ\text{R}$



(c)  $V/V_o = 0.706$ ;  $T \approx 5000^\circ\text{R}$

Figure 43. Oscillograms showing attenuation in bare rhenium sensor self-heated in graphite felt. Sensor length approximately 2 inches. Data obtained with experimental arrangement of Fig. 42.





Amplitude as a function of time for a freely decaying vibration. The product  $f_0$  times  $t_A$  represents the number of vibrations required for the amplitude to decrease from the value  $A$  to  $A/e = 36.8\%$ .

Figure 45a. Schematic of a resonance method for the measurement of the modulus of elasticity and damping, after F. Förster, Magnaflux Corp. Bulletin MT-7.

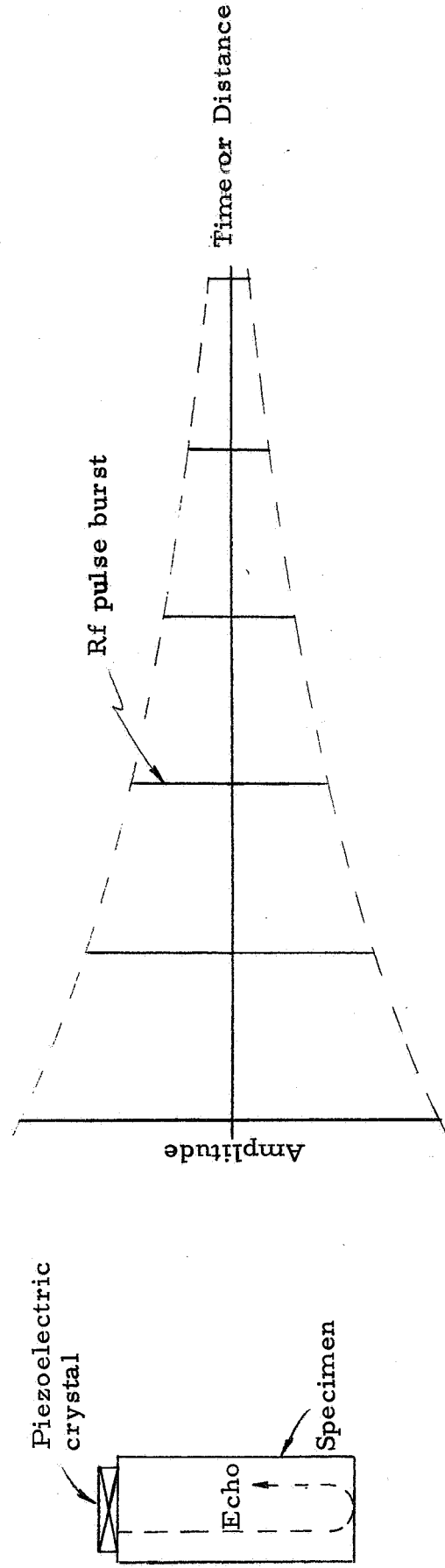


Figure 45b. Schematic of attenuation measurement using multiple echoes in bar. Diagram simplified for illustrative purposes.

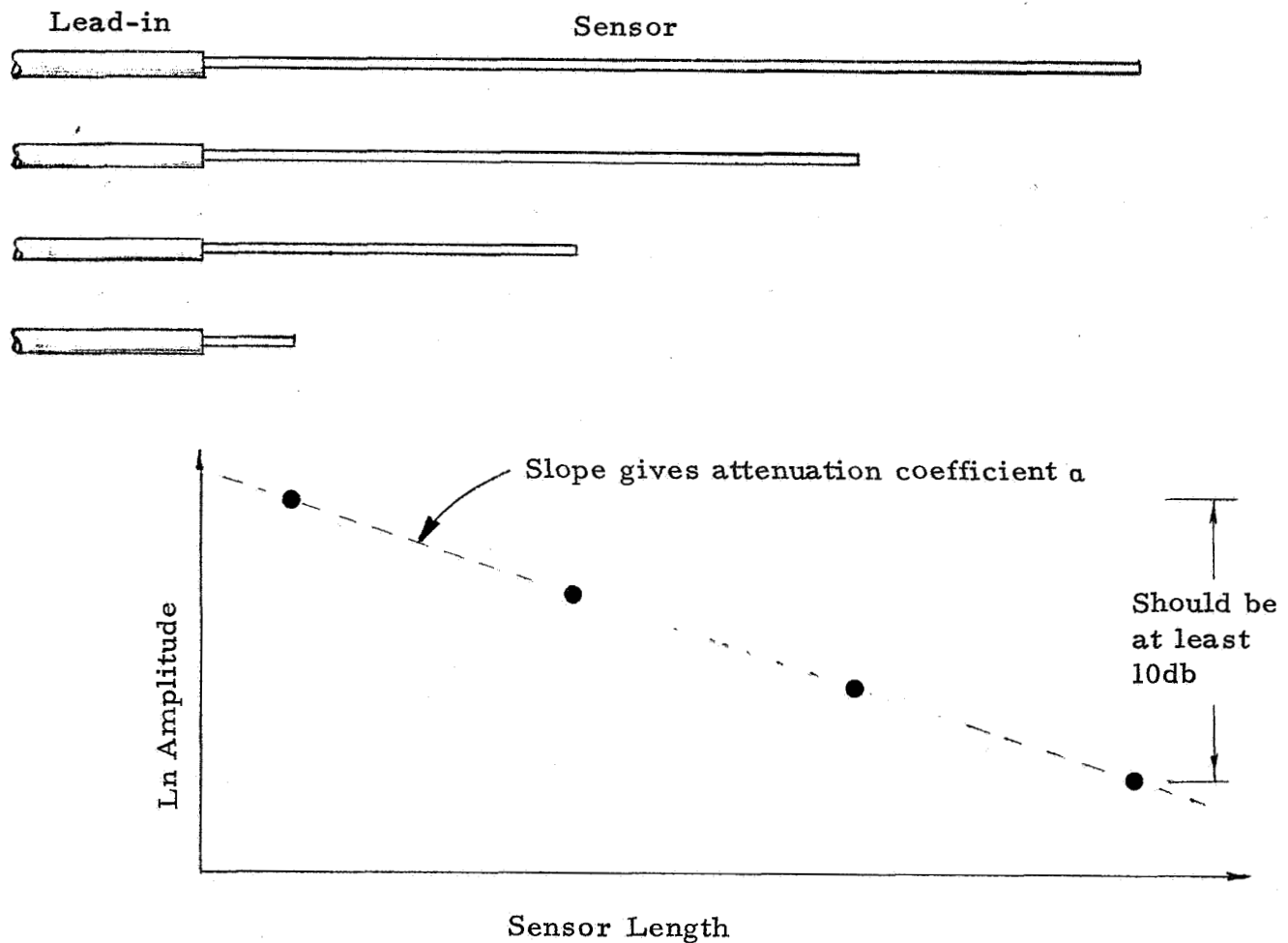
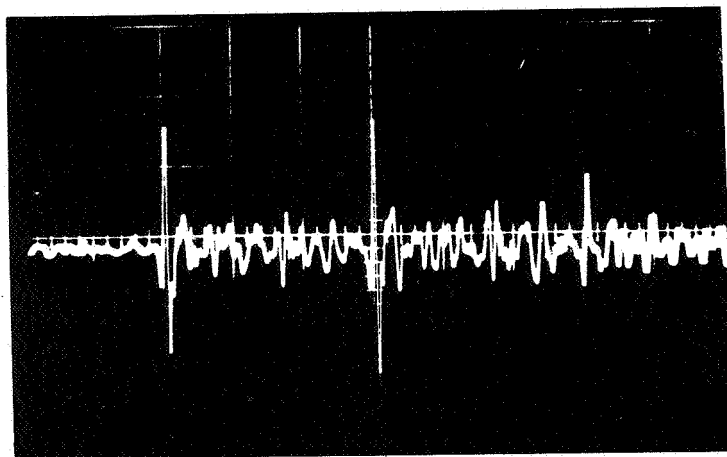


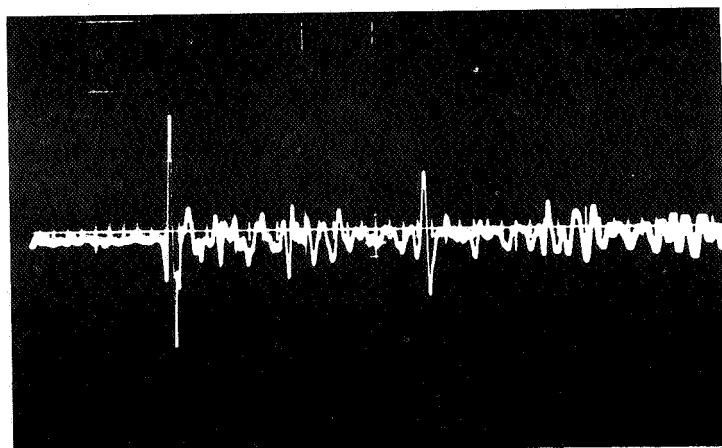
Figure 45c. Measurement of the attenuation coefficient using differential path length.

For a given temperature,  $T_1$ , frequency  $f_1$  and vibration mode  $V_1$ , amplitudes  $A$  and  $B$  are measured at the beginning ( $B$ ) and end ( $A$ ) of one or more sensors. This determines  $a$  for the conditions  $T_1$ ,  $f_1$ ,  $V_1$ , for a sensor of material  $M_1$  having a structure  $S_1$ . Procedure may be repeated as a function of  $T$ ,  $f$ , etc. Additional parameters of interest may include environment  $E$ , specimen history  $H$ , etc.

In the simplest case of only one sensor length  $x$ , if the room temperature sensor echo amplitudes are  $A_{\text{cold}}$  and  $B_{\text{cold}}$ , and the high temperature amplitudes are  $A_{\text{hot}}$  and  $B_{\text{hot}}$ , the increase in  $a$  due to heating from the "cold" to the "hot" condition is  $a = (1/2x) \ln \left[ (B_{\text{hot}}/B_{\text{cold}}) (A_{\text{cold}}/A_{\text{hot}}) \right]$  or  $a = (1/2x) \ln \left[ (A/B)_{\text{cold}} / (A/B)_{\text{hot}} \right]$ . If  $B_{\text{cold}} = B_{\text{hot}}$ , this reduces to  $a = (1/2x) \ln \left[ A_{\text{cold}} / A_{\text{hot}} \right]$ . See, for example, Fig. 46. Also, at room temperature,  $a_{\text{room temp}}$  can be estimated by comparing the observed  $A/B$  ratio with that predicted from Figs. 15a, b or c. That is to say,  $a_{\text{room temp}} = (1/2x) \ln \left[ (A/B)_{\text{Fig. 15}} / (A/B)_{\text{observed}} \right]$ .



Room temperature



High temperature  
~ 4300°R

→ | ← Sweep,  
50 μsec/cm

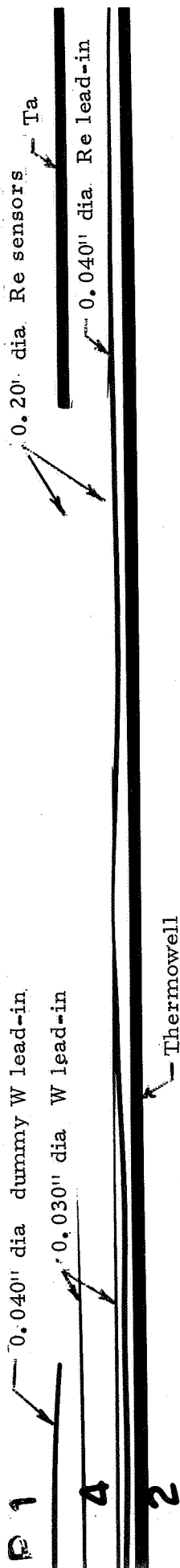
Figure 46. Oscillograms showing attenuation in self-heated tungsten wire. Specimen is about 1 ft long (acoustic path = 2 ft). From transit time ratio,  $148 \mu\text{sec}/181 \mu\text{sec} \approx 0.82$ , temperature is estimated from Fig. 12 to be  $\sim 4300^\circ\text{R}$ . From amplitude ratios at room and elevated temperature, attenuation is estimated as follows. End echo amplitude ratio is about  $1.8/0.9 = 2$ , i. e., a 6 db loss due to high temperature (change in lead-in attenuation is negligible in the present case). The attenuation coefficient is therefore  $\alpha = 6\text{db}/2 \text{ ft} = 3 \text{ db/ft}$ , at  $\sim 4300^\circ\text{R}$ , frequency  $\sim 300 \text{ kHz}$ . Above data were obtained with system of Fig. 2, operated in single pulse mode.

26

WANL 45312

V

6.28.67 W.0.90246



39

WANL 45312

V

6.28.67 W.0.90246

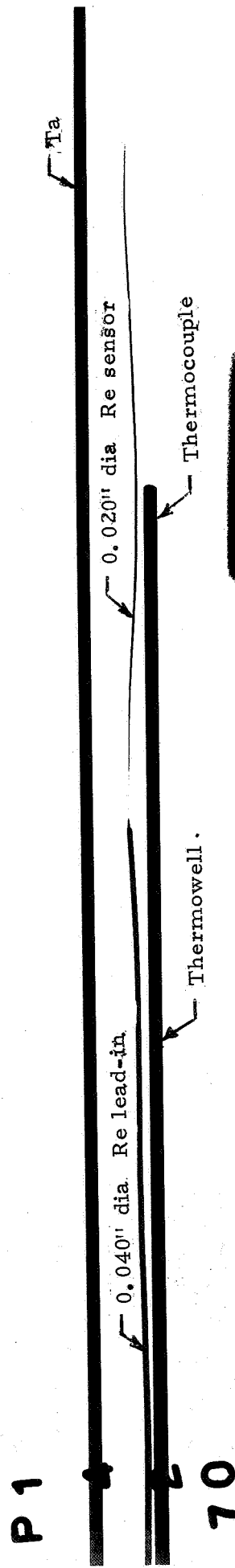
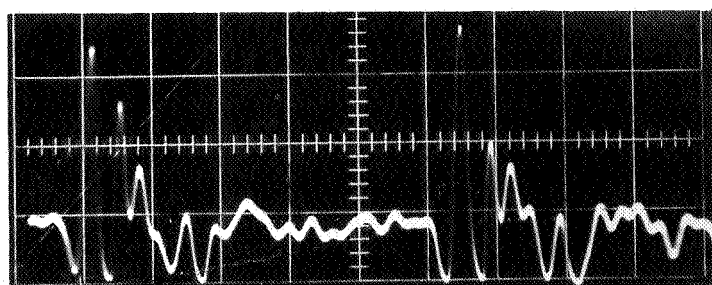
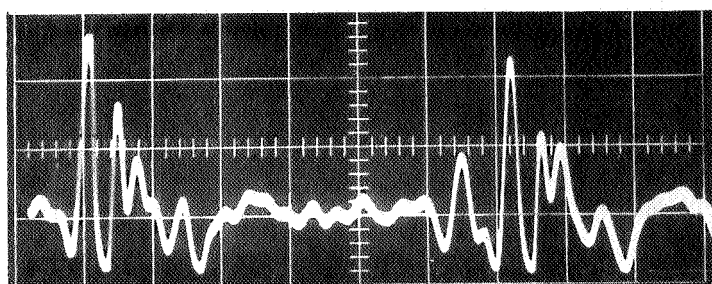


Figure 47: Identification of Key Items in WANL Tests

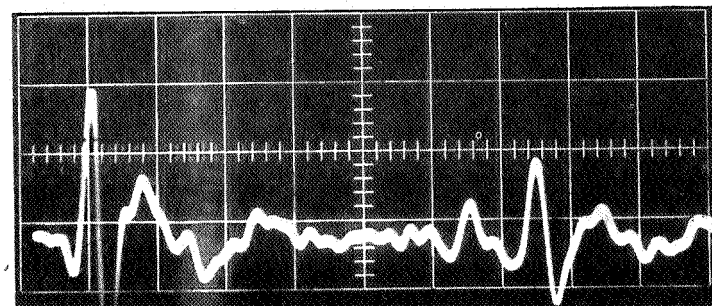
of June 28, 1967



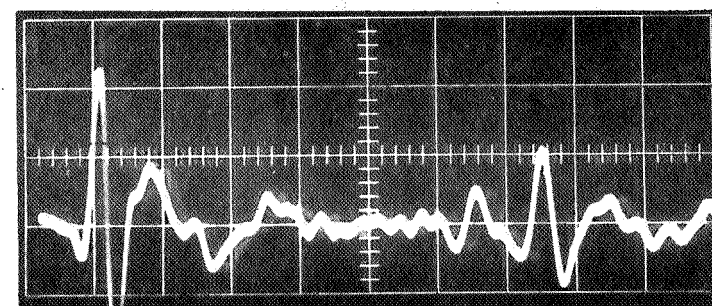
(a) 1337 hours Room Temperature  
10  $\mu\text{sec}/\text{cm}$  1 v/cm



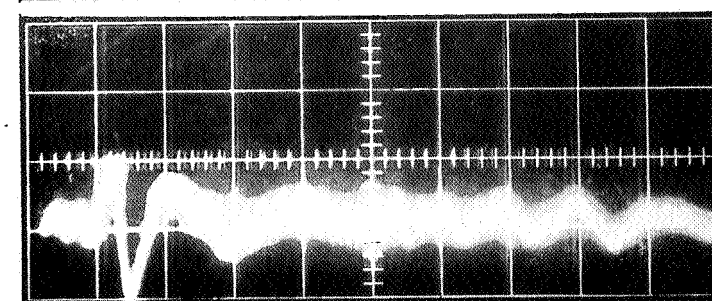
(b) 1409 hours  
10  $\mu\text{sec}/\text{cm}$  1 v/cm



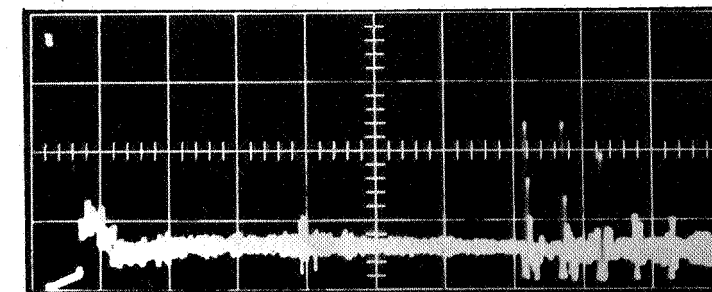
(c) 1428 hours  
10  $\mu\text{sec}/\text{cm}$  0.5 v/cm



(d) 1434 hours  
10  $\mu\text{sec}/\text{cm}$  0.5 v/cm



(e) 1441 hours  
10  $\mu\text{sec}/\text{cm}$  0.5 v/cm



(f) 1500 hours  
100  $\mu\text{sec}/\text{cm}$  2 v/cm

Figure 48. Oscillograms of bare all-rhenium wire line tested June 28, 1967  
- at WANL.

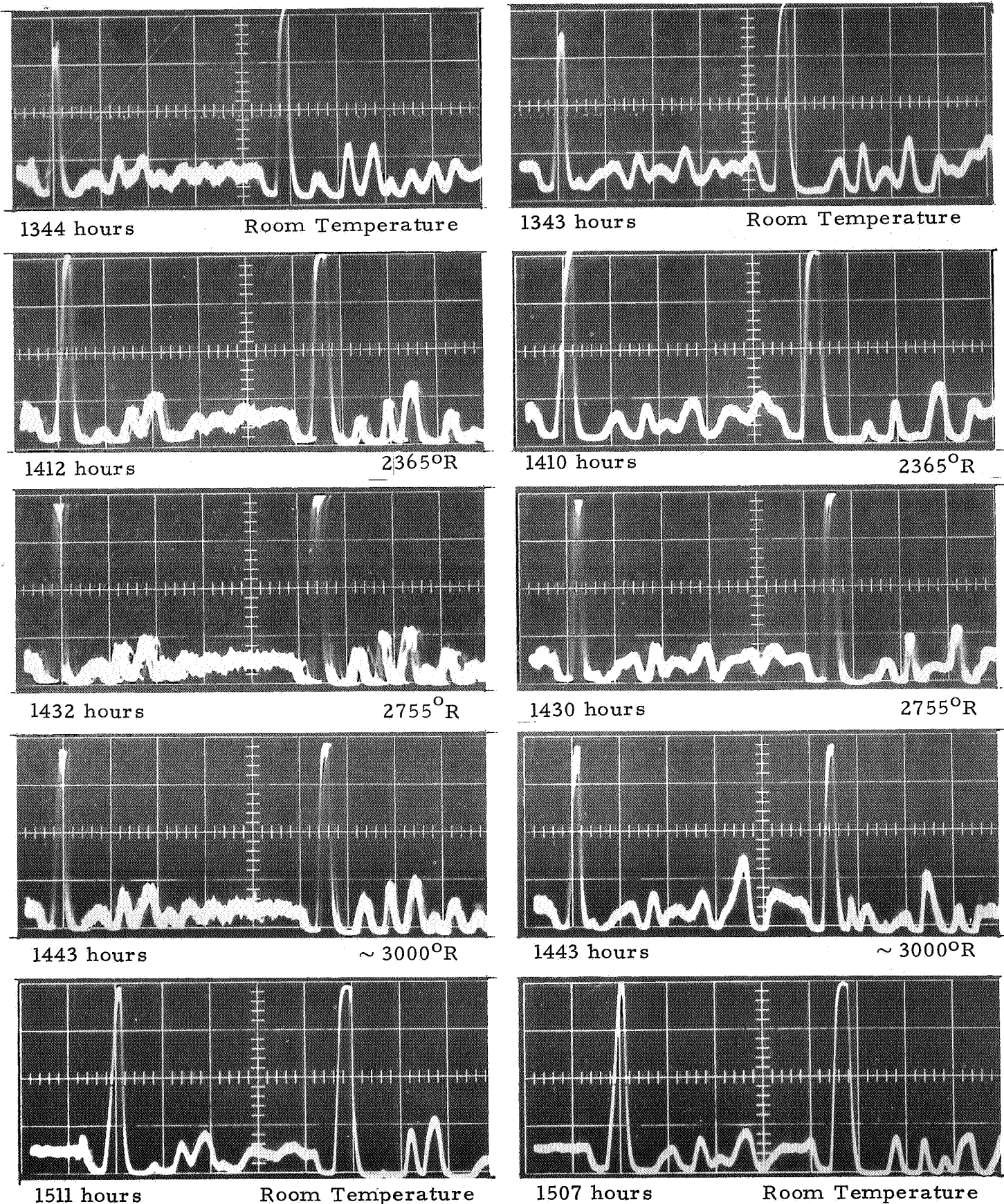


Figure 49. Oscillograms of echoes in 0.020" dia x 5" long rhenium sensor, welded to 0.030" dia centerless ground tungsten lead-in. Wires tested bare in WANL oven, June 28, 1967. Left column, specimen "A"; right column, specimen "B". Sweep, 10  $\mu$ sec/cm. Sensitivity, 2 v/cm.

Room Temp.

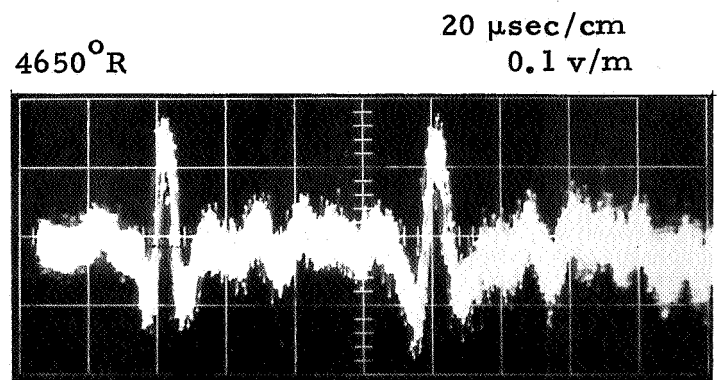
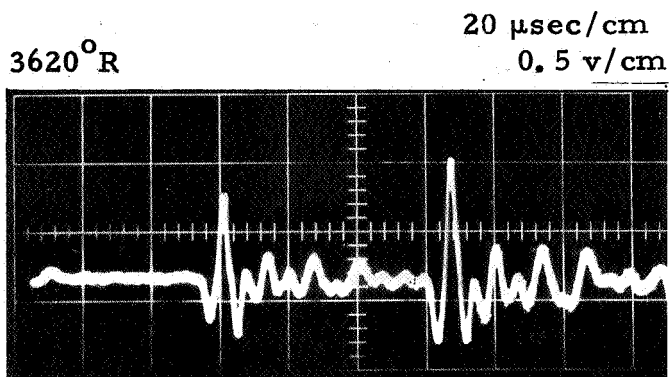
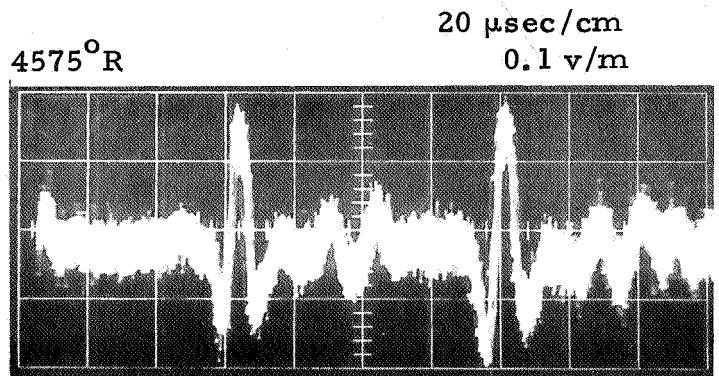
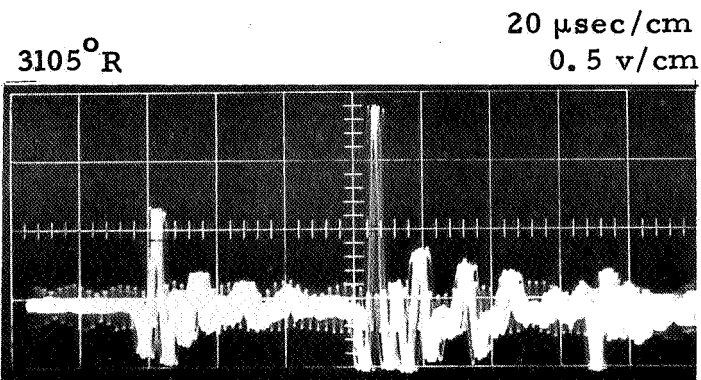
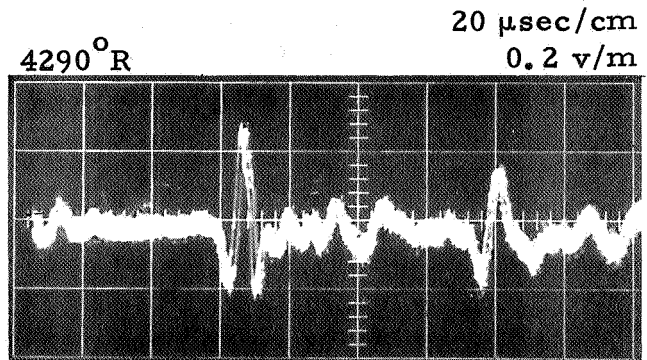
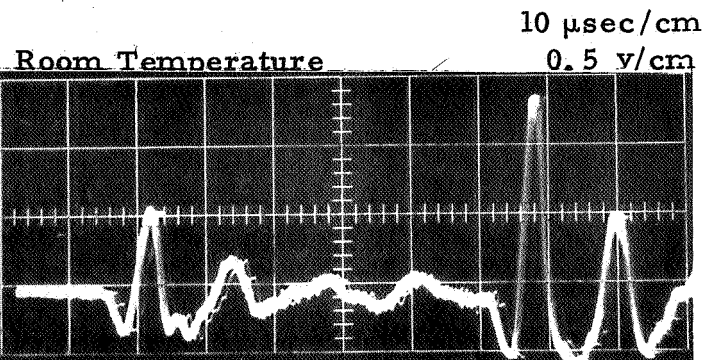
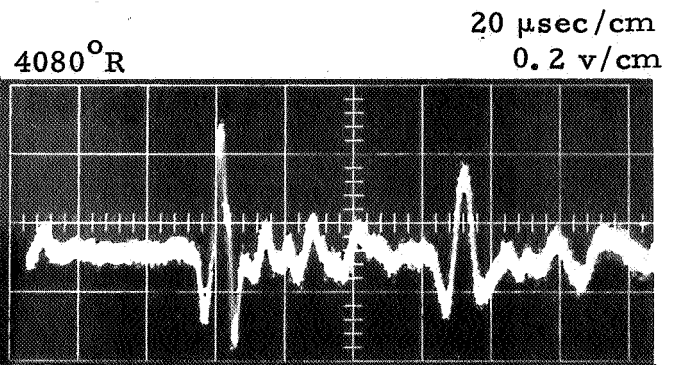
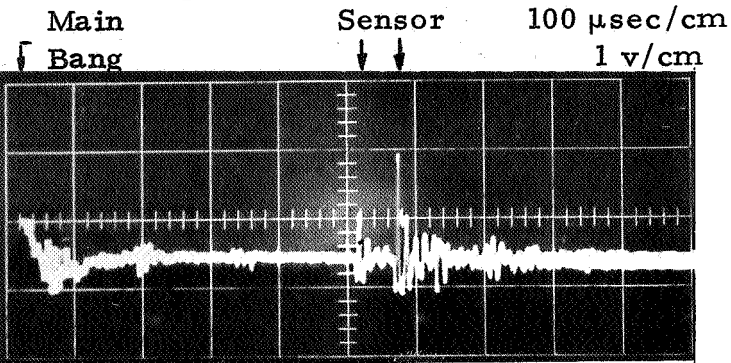


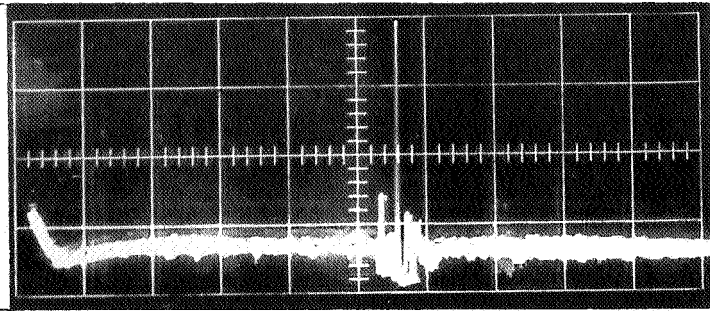
Figure 50. Oscillograms of 5" bare rhenium sensor, 0.020" dia, flash butt welded to 0.030" dia tungsten lead-in wire. Date of test, June 30, 1967. (Switch Point 1).

Room Temperature

Main  
Bang

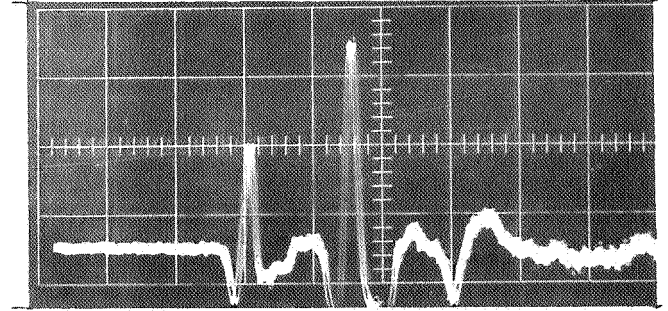
Sensor  
↓ ↓

100  $\mu\text{sec/cm}$   
1 v/cm



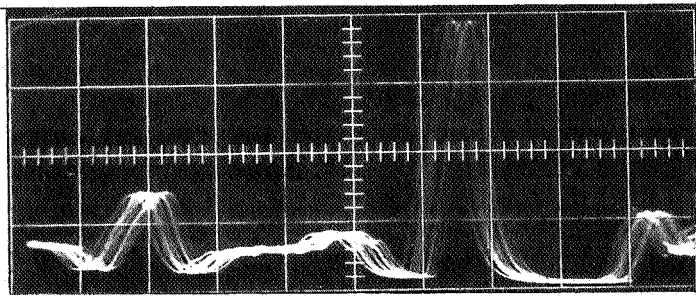
4300°R

20  $\mu\text{sec/cm}$   
0.5 v/cm



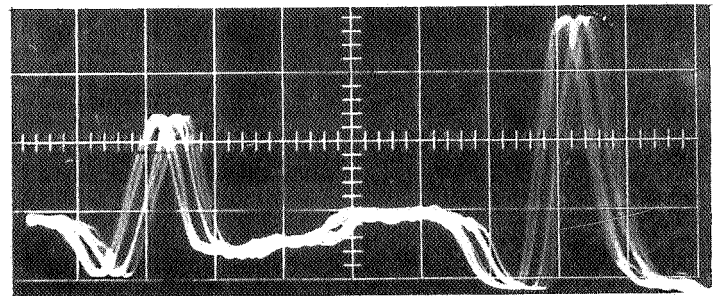
Room Temperature

5  $\mu\text{sec/cm}$   
1 v/cm



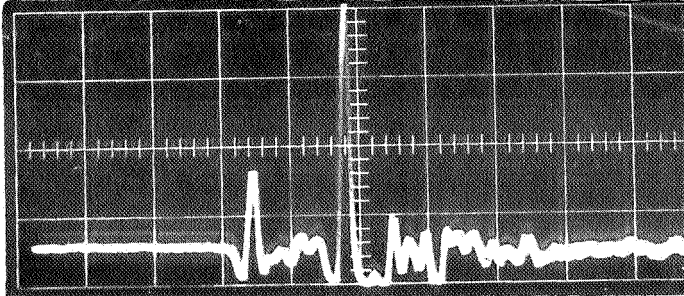
4315°R

5  $\mu\text{sec/cm}$   
0.5 v/cm



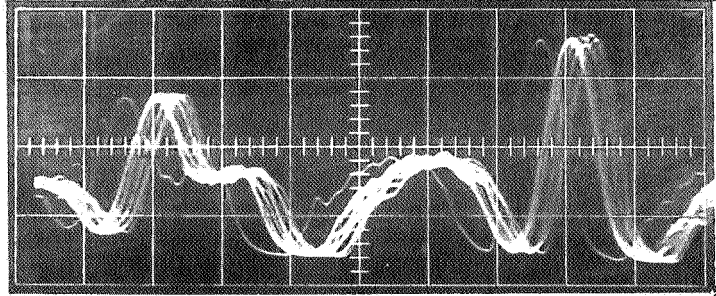
3170°R

20  $\mu\text{sec/cm}$   
1 v/cm



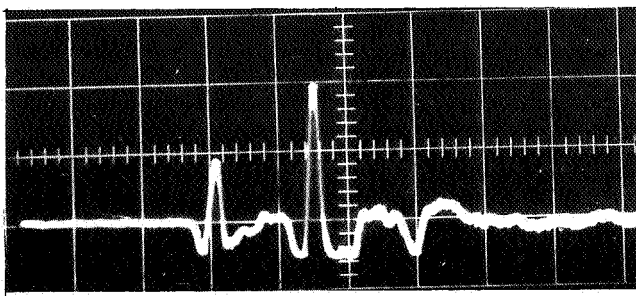
4500°R

5  $\mu\text{sec/cm}$   
0.5 v/cm



4080°R

20  $\mu\text{sec/cm}$   
1 v/cm



4765°R

5  $\mu\text{sec/cm}$   
0.5 v/cm

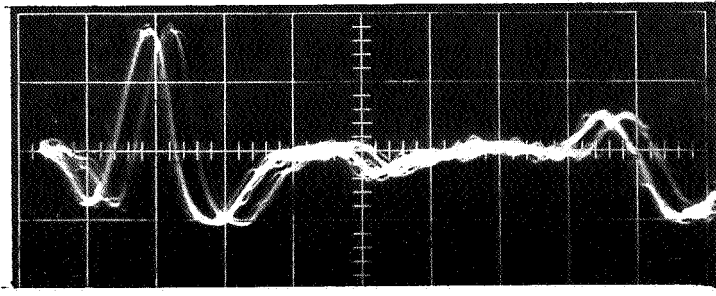
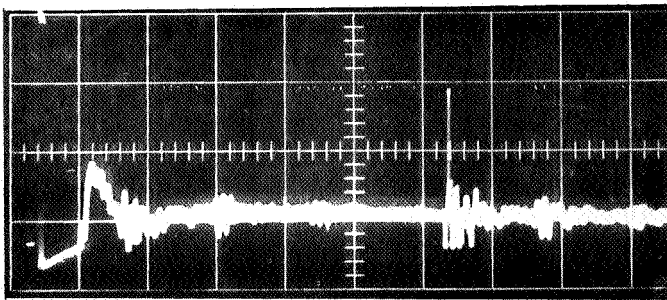
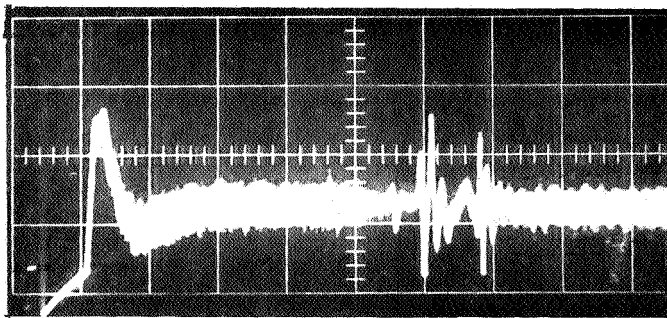


Figure 51. Oscillograms of 2" bare rhenium sensor 0.030" dia flash butt welded to 0.040" dia tungsten lead-in wire. Date of test, June 30, 1967. (Switch Point 2).



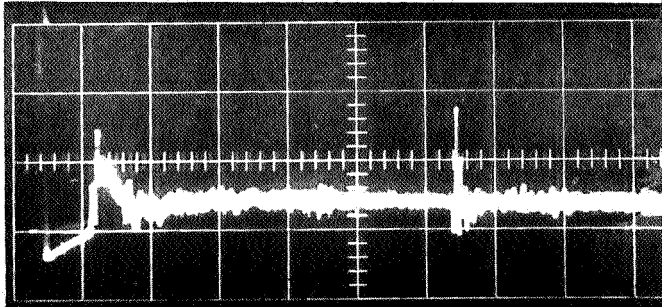
0.030" dia W lead-in wire

4085°R, on cooling. ~1434 hrs, 1 v/cm



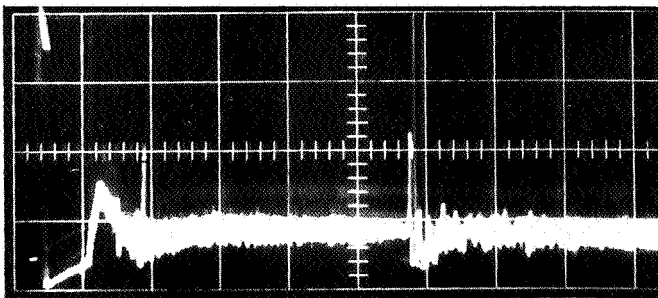
0.040" dia W lead-in wire

5000°R, on heating. ~1432 hrs, 0.5 v/cm



0.040" dia Re lead-in wire

~4000°R, on cooling. ~1435 hrs, 1 v/cm



0.030" dia W lead-in wire, in sheath

~4000°R, on cooling. ~1435 hrs, 1 v/cm

Figure 52. Echoes from end of lead-in wires, after loss of sensors in WANL test, June 30, 1967. Sweep, 100  $\mu$ sec/cm. From top to bottom, switch points 1 to 4.

Figure 53

Comparison of temperatures in  
WANL graphite/hydrogen oven using  
ultrasonic, pyrometric and thermo-  
couple means.

Date of Test: June 30, 1967.

